Master's Thesis

A thesis submitted in fulfillment of the requirements for the degree of joint master program in space science and technology - spacemaster (ltu) and for the degree of master in cybernetics and robotics at czech technical university (ctu).

FORESAIL-2 AOCS Trade Studies and Design

AUTHOR

Guillaume Le Bonhomme
Luleå University of Technology
Joint MSc in Space Science & Technology
Czech Technical University
MSc in Cybernetics & Robotics

SUPERVISORS

Assistant Professor Jaan Praks
Postdoctoral Researcher Andris Slavinskis

EXAMINERS

Assistant Professor Martin Hlinovsky
Assistant Professor Kristian Hengster-Movric
Senior Lecturer Anita Enmark

August 14, 2020

MASTER'S THESIS ASSIGNMENT

I. Personal and study details

Student's name: **Le Bonhomme Guillaume** Personal ID number: **492120**

Faculty / Institute: **Faculty of Electrical Engineering**

Department / Institute: **Department of Control Engineering**

Study program: **Cybernetics and Robotics**

Branch of study: **Cybernetics and Robotics**

II. Master's thesis details

Master's thesis title in English:

FORESAIL-2 AOCS trade studies and design

Master's thesis title in Czech:

FORESAIL-2 AOCS obchodní studie a návrh

Guidelines:

FORESAIL-2 will demonstrate a feasibility to utilize and characterize a nanosatellite and its instruments for scientific purposes in a high-radiation environment. The thesis objective is the trade study of the performance of selected actuators and sensors in order to choose the ones that are the most adapted to the FORESAIL-2 mission objectives and requirements.
1. A study of which attitude sensors, actuators and propulsion systems can fulfil the mission requirements.
2. A trade-off study between different solutions.
3. Find out the most optimal solution(s) and write one or two recommendations.

Bibliography / sources:

[1] Berlin Peter - Satellite Platform Design, 6th Edition - Lulea University of Technology, 2014
[2] Macdonald Malcom, Badescu Viorel – The International Handbook of Space Technology - Springer-Verlag Berlin Heidelberg, 2014
[3] Fortescue Peter, Swinerd Graham, Stark John - Spacecraft Systems Engineering, 4th Edition – Wiley, 2011

Name and workplace of master's thesis supervisor:

Dr. Andris Slavinskis, Department of Electronics and Nanoengineering, Aalto University School od Electrical Engineering, Maarintie 8, 02150 Espoo, Finladn

Name and workplace of second master's thesis supervisor or consultant:

Ing. Martin Hlinovský, Ph.D., Department of Control Engineering, FEE

Date of master's thesis assignment: **20.01.2020** Deadline for master's thesis submission: **14.08.2020**

Assignment valid until:
by the end of winter semester 2021/2022

Dr. Andris Slavinskis Supervisor's signature	prof. Ing. Michael Šebek, DrSc. Head of department's signature	prof. Mgr. Petr Páta, Ph.D. Dean's signature

III. Assignment receipt

The student acknowledges that the master's thesis is an individual work. The student must produce his thesis without the assistance of others, with the exception of provided consultations. Within the master's thesis, the author must state the names of consultants and include a list of references.

. _____
Date of assignment receipt

_____
Student's signature

Declaration

I declare that the presented work was developed independently and that I have listed all sources of information used within it in accordance with the methodical instructions for observing the ethical principles in the preparation of university theses.

Date and place : Prague, August 14, 2020 Signature:

Abstract

This thesis aims to design a reliable CubeSat platform, including the avionic subsystems that can sustain a high radiation environment for a mission having a lifetime of at least six months. The science instruments put stringent requirements on the platform to achieve and maintain the desired spin rate. The simulation background is set up in Systems Tool Kit (STK). A trade-off analysis for the Attitude and Orbit Control System (AOCS) of FORESAIL 2 was done, focusing on the actuators and their ability to offer the right amount of torque to fulfill the tether deployment. Mission design analyses were performed to conclude on the form factor of the CubeSat, its ability to generate power, its compliance with the Space Debris Mitigation (SDM) technical requirements, and the total radiation dose accumulated. It was found that a 6U form factor is preferred to allocate more space for each subsystem, alongside with generating enough power for the satellite to work in all modes wanted. The mission is compliant with European Cooperation for Space Standardization (ECSS) and International Organization for Standardization (ISO) standards if the CubeSat is to be launched in September 2022. To allow a threshold limit of 10 $krads$ on the components of the satellite, a shielding wall of 7 mm should be implemented on the CubeSat's structure. Major requirements for the designed mission were written to initialize the investigation on the sensors and actuators. The results showed that only a propulsion system provided the necessary angular momentum to deploy the tether. The lack of magnetic field makes magnetorquers almost unusable in the desired orbit, leaving reaction wheels as the only option remaining to assist the propulsion units. The different analyses and simulations led to a final AOCS configuration composed of five various sensors (Sun sensors, magnetometers, a GPS, an IMU, and housekeeping sensors) for the attitude determination. A propulsion system and reaction wheels will provide the necessary control over the satellite.

Acknowledgements

Firstly, I would like to express my most significant appreciation towards my supervisors, Professor Jaan Praks, Postdoctoral Researcher Andris Slavinskis, Postdoctoral Researcher Muhammad Rizwan Mughal, and Doctoral Candidate Zainab Saleem. They have been very helpful and provided me with advice and guidance during my stay at Aalto University. It was a fantastic opportunity to discover the space industry, where I learned a lot about designing a satellite from scratch. My stay in Finland made me find out the so-called Digital Mission Engineering side when planning a mission, which I hope to work on in the future.

In addition to my supervisors, I would like to pay my special regards to Assistant Professor Martin Hlinovský, Assistant Professor Kristian Hengster-Movric, and Senior Lecturer Anita Enmark for being my examiners.

I wish to express my sincere appreciation to Dr. Victoria Barabash for enrolling me in the Joint Master Program in Space Science and Technology – SpaceMaster. It was the best educational experience I received by far.

I wish to thank all the people whose assistance was a milestone in the completion of this project. Throughout my studies, I have met fantastic people who supported me and encouraged me. I want to thank my girlfriend, Cristina, for sending irreplaceable support and love despite the distance due to the COVID-19 situation. I am also grateful to Maximilian, Niels, Roger, Mauro, Lucas, David, Javier, Max, Jose, Paula, Patricia, Thibault, Florent, and Richard for having beautiful friendships.

Last but not least, I am indebted to my parents and sisters who supported me during my entire life so that I could achieve my dreams and goals.

Contents

List of Figures

List of Tables

List of Symbols

T_a	Aerodynamic drag torque	$N \cdot m$
c_{pa}	Aerodynamic pressure center	m
θ	Angle between local vertical and Z principal axis	$^\circ$
h_{max}	Angular momentum produced by the reaction wheel	$N \cdot m \cdot s$
AU	Astronomical unit	AU
ρ	Atmospheric density	$kg \cdot m^{-3}$
c_m	Center of mass	m
R	Distance from the center of Earth	m
C_d	Drag coefficient	N/A
μ	Earth gravitational constant	$m^3 \cdot s^{-2}$
$E_{required}$	Energy required for tether deployment	$W \cdot h$
λ	Function of magnetic latitude	N/A
T_{mag}	Generated torque from magnetorquer	$N \cdot m$
T_g	Gravity gradient torque	$N \cdot m$
I_{max}	Greatest inertia of the satellite	$kg \cdot m^{-2}$
h_{disc}	Height of the disc	m
h_{ring}	Height of the ring	m
I_{disc}	Inertial momentum of the disc	$kg \cdot m^{-2}$
I_{ring}	Inertial momentum of the ring	$kg \cdot m^{-2}$
μ_0	Magnetic constant	$m \cdot kg \cdot s^{-2} \cdot A^{-2}$
m_{mag}	Magnetic dipole	$A \cdot m^2$
B	Magnetic field strength	T
M	Magnetic moment of the Earth multiplied by μ_0	$T \cdot m^3$
m_{disc}	Mass of the disc	kg
m_s	Mass of FORESAIL-2	kg
m_{RW}	Mass of the reaction wheel	kg
m_{ring}	Mass of the ring	kg
ρ_{mat}	Material (iron) density	$kg \cdot m^{-3}$
I_{xx}	Moment of inertia about the x axis	$kg \cdot m^{-2}$
I_{yy}	Moment of inertia about the y axis	$kg \cdot m^{-2}$
I_{zz}	Moment of inertia about the z axis	$kg \cdot m^{-2}$
n	Number of turns of the wire	N/A
ω_{max}	Operational speed of the motor	RPM
t_{orbit}	Orbital period	s
v	Orbital velocity	$m \cdot s^{-1}$
$P_{thruster}$	Power consumption of the propulsion unit	W
r_{disc}	Radius of the disc	m

r_{ring}	Radius of the ring	m
A_r	Ram area	m^2
q	Reflectance factor	N/A
D	Residual dipole moment of the spacecraft	$A \cdot m^2$
T_m	Residual magnetic dipole torque	$N \cdot m$
ϕ	Solar constant adjusted to actual distance	$W \cdot m^{-2}$
T_s	Solar radiation pressure	$N \cdot m$
c_{ps}	Solar radiation pressure center	m
I_{sp}	Specific impulse	s
c	Speed of light	$m \cdot s^{-1}$
φ	Sun incidence angle	$^\circ$
A_s	Sunlit surface area	m^2
T	Thrust generated by the propulsion unit	$N \cdot s$
$t_{maneuver}$	Time needed to deploy the tether	s
t_f	Time needed to rotate FS-2 using the reaction wheel	s
I_t	Total effective propellant mass	kg
I_t	Total impulse	$N \cdot s$
$I_{t_{required}}$	Total impulse required to deploy the tether	$N \cdot s$
I_{RW}	Total inertial momentum of the reaction wheel	$kg \cdot m^{-2}$
T_{dist}	Total magnitude of external disturbances	$N \cdot m$
A_{mag}	Vector area of the coil	m^2

Physical constants

AU	Astronomical unit	$1\ AU = 149597870700\ m$
μ	Earth gravitational constant	$3.98600441 \cdot 10^{14}\ m^3 \cdot s^{-2}$
g_0	Gravitational acceleration	$9.80665\ m \cdot s^{-2}$
μ_0	Magnetic constant	$1.25663706 \cdot 10^{-6}\ m \cdot kg \cdot s^{-2} \cdot A^{-2}$
ϕ	Solar constant at 1 AU	$1366\ W \cdot m^{-2}$
c	Speed of light	$299792458\ m \cdot s^{-1}$

Abbreviations

ACS	Attitude Control System
ADCS	Attitude Determination and Control
ADS	Attitude Determination System
AOCS	Attitude and Orbit Control System
APS	Active Pixel Sensor
CCD	Charge Coupled Device
CPM	Coarse Pointing Mode
CD	Coulomb Drag
CMG	Control Moment Gyros
COTS	Commercially Off The Shelf
CROC	Cross Section of Complex Bodies
DPS	Deep Space Positioning System
DRAMA	Debris Risk Assessment and Mitigation Analysis
EMI	Electro-Magnetic Interferences
ECSS	European Cooperation for Space Standardization
ESA	European Space Agency
FOG	Fibre Optic Gyros
FPM	Fine Pointing Mode
FS	FORESAIL
FS-1	FORESAIL-1
FS-2	FORESAIL-2
GEO	Geostationary Earth Orbit
GNSS	Global Navigation Satellite System
GPS	Global Positioning System
GTO	Geostationary Transfer Orbit
HEO	High Earth Orbit
HRG	Hemispherical Resonator Gyros
IMU	Inertial Measurement Unit
IR	Infrared
IADC	Inter-Agency Space Debris Coordination Committee
ISO	International Standards Organization
LEO	Low Earth Orbit
MASTER	Meteoroid and Space Debris Terrestrial Environment Reference
MEO	Medium Earth Orbit
NASA	National Aeronautics and Space Administration
OMDM	Orbit Maintenance and Deorbit Mode
OSCAR	Orbital SpaceCraft Active Removal

PMW	Pulse Width Modulation
RCS	Reaction Control System
REPE	Relativistic Electron and Proton Experiment
RHBD	Radiation Hardening By Design
RLG	Ring Laser Gyros
RME	Radiation Mitigation Experiment
RPM	Revolutions Per Minute
SM	Safe Mode
SWaP	Size Weight and Power
SRP	Solar Radiation Pressure
SDM	Space Debris Mitigation
STK	Systems Tool Kit
TRL	Technology Readiness Level
TPDM	Tether Pre-Deployment Mode
TID	Total Ionizing Design
ULF	Ultra Low Frequency
VSG	Vibrating Structure Gyros

1 Introduction

The growth and standardization of miniaturized satellites such as CubeSats have brought a new era to the space industry by allowing more actors to join the space movement. During the past few years, many universities and startups could rise by starting their own CubeSat thanks to lower costs and faster design processes. This technology was proved many times to be efficient LEO, with the ambition to go even further in HEO, GTO, GEO. FORESAIL-2 is a mission designed and developed by the Finnish Center of Excellence for Research in Sustainable Space. It aims to demonstrate the feasibility of small satellite platforms for scientific and technology demonstration purposes in a high-radiation environment. The science goal is to use a nanosatellite to study the role of ULF waves in accelerating, transporting, and scattering electrons in the Van Allen radiation belts. Another science objective is to deploy a thin, long charged tether for coulomb drag and scientific plasma measurements.

The author of the thesis had the intent to make this work easy to read and follow. The introduction is followed by a literature review (section 2) where a special attention is put on the desired orbit, CubeSats and missions to GTO, and the heritage of FORESAIL-2. Following the literature review is the theoretical background (section 3) where the subsystem is explained alongside with the different technologies available to determine the final design. The trade studies (section 4) come right after where the orbital propagator model is set up for simulations, analyses, and calculation. The environment is being studied to determine limits, constraints, and requirements for the AOCS design. As a result, calculation on actuators follow the latter to determine what is the best option to go for. A final AOCS configuration is resulting from this section with various COTS availability and a description of the modes architecture. The end of the thesis (section 5) will conclude on the work accomplished, and states recommendations for future work to be done.

2 Literature review

2.1 Characteristics of GTO

A Geosynchronous Transfer Orbit also known as Geostationary Transfer Orbit is a highly elliptical orbit with the perigee being in Low Earth Orbit and the apogee crossing to Geosynchronous Earth Orbit. More information about GTO can be seen in table 2.1. [1]

Element	**Value**
Perigee	Usually restricted to a few hundred kilometers above the Earth's surface
Apogee	$\sim 35786\ km$
Eccentricity	Highly elleptical, usually from 0 to 0.9
Period	$\sim 10.5\ hours$
Inclination	$i < 90°$ (subject to the launch site) The majority of the missions have $i < 10°$
Argument of perigee	Such that apogee occurs on or near the equator

Table 2.1: Characteristics of GTO.

Typical characteristics of a GTO orbit can be found in table 2.2, respecting the constraints outlined in table 2.1.

Element	**Value**
Perigee	$500\ km$
Apogee	$35786\ km$
Semi-major axis	$24514\ km$
Eccentricity	0.72
Argument of perigee	0.00°
Orbital period	$10.61\ h$

Table 2.2: Typical characteristics of a GTO orbit.

Because of its orbital characteristics (inclination and eccentricity), the CubeSat will be influenced by changes in temperature where the primary sources are the Sun and the Earth loads. [2] The satellite will spend more time around the apogee due to the

decreasing speed and, therefore, will be influenced much more by thermal radiation coming from the Sun than from the Earth. [3]

The different heat sources can be found in table 2.3 below.

Heat source	Value
Solar flux	Annual average of $1367\,Wm^{-2}$ $1414\,Wm^{-2}$ during winter solstice $1322\,Wm^{-2}$ during summer solstice
Earth radiation	Average value of $230\,Wm^{-2}$ in LEO
Earth albedo	Average value of $390\,Wm^{-2}$ in LEO

Table 2.3: External heat sources influencing the CubeSat.

When oscillating from low to high altitudes, the spacecraft will be influenced by changes of the magnetic field strength. It is a fact that the magnetic field is much stronger in LEO, and when approaching the apogee this one will have no influence on the CubeSat because of its weakness. Using SPENVIS (see table 2.2 for implemented values), the magnetic field strength as a function of time has been simulated for the given orbit. Figure 2.1 outlines the rising magnetic field strength each time the CubeSat passes by the perigee with peaks of about $\sim 0.3\,Gauss$. The Gauss is the unit measurement for magnetic field flux density, or in other words, its intensity ($1\,Gauss$ is equal to $10^{-4}\,T$).

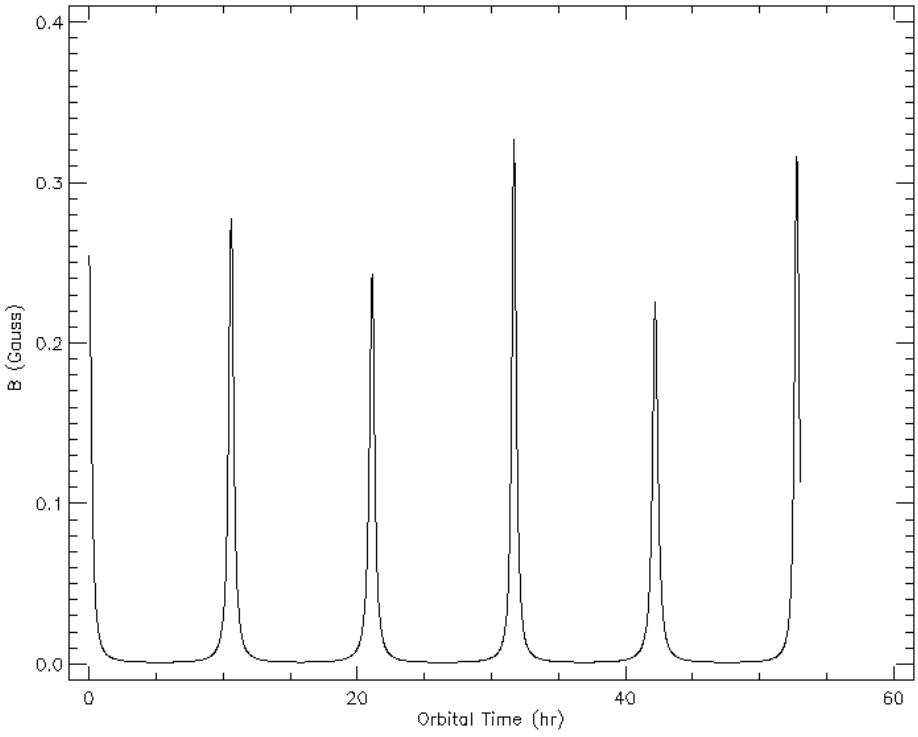

Figure 2.1: Magnetic field strength as a function of time for 5 orbits.

2.2 General description of space environment

The orbit of the CubeSat is of an elliptical sort with high eccentricity. It is known that the spacecraft will go through numerous environments, although not exceeding beyond the Earth's magnetosphere during normal circumstances. The characteristic interactions with the environment for each orbital segment has to be considered. Based on the mission characteristics, the CubeSat will pass two of the following orbital regions and even reach GEO which is located just at the lower boundary of the High Earth Orbit region. [4]

Orbit type	Altitude
LEO	$h < 2000\ km$
Medium Earth Orbit (MEO)	$2000\ km < h < 35786\ km$
HEO	$h > 35786\ km$

Table 2.4: Orbital regions (where h is the altitude in km).

The orbits mentioned above are among the most crowded areas surrounding Earth (see figure 2.2). Artificial debris that originated from discontinued man-made objects such as communication satellites are a serious hazard for spacecraft crossing their path. [5]

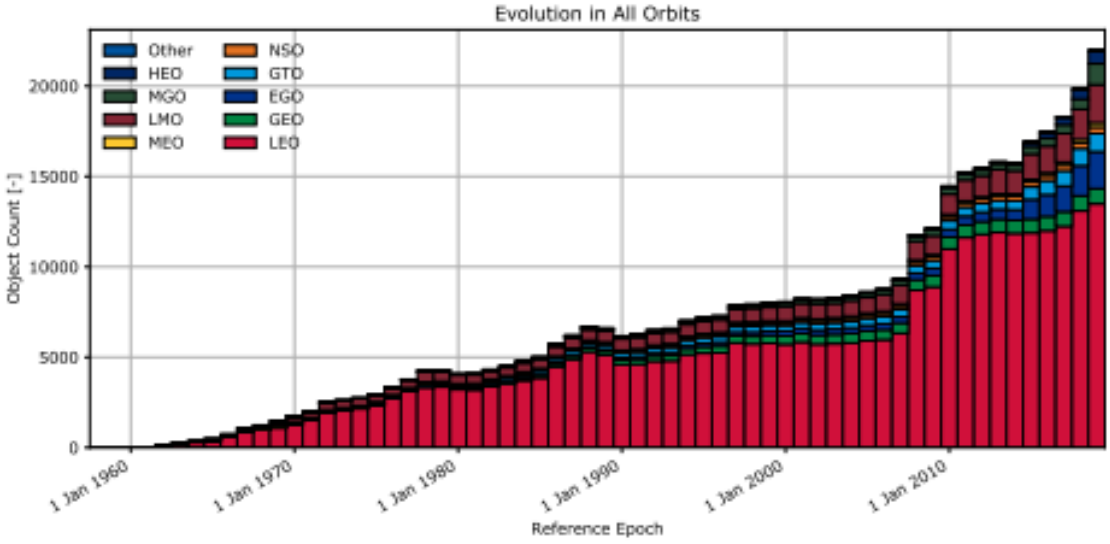

Figure 2.2: Evolution of the number of objects in space for all orbits. [5]

2.2.1 Neutral environment

The CubeSat does not spend a long time in the LEO orbital region. Nonetheless, this one will still be affected by the neutral environment. The neutral environment causes the drag effect, sputtering, surface erosion and spacecraft glow. The vacuum environment is characterized by its low pressure and absence of usual atmosphere. However, it includes atmospheric gas (that does not affect spacecrafts for higher altitude such as in the MEO orbital region for instance) that will impact the surface

of the CubeSat and causes the drag effect mentioned earlier (see section 3.2.1 for more information and formula). This is a dangerous force as it can drag back the satellite to the Earth's surface if a propulsion system is not used to keep it in orbit. [6]

Another important parameter to take in account is the surface erosion mentioned above. Atomic oxygen is the prominent gas in the neutral environment, collisions between this last one and the CubeSat can induce unwanted chemical reactions and, therefore, leads to surface erosion. [7] The rate of the surface loss is given by the following equation:

$$\frac{dx}{dt} = RE\phi \tag{2.1}$$

where RE is the reaction efficiency of the material and ϕ the atomic oxygen flux.

To prove a point, the total mass density relative to the orbital time has been simulated as seen in figure 2.3.

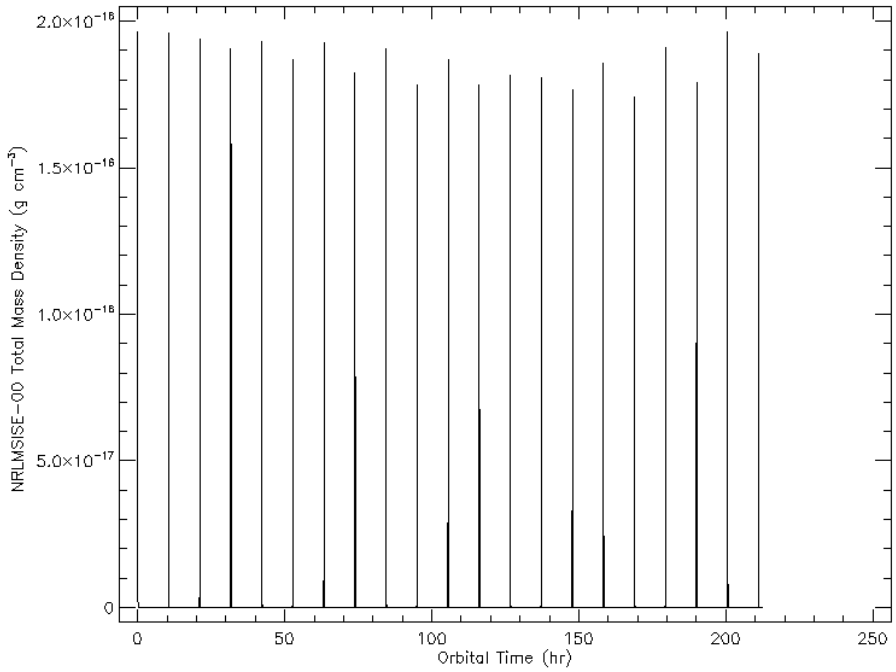

Figure 2.3: Total mass density as a function of time for 20 orbits.

It can be observed that each time the CubeSat would go back to the perigee, the total mass density reaches a maximum of about $2.0 \cdot 10^{-16}\, g \cdot cm^{-3}$. Once the perigee is passed, the total mass density will decrease before reaching the apogee. This plot demonstrates that the amount of atmospheric gas the spacecraft will receive is way larger at low altitudes.

Figure 2.4 below zooms in on the LEO region (between 200 and 2000 km) where the CubeSat is affected the most by the neutral environment. The maximum amount of atmospheric drag that the CubeSat will endure is reached for altitudes below 500 km.

It is an important information to keep in mind for the rest of the analyses performed in this thesis, especially for one scientific payload that will be implemented in the satellite (see section 2.6.3 for more details).

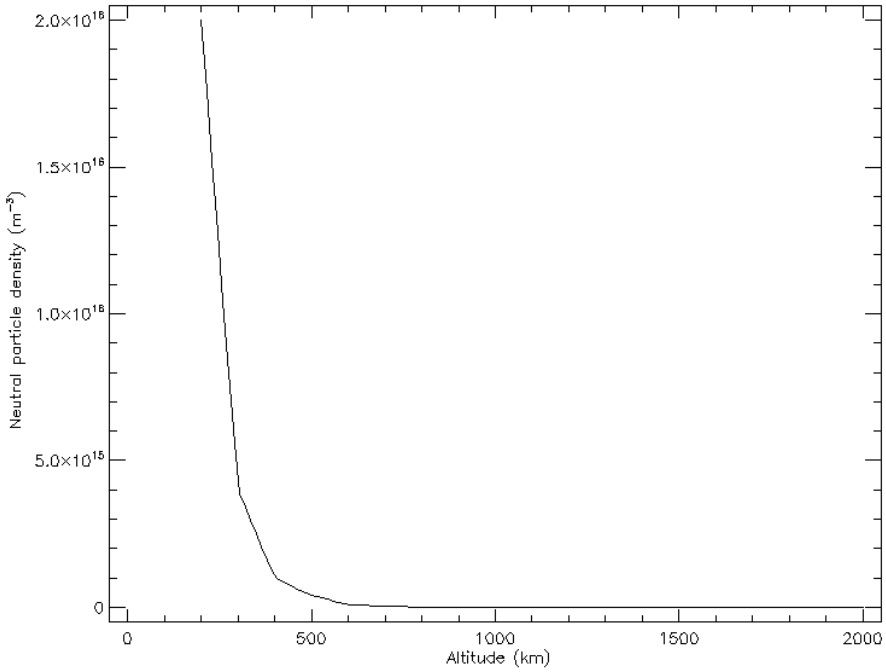

Figure 2.4: Total neutral particle density density as a function of the altitude in LEO.

2.2.2 Plasma environment

The chosen mission design requires the CubeSat to pass the ionosphere, plasmasphere and plasmapause. Those three regions differ in their electron density and thus have different effects on the satellite. The ionosphere is the transition layer between the relatively unionized region of the atmosphere and the fully ionized plasmasphere. It ranges from 60 km to 1000 km of altitude. The plasmasphere consists of hydrogen ions and electrons and is defined by a electron density of $10^{10}\ m^{-3}$ to $10^{11}\ m^{-3}$. Between four and seven Earth radii, the plasmasphere reaches the plasmapause, where the electron density drops to a value of $10^{5}\ m^{-3}$ to $10^{6}\ m^{-3}$. The electron density is non-constant as it strongly depends on solar activity, day/night cycle and leads to a charging of the CubeSat, which may harm its electronic components. [8]

2.2.3 Radiation environment

Electromagnetic and corpuscular environment delineate the radiation environment that the satellite will have to go through. The electromagnetic radiation environment describes the radiation emitted from the Earth, EMI emitted from the spacecraft, electromagnetic waves emitted by the plasma and ambient solar photon flux. On the other hand, the corpuscular radiation environment describes the ambient flux of particles (neutrons, electrons, protons and heavy ions).

One big parameter to take in account is the fact that the CubeSat will fly through the Van Allen radiation belts. The Van Allen radiation belts are divided in two, one inner belt and one outer belt. Depending in which orbital zone the CubeSat will be, different impacts will occur. The two belts are filled with energetic charged particles, and clutched together by the Earth's magnetic field. These particles are composed by the flux of cosmic rays or solar wind particles which are bombarding the Earth's atmosphere. They collide with molecules in the atmosphere and create high-energy particles, which then becomes concentrated into two belts. [9]

The inner belt ranges from 1000 to to 6000 km. Thus, it will have more impact on the satellite when this one will be in the LEO orbital region. High energy protons ($> 100\ MeV$) and high energy electrons ($1 - 10\ MeV$) are present in this location of the Van Allen Belts. The outer belt ranges from 13000 to 60000 km. Thus, it will have more impact on the satellite when this one will be in the MEO orbital region. This region is mainly composed of high energy electrons ($0.1 - 10\ MeV$). [10]

Radiation will rise when passing trough the inner and outer belts. It is, therefore, important to run simulations in order to determine the amount of shielding the spacecraft will need to protect its critical components for the Attitude and Orbit Control System.

SPENVIS has been used to simulate the proton and electron fluxes at different energies, based on the AP-8 and AE-8 models. This is not a full simulation of the radiation environment (see section 4.6 for the full simulation in STK), and one cannot conclude on the shielding thickness needed with the numbers obtained. Still, they give an overview of the environment and what to expect when planning a mission at GTO altitudes.

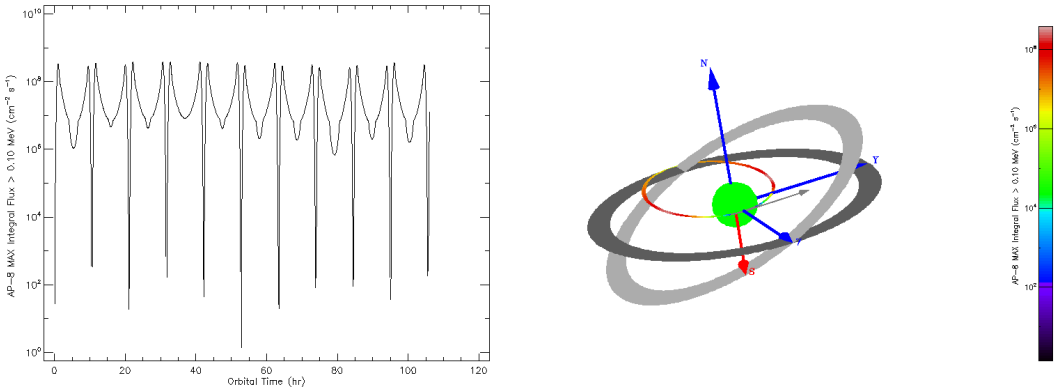

(a) Trapped proton flux as a function of time for 10 orbits.

(b) 3D view of the trapped proton flux.

Figure 2.5: Proton integral flux greater that 0.1 MeV as a function of time (10 orbits) and in a 3D view.

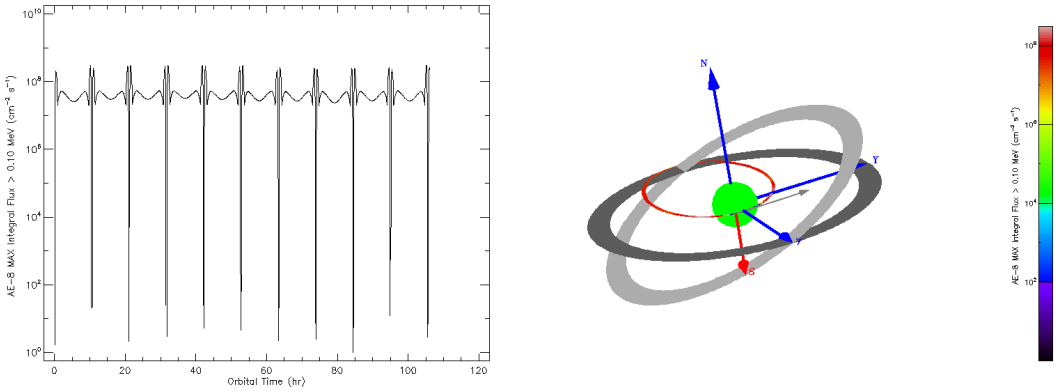

(a) Trapped electron flux as a function of time for 10 orbits.

(b) 3D view of the trapped electron flux.

Figure 2.6: Electron integral flux greater that 0.1 MeV as a function of time (10 orbits) and in a 3D view.

Figures 2.5 and 2.6 show that for a big amount of time during the mission (approximately eight hours per orbit), the spacecraft will be affected by a constant flux of 0.1 MeV protons and electrons, with a maximum of about $\sim 10\, cm^{-2} \cdot s^{-1}$. The only time when this flux will lower a bit is when approaching the perigee (LEO orbital region).

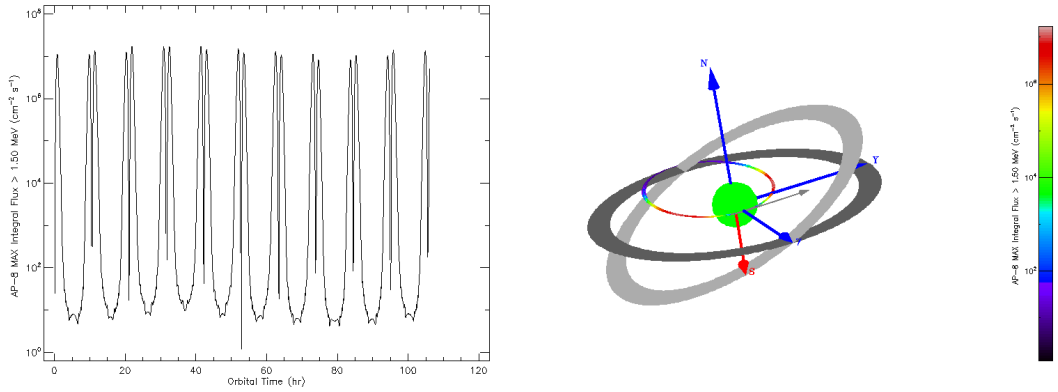

(a) Trapped proton flux as a function of time for 10 orbits.

(b) 3D view of the trapped proton flux.

Figure 2.7: Proton integral flux greater that 1.5 MeV as a function of time (10 orbits) and in a 3D view.

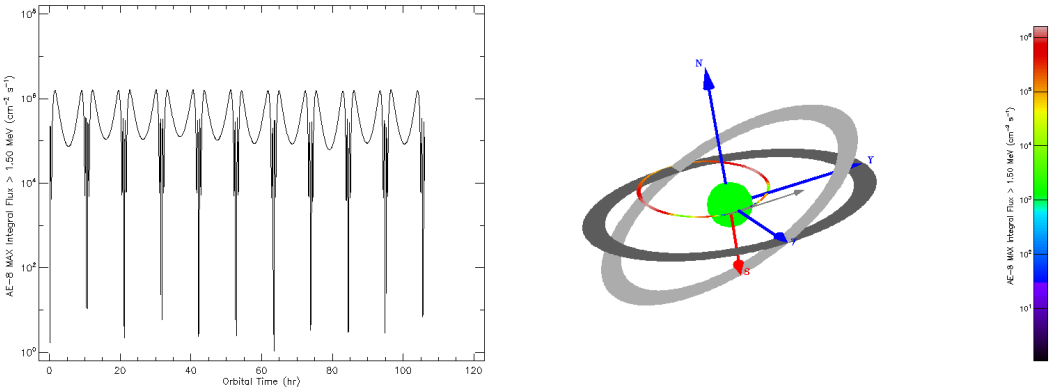

(a) Trapped electron flux as a function of time for 10 orbits.

(b) 3D view of the trapped electron flux.

Figure 2.8: Electron integral flux greater that 1.5 MeV as a function of time (10 orbits) and in a 3D view.

Figures 2.7 and 2.8 show the same phenomena but for a proton and electron flux of 1.5 MeV. Here, the proton flux is not constant at all and increase sharply when the spacecraft is entering the LEO orbital region and, therefore, approaching the perigee. The maximum proton flux that the spacecraft will receive will be approximately $\sim 10^7\ cm^{-2} \cdot s^{-1}$. On the other hand, the electron flux will stay rather constant, with an average value of about $\sim 10^6\ cm^{-2} \cdot s^{-1}$.

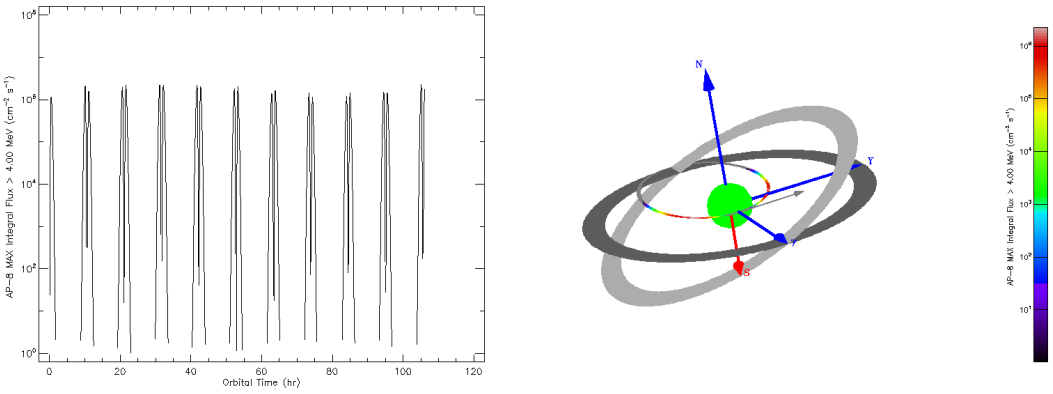

(a) Trapped proton flux as a function of time for 10 orbits.

(b) 3D view of the trapped proton flux.

Figure 2.9: Proton integral flux greater that 4.0 MeV as a function of time (10 orbits) and in a 3D view.

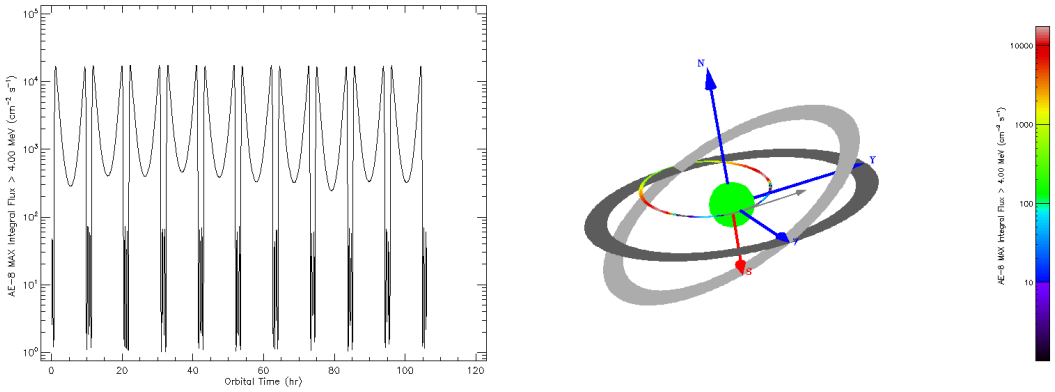

(a) Trapped electron flux as a function of time for 10 orbits.

(b) 3D view of the trapped electron flux.

Figure 2.10: Electron integral flux greater that 4.0 MeV as a function of time (10 orbits) and in a 3D view.

Figures 2.9 and 2.10 show that for high energy proton flux ($> 4\,MeV$), the CubeSat will be affected mainly in the LEO orbital region where this one will encounter the spacecraft only when it approaches the perigee (peaks of about $\sim 10^6\,cm^{-2} \cdot s^{-1}$). The electron flux will be a bit more constant, with a drop of the flux when the spacecraft goes from the inner belt to the outer belt (peaks of about $\sim 10^4\,cm^{-2} \cdot s^{-1}$). To summarize, it seems to be that the inner belt will have a greater effect in terms of high fluxes but as the spacecraft will stay for a longer time around the apogee, it can't be neglected, on the contrary.

2.3 Application of GTO

This type of orbit is usually used to transfer any kind of spacecraft or satellite to GEO. The launch site influences on the inclination of the GTO, it is usually preferred to have it near the equator. It is so far the most energy efficient way to inject communication satellites for instance to the targeted GEO. Nonetheless, it is needed to take into consideration the amount of time such a transfer takes (regardless of the efficiency) when designing the on-board components of the satellite. As seen in the previous section, the CubeSat will be exposed for quite a time to radiation making missions to GTO unsuitable for long periods and too massive (in terms of money especially) satellites. [11]

2.4 CubeSats and missions to GTO

2.4.1 CubeSats

CubeSats fall in the category of nanosatellites (see table 2.5). It is a class of satellite that uses a specific and standardized size of $10\,cm \times 10\,cm \times 10\,cm$ known as 1U. The size of such satellites can be augmented into 2U, 3U, 6U or even 12U for instance (1U, 6U and 12U being the most common as seen in figure 2.11). [12]

Category	Mass
Minisatellite	$100 - 180\ kg$
Microsatellite	$10 - 100\ kg$
Nanosatellite	$1 - 10\ kg$
Picosatellite	$0.01 - 1\ kg$
Femtosatellite	$0.001 - 0.01\ kg$

Table 2.5: Categories of SmallSats. [13]

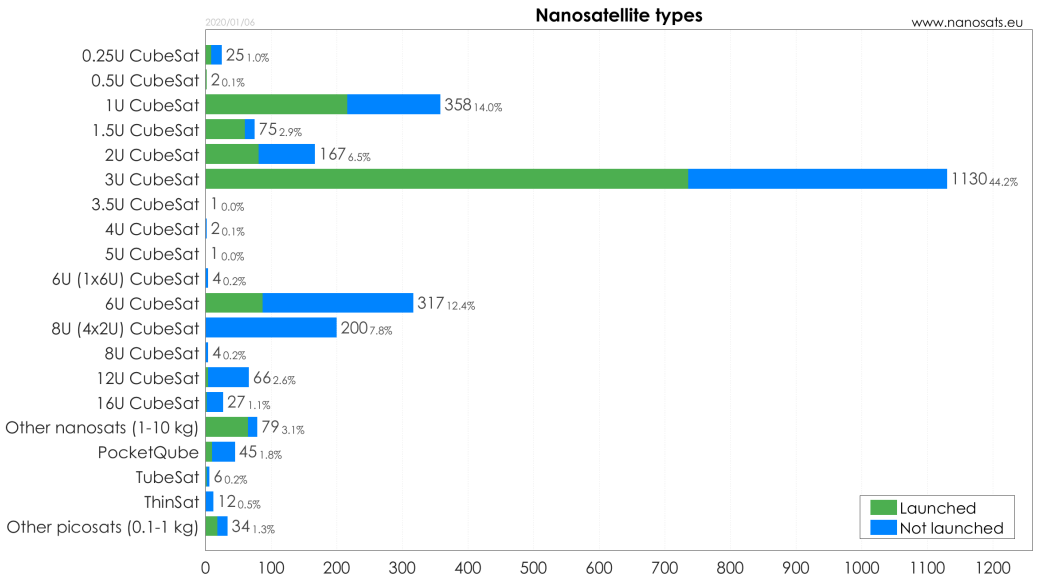

Figure 2.11: Number of CubeSats launched/planned on being launched according to their size. [14]

Ever since the fist CubeSat was developped (in 1999 by California Polytechnic State University at San Luis Obispo and Stanford University [12]), the development never stopped increasing to become an entire industry of its own adulated by universities, companies and governments for being an education platform and a useful tool for space exploration. CubeSats provide a low deployment cost and the possibility of being launched in constellation. In addition to that, the risk is minimized as the cost of a mission is much lower than it would be with a larger satellite and COTS components are available. [15]

Another argument for the popularity of CubeSats in the space industry can be seen in the figure 2.12. Ever since the first launch in 2003, the number of missions have never stopped growing drastically and reached 1027 as of 2019 (including launch failures). [14] An interesting statistic is the number of nanosatellites using propulsion modules. A small amount of about 60 nanosatellites are using such a technology and it could be interesting to focus on those missions as the thesis will talk about the feasibility of using thrusters as a mean for attitude control.

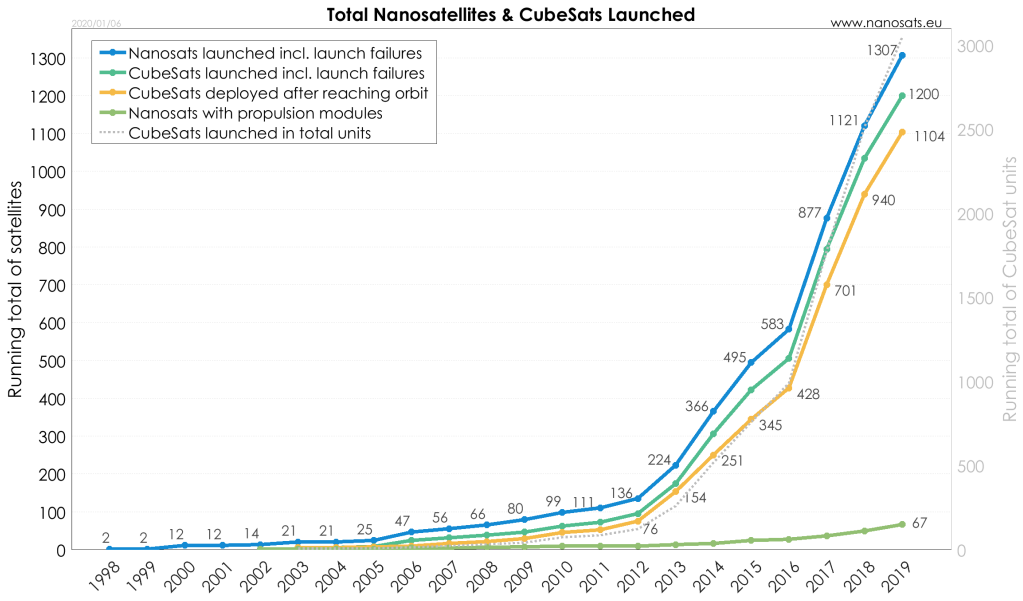

Figure 2.12: Number of CubeSats (in yellow) and nanosatellites (in blue) launched since 1998. [14]

2.4.2 Missions to GTO

Figure 2.13 outlines that no missions have been designed yet to accommodate a nanosatellite in GTO. Most of the missions are being designed to be in LEO except two that will flyby Mars and go to deep space. Even though those last ones are not directly similar to the mission studied in this thesis, they share some elements and will, therefore, be studied in this section.

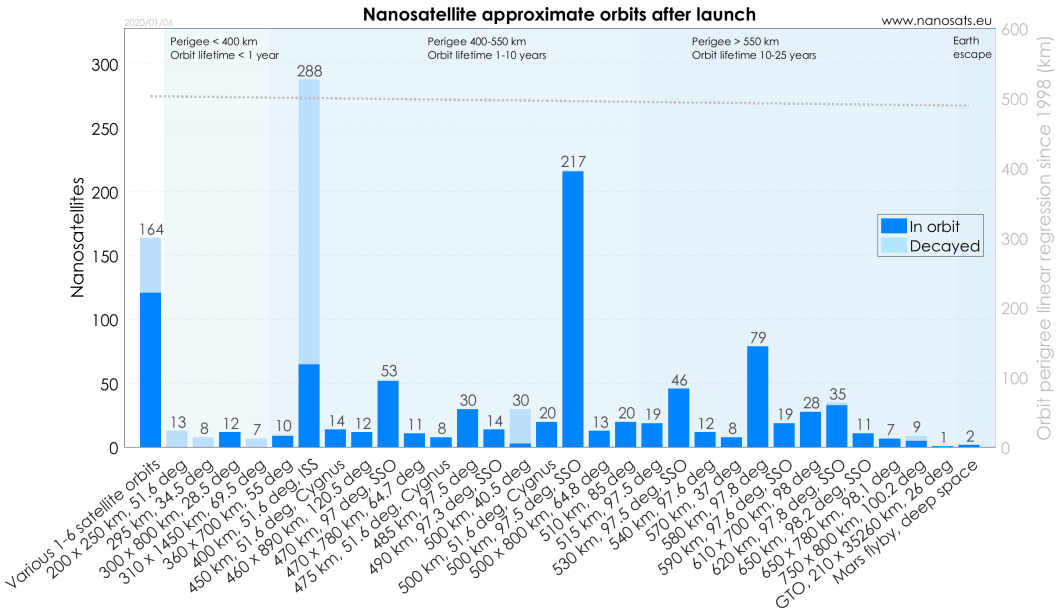

Figure 2.13: Altitudes of numerous nanosatellites lauched in the past few years. [14]

Because of the trend that can be seen in figure 2.13, designing a mission to GTO is particularly challenging as flight heritages are limited, implying that new ways of determining and controlling the attitude need to be found.

MarCO

MarCO consists of two 6U CubeSats, MarCO-A and MarCO-B, flying separately to Mars. It is the first mission involving CubeSats going to deep space and to another planet. Two identical CubeSats are launched for redundancy purposes.

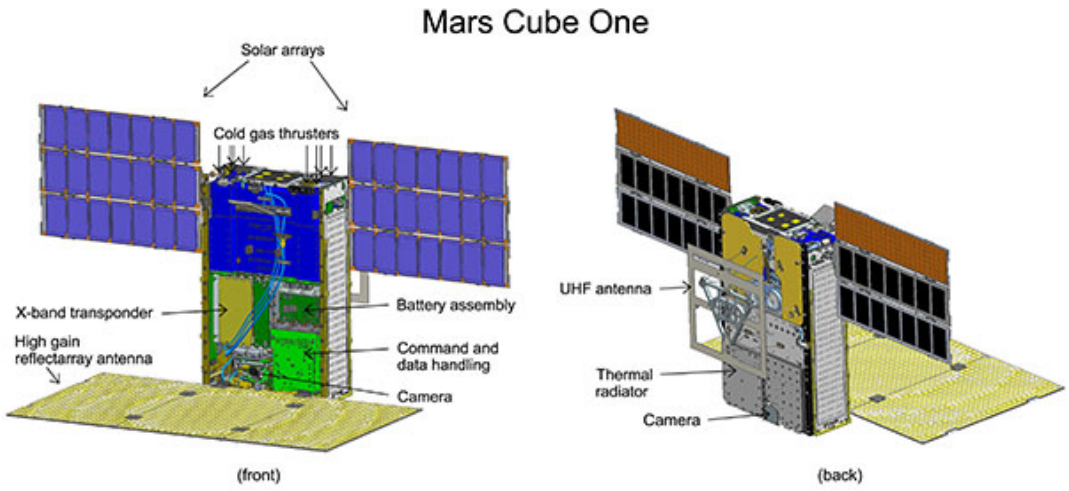

Figure 2.14: Illustration of one MarCO CubeSat with antennas and solar arrays deployed. [16]

The AOCS of each CubeSats consist of a star stracker, sun sensors, gyroscopes, cold gas thrusters and three-axis reaction wheels. The propulsion system operates so that four thrusters are used for attitude control (desaturating the reaction wheels) and four thrusters are used for correcting the trajectory. Added together, the propulsion system consists of eight thrusters capable of releasing a compressed R236FA gas in different directions. [16] Using a propulsion based AOCS is an obligation for this mission as usual actuators such as magnetorquers cannot be used because of the lack of magnetic field in deep space.

SpectroCube

SpectroCube by the European Space Agency is a 6U CubeSat built for astrochemistry and astrobiology research beyond LEO. The nanosatellite would weigh around 12 kg with the scientific payload occupying a minimum of one third of the volume while the remaining space is reserved for the subsystems (power, propulsion, attitude control, communication and on-board computer).

The CubeSat is designed to be launched with an altitude above 2000 km and three potential orbits are being studied: GTO (baseline configuration), super-GTO, and Molniya. The latest information makes this mission very interesting to compare with the one dealt in this thesis.

Looking at the AOCS, SpectroCube will use four reaction wheels for attitude control, three magnetorquers to desaturate the reaction wheels and sun sensors for pointing accuracy. The propulsion system is only used to raise or lower the orbit and will operate with cold gas. [17]

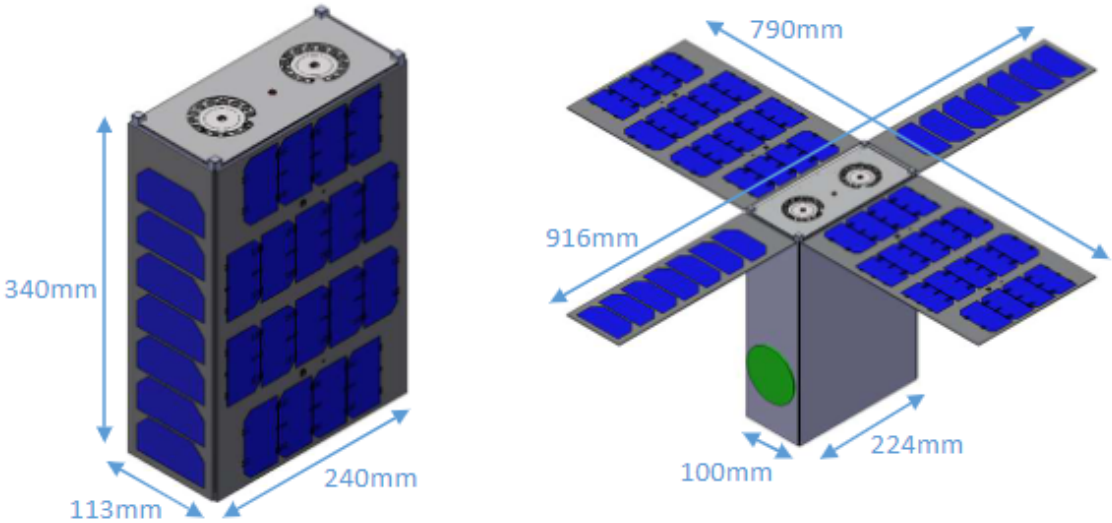

Figure 2.15: SpectroCube baseline design. [17]

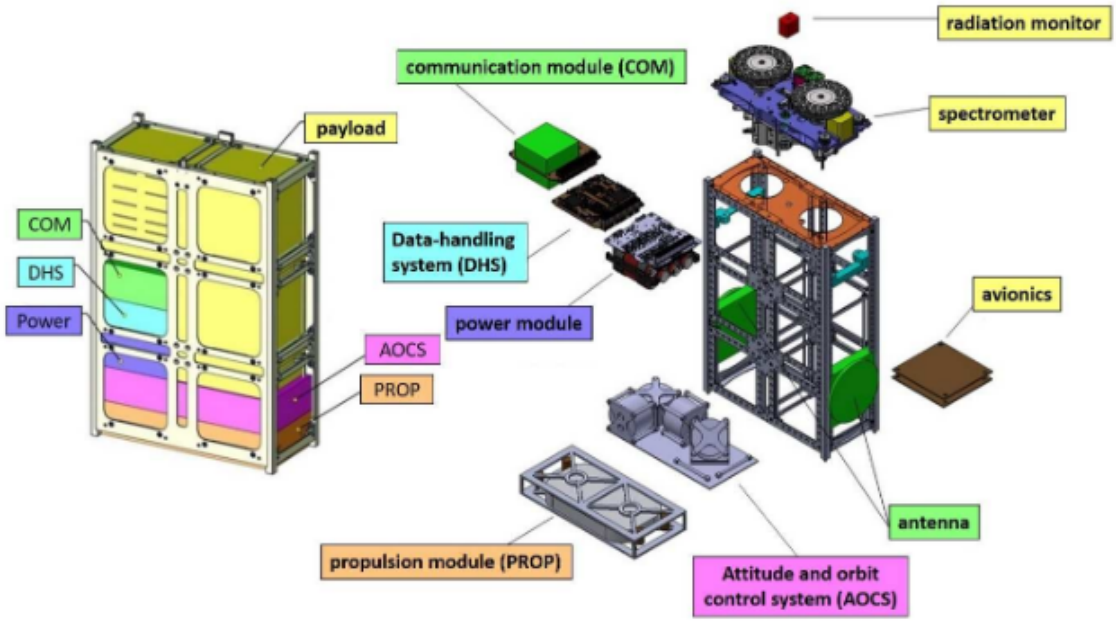

Figure 2.16: Configuration and placement of the subsystems inside SpectroCube. [17]

GTOSat

GTOSat by the National Aeronautics and Space Administration is a 6U CubeSat designed to study the dynamics of outer belt electrons and supposed to be launched in early 2021.

This mission seems to host similar instruments as FORESAIL-2 making it very interesting to study especially for the sensors and actuators used for the AOCS. [18] The nanosatellite will be built on the Dellingr-X platform to assure that it will be able to withstand the environment more destructive than in typical orbits. Using this platform and for the need of the payloads, NASA wants to achieve a pointing accuracy fewer than 1° and a pointing determination of 18 *arcsec*. [19] This information is very important to know because looking at the section 2.6.3, it can be seen that FORESAIL-2 shares a pointing accuracy very similar to the one of Dellingr-X platform. Furthermore, as for the mission studied in this thesis, the use of a magnetometer on GTOSat requires the implementation of an extendable boom. The Electro-Magnetic Interferences emitted by this instrument would in fact cause troubles for the on-board electronics. A consequence is the placement of the magnetometer outside of the CubeSat frame.

The AOCS consists of a reaction wheel system combined with magnetorquers for stability and momentum dumping. The sensors should be multiple fine and coarse sun sensors for pointing, and an Inertial Measurement Unit consisting of three accelerometers, three gyroscopes and depending on the heading requirement, three magnetometers. [20] Looking at figure 2.17, an overview of subsystems placement is displayed. The magnetorquers are used inside $L \sim 3$ for momentum dumping of reaction wheels. It is a critical data as including magnetorquers in the AOCS instead of propulsion based attitude control could reduce the price of the CubeSat unduly. In the same way, a potential size of 3U could be considered instead of the initial one of 6U.

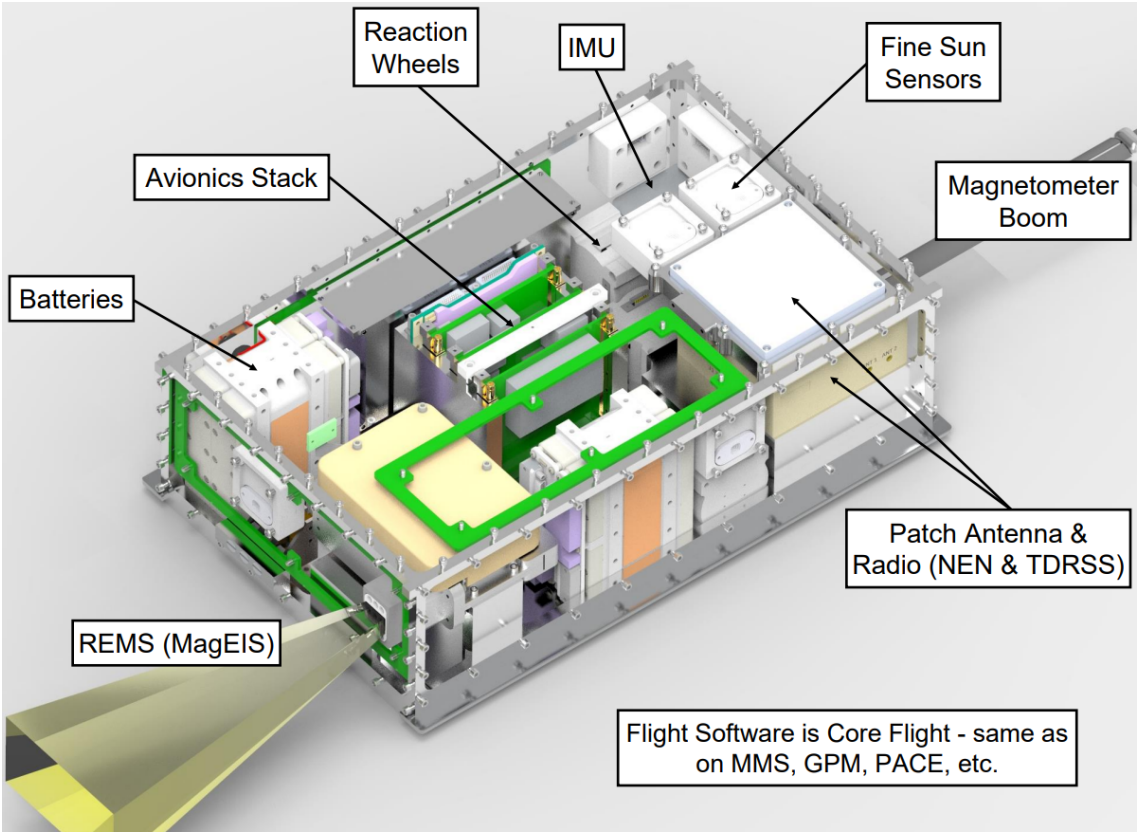

Figure 2.17: Observatory overview of GTOSat. [18]

To summarize, GTOSat is a low-cost ($4.35 M) 6U CubeSat designed to study electron dynamics in the outer radiation belts. It will carry two Van Allen Probe and flight-proven instruments and is, so far, the best heritage mission (even though still on going) that the FORESAIL-2 team can look at principally due to the fact that the size of the two CubeSats is the same (6U), the targeted orbit is the same (GTO) and the science objectives alongside with the payloads are analogous.

2.5 Heritage mission - FORESAIL-1

The FORESAIL-1 satellite, whose subsystems are currently being tested in Aalto university will serve as an heritage mission for FORESAIL-2. Both FORESAIL-1 and FORESAIL-2 are "*funded by the Finnish Academy of Science, the Finnish Centre of Excellence in Research of Sustainable Space encompasses three microsatellite missions for the investigation of a multitude of kinetic processes in near-Earth space, while deploying novel methods for propulsion and space debris reduction.*" [21]

FORESAIL-1 mission has two objectives consisting of measuring radiation belt losses alongside with demonstrating the feasibility of de-orbiting a CubeSat in LEO using plasma brake to manipulate the orbit at the end of the mission. It is a designed 3U CubeSat (see figure 2.18) holding two payloads: a particle telescope (PATE) and a plasma break.

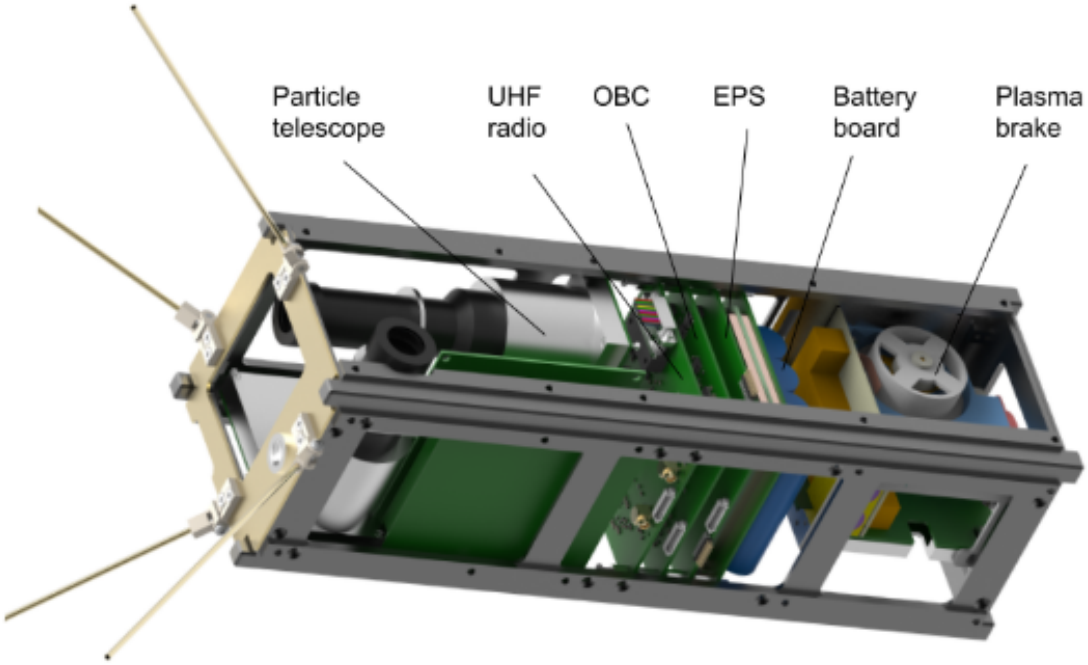

Figure 2.18: FS-1 3U CubeSat - satellite subsystem locations without shielding. [21]

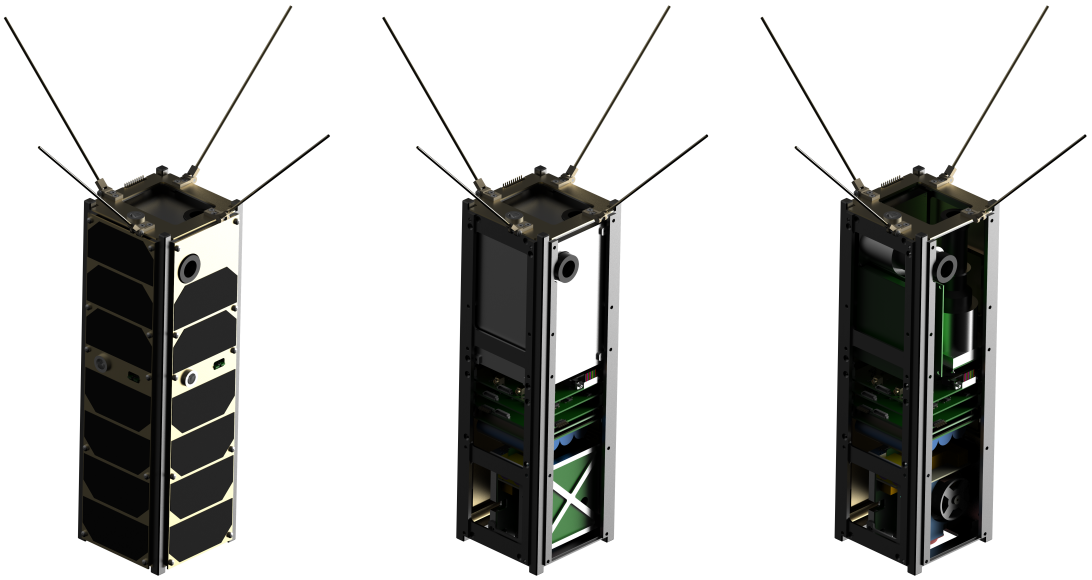

Figure 2.19: Renders for FORESAIL-1. [22]

Those instruments, even though different, are similar to the ones assigned for FS-2 (see section 2.6). Nonetheless, the same team is taking care of both FS-1 and FS-2 payloads which can help to estimate important data such as power budget, link budget and mass budget.

2.6 FORESAIL-2

2.6.1 Mission overview

The FORESAIL-2 mission is funded by the Academy of Finland, FORESAIL and must comply with the original proposal. FORESAIL-2 alongside with the entire FORESAIL project has the following objectives: maintain strong collaboration within the consortium, establish the Finnish Space Science Program, and raise awareness and provide solutions for space sustainability issues.

Space is becoming more and more a topic of interest for every institution in the world. As a result, a lot of missions have been launched ever since the space conquest started, ranging from sending men on the Moon to CubeSats designed by students as a project. The consequence is that the number of satellites increased and is increasing exponentially. The latest statement threatens the sustainable use of space, as without removal, space debris will make critical orbits unusable. Another central factor affecting spacecraft lifetime is the radiation environment, which is unpredictable due to an incomplete understanding of plasma dynamics. [23]

The mission statement goes as follow: "*FORESAIL-2 will build on the FORESAIL-1 results - measurements of radiation belt losses and demonstrate deorbiting in LEO. FORESAIL-2 will demonstrate a feasibility to utilize and characterize a nanosatellite and its instruments for scientific purposes in a high-radiation environment.*" [23]

2.6.2 Science and technology objectives

Ultra Low Frequency

What is the role of ULF waves in accelerating, transporting, and scattering of electrons in the Earth's radiation belts as a function of solar wind driving and magnetospheric activity?

- Quantify the role of ULF waves (Pc5 and EMIC) for the response of the radiation belt electrons over a wide range of energies and locations as a function of solar wind structures.
- Explore the impact of solar wind drivers and magnetospheric activity on the ULF Pc5 ($2\,mHz - 5\,Hz$) and EMIC ($0.1 - 5\,mHz$) wave properties.
- Integrate the data with measurements by the other spacecraft in the solar wind and magnetosphere, and from ground-based facilities to resolve whether waves are externally transferred or internally generated waves. Characterise the response of electrons.

How do ULF waves and turbulence transmit within the inner magnetosphere?

- Characterize how wave properties vary as waves travel within the inner magnetosphere.
- Characterize the spatial variation of wave properties in as large a range of L-shells and polar angles as possible.
- Characterize the temporal variations of the wave properties, as a function of solar wind driving conditions.

Coulomb Drag

How does the CD force depend on plasma parameters and tether voltage?

- Characterise the relationship between the CD force and plasma density in various plasma environments.
- Characterise the relationship between the CD force and the tether voltage.

2.6.3 Instruments

Relativistic Electron and Proton Experiment telescope

The REPE telescope is built to satisfy measurement requirements for the science goal regarding ULF waves. The detector consists of two stacked elements, a silicon and a scintillator. The silicon detector stack on the top would count particles in the energy range of $300 - 1000\,keV$ and the scintillator in the range of $1 - 8\,MeV$. It works in a scanning mode with the spin axis perpendicular to the magnetic field vector. [23]

Duty cycle per orbit	90 %
Total number of orbits	200 (ideally one year)
Data rate	Spin rate dependent $300\,bit \cdot s^{-1}$
Power consumption	$2.0\,W$

Table 2.6: Data products of the minimal science case for REPE.

Magnetometer

The magnetometer will contribute to satisfy measurement requirements for the science goal regarding ULF waves. In an ideal case, it would measure the magnetic field vector in a frequency range of $1\,mHz$ to $10\,Hz$ with the sampling between 10 and $100\,Hz$. It is needed to analyse if the need of a boom is necessary or not for the implementation of the magnetometer. A minimum orbital altitude range should be between two and five Earth radii while a maximum inclination of 45° (equatorial orbit) needs to be achieved. The attitude knowledge should be better than 1.5° for the ULF wave mode and position knowledge should be in the range of hundred of kilometers in order to interpret scientifically the data in post processing. [23]

Duty cycle per orbit	>2 Earth radii, some orbits can be skipped
Total number of orbits	200 (ideally one year)
Data rate	$100-200\,bit \cdot s^{-1}$ with one sensor
Power consumption	$0.6\,W$

Table 2.7: Data products of the minimal science case for the magnetometer.

CD experiment

The CD tether will be used both for drag measurements and as a scientific plasma instrument. It will contribute to the first two science objectives. The CD force will be estimated by measuring changes in spin rate while the plasma density will be characterised by measuring the tether current. A gold tether and an aluminium tether were both considered to accomplish the science objective. The aluminium tether has been chosen after a workshop with the science team designing the payloads. However, it is still of interest to write down the numbers calculated for the gold tether. Assuming a $300\,m$ long aluminium tether, the mass would be $3.3\,g$ with the tether tip mass being approximately $\sim 2.5\,g$. The equivalent phase angle difference would reach 1.6°. With a golden material, the tether would be $300\,m$ long, would weigh $26\,g$ and would introduce a difference in the phase angle of $\sim 0.4°$. The Attitude Determination System must be able to measure changes in the phase angle. [23]

Charge	$1\,kV$
Duty cycle per orbit	$100\,\%$
Total number of orbits	110 to estimate the plasma density > 20 to estimate the Coulomb drag force
Data rate	$15\,bit \cdot s^{-1}$
Power consumption	$0.6\,W$

Table 2.8: Data products of the minimal science case for the CD experiment.

3 Theoretical background

3.1 Spacecraft model

3.1.1 Definition of the axes

FORESAIL-2 is a typical 6U CubeSat with an extended boom to accommodate a magnetometer. A 3D model (see figure 3.1) was built in a CAD software and modified in Blender to give it the right dimensions and the correct axes definition. The advantage of using this model is that the extended boom is already implemented. It can come very handy when making further analysis on orbital decay, as the area exposed to the Sun will be more accurate than for a general 6U CubeSat model.

The requirements of the payloads set the definition of the axes. Some on-board instruments require to work with the magnetic field, thus, this vector needs to be normal to the one of the spin axis. Therefore, the spin axis Y always lies within the orbital plane and is perpendicular to the orbit normal vector. The Z-axis lies within the tether deployment vector and the X-axis is, by the right-hand rule, defined to be normal to the 3U face of the CubeSat.

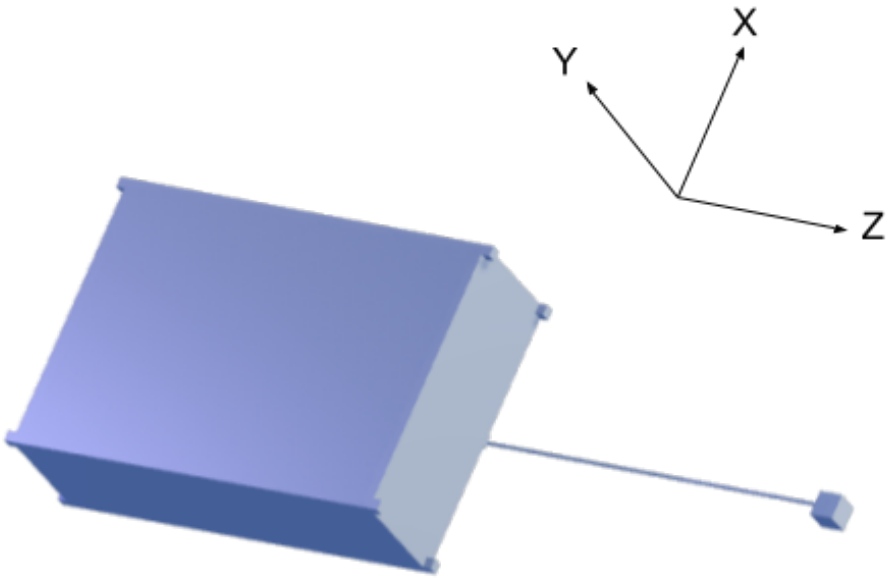

Figure 3.1: Reference frame of FORESAIL-2.

3.1.2 Moment of inertia

The moment of inertia of a body is measured in a certain direction, about a rotation axis, and trough a chosen point. It expresses the difficulty of producing an angular acceleration on the body about the rotation axis. As an example, one can take a body with a high moment of inertia that is rotating. It will be difficult to stop the rotation of the body. In other words, the body will resist infused angular acceleration. The moment of inertia plays the same role for rotational movements as the mass does for translational movements. [24]

The 6U CubeSat can be represented as a rectangular prism in order to calculate the inertia tensor points I_{xx}, I_{yy}, and I_{zz}. The chosen point for the calculation is set at the center of gravity of the satellite.

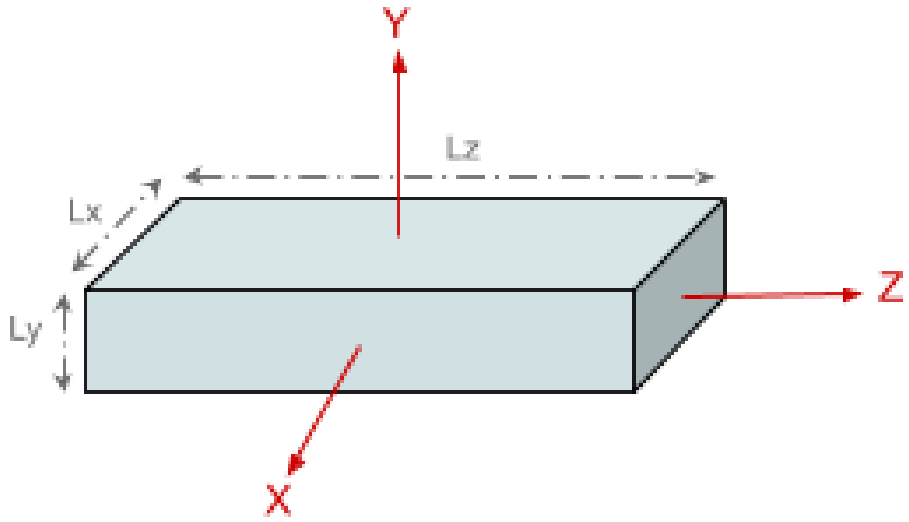

Figure 3.2: FORESAIL-2 CubeSat as a rectangular prism for moments of inertia.

The derivation for any of the axes is the same, so only the calculation for I_{zz} will be shown here. Using equation 3.1 below:

$$I_{zz} = \iiint_{\beta} \rho(x^2 + y^2)\, dxdydz \tag{3.1}$$

one can make the following derivation:

$$
\begin{aligned}
I_{zz} &= \int_{-\frac{L_z}{2}}^{\frac{L_z}{2}} \int_{-\frac{L_y}{2}}^{\frac{L_y}{2}} \int_{-\frac{L_x}{2}}^{\frac{L_x}{2}} \rho(x^2+y^2)\, dxdydz \\
I_{zz} &= \int_{-\frac{L_z}{2}}^{\frac{L_z}{2}} \int_{-\frac{L_y}{2}}^{\frac{L_y}{2}} \left[\rho\left(\frac{1}{3}x^3+y^2x\right)\right]_{x=-\frac{L_x}{2}}^{x=\frac{L_x}{2}} dydz \\
I_{zz} &= \int_{-\frac{L_z}{2}}^{\frac{L_z}{2}} \int_{-\frac{L_y}{2}}^{\frac{L_y}{2}} \rho\left(\frac{1}{12}L_x^3+y^2L_x\right) dydz \\
I_{zz} &= \int_{-\frac{L_z}{2}}^{\frac{L_z}{2}} \left[\rho\left(\frac{1}{12}L_x^3y+\frac{1}{3}y^3L_x\right)\right]_{y=-\frac{L_y}{2}}^{y=\frac{L_y}{2}} dz \\
I_{zz} &= \int_{-\frac{L_z}{2}}^{\frac{L_z}{2}} \rho\left(\frac{1}{12}L_x^3L_y+\frac{1}{12}L_xL_y^3\right) dz \\
I_{zz} &= \left[\rho L_xL_y\frac{1}{12}\left(L_x^2+L_y^2\right)z\right]_{z=-\frac{L_z}{2}}^{z=\frac{L_z}{2}} \\
I_{zz} &= \rho L_xL_yL_z\frac{1}{12}\left(L_x^2+L_y^3\right)
\end{aligned}
$$

The mass of the rectangular prism can be written as $m_s = \rho L_x L_y L_z$. Therefore, one can write the moment of inertia I_{zz} as:

$$I_{zz} = \frac{1}{12}m_s\left(L_x^2+L_y^2\right) \tag{3.2}$$

By identification, the moments of inertia I_{xx} and I_{yy} are:

$$I_{xx} = \frac{1}{12}m_s\left(L_y^2+L_z^2\right) \tag{3.3}$$

$$I_{yy} = \frac{1}{12}m_s\left(L_x^2+L_z^2\right) \tag{3.4}$$

Taking the usual dimensions of $10\,cm \times 20\,cm \times 30\,cm$ for a 6U CubeSat and a maximum mass $m_s = 7\,kg$, the moments of inertia of FORESAIL-2 are $I_{xx} = 0.076\,kg\cdot m^2$, $I_{yy} = 0.058\,kg\cdot m^2$, and $I_{xx} = 0.029\,kg\cdot m^2$.

3.2 AOCS design

When designing the AOCS, one needs to take into account internal and external disturbances. Generally, more surveillance is accorded to external disturbances as they disturb continuously the angular momentum of the satellite. External disturbances usually come from four different phenomena: solar radiation pressure (acts above 700 km but is dependant on the solar activity), aerodynamic drag torque (usually under 500 km), gravity gradient torque (500 km - 35000 km), and residual magnetic dipole torque (500 km - 35000 km). A thrust misalignment in case propulsion units are used can also be the cause of disturbances acting on the spacecraft, at any

heights. [25] Internal disturbances, that do not change the angular momentum of the system, can come from fuel movement, mechanisms, general mass movement, or flexible appendages. This section, will focus primarily on the external ones as they rule the design of crucial parts of the AOCS subsystem.

3.2.1 External disturbances

Before a satellite decays, the attitude of the latter gets continually disturbed by different forces, called disturbance torques. These forces need to be taken into account when designing the AOCS, to make sure the spacecraft operates as it should. This section will discuss how to calculate these external disturbances, and estimate their magnitude over the CubeSat (worst case values). [25]

Solar radiation pressure

It comes from the mechanical pressure imposed from the photons. A torque can result from the difference between the pressure center and the center of mass. [26]

$$T_s = \frac{\Phi}{c} A_s \left(1+q\right) \left(c_{ps} - c_m\right) cos\left(\varphi\right) \tag{3.5}$$

The reflectance factor is not constant, but assuming it is, a fist order approximation can be done and $q = 0.6$. The worst case happens when the sun incidence angle is normal to the surface of the satellite, that is $\varphi = 0°$. The center of mass is assumed to be located in the center of the satellite, and the solar radiation pressure center acts along the biggest face of the CubeSat. Using equation 3.5, one can estimate the torque generated by the solar radiation pressure:

$$T_s = \frac{1366}{299792458} \cdot (0.2 \cdot 0.3) \cdot (1+0.6) \cdot (0.15-0) \cdot \cos(0) = 6.561 \cdot 10^{-8}\ Nm$$

Aerodynamic drag torque

It comes from the air pressure present in LEO. [26]

$$T_a = \frac{1}{2} C_d A_r v^2 \left(c_{P_a - c_m}\right) \rho \tag{3.6}$$

Because of the eccentricity of the orbit chosen for the mission, it is rather difficult to obtain an accurate number for the aerodynamic drag torque. Many assumptions need to be made in order to estimate, including a high error margin, the resulting torque. The atmospheric density at $300\ km$ is taken as a baseline, that is $\rho = 4.840 \cdot 10^{-11}\ kg \cdot m^3$. At this altitude, the velocity of a satellite in a circular orbit is $v = 7800\ m \cdot s^{-1}$. Using 2.5 as the drag coefficient and using equation 3.6, one can calculate the aerodynamic drag torque:

$$T_a = \frac{1}{2} \cdot 2.5 \cdot (0.2 \cdot 0.3) \cdot 7800^2 \cdot (0.15-0) \cdot 4.840 \cdot 10^{-11} = 3.313 \cdot 10^{-5}\ Nm$$

The estimated number seems too high for the planned GTO orbit. Indeed, this is due to the fact that the satellite does not stay in a circular orbit at 300 km altitude. As a matter of fact, it can be estimated that the CubeSat remains in the LEO region for about 18 % of the orbital period. Taking this information in account, the resulting torque converges to a lower value of $5.963 \cdot 10^{-6}\ Nm$. Precise calculation is very difficult. In addition to that, the atmospheric density varies substantially between day and night.

Gravity gradient torque

It comes from the difference between the center of gravity and the center of mass. There exists a difference since the gravity field is not uniform. [26]

$$T_g = \frac{3\mu}{2R^3}|I_z - I_y| sin\,(2\theta) \tag{3.7}$$

Again, the eccentricity of the orbit makes it complicated to estimate a good value. Because of the time spent in MEO and GEO, a solution can be to take the average value for the distance from the center of Earth, that is 24414 km. Using the moments of inertia calculated in a previous section for a 6U CubeSat, and an attitude control accuracy of 2°, the gravity gradient torque can be calculated:

$$T_g = \frac{3 \cdot 3.98600441 \cdot 10^{14}}{2 \cdot (24414 \cdot 10^3)^3} \cdot |0.029 - 0.058| \cdot sin\,(2 \cdot 0.035) = 8.312 \cdot 10^{-11}\ Nm$$

Residual magnetic dipole torque

The residual magnetism of the spacecraft results in a torque from the Earth's magnetic field. [26]

$$T_m = DB = D\left(\frac{M}{R^3}\lambda\right) \tag{3.8}$$

The residual dipole moment of a satellite can be obtained only while testing it. The problem here is that the CubeSat is still in the mission design phase, thus making it impossible to obtain an accurate value. A way to estimate a value for a 6U CubeSat is to have a look at similar satellites that have already been tested. Typical values range from 0.2 to 20 $A \cdot m^2$. Nonetheless, those values concern spacecraft with dimensions superior to nanosatellites. According to [27] and [28], a value of 0.2 $A \cdot m^2$ seems to be a safe guess for a 6U CubeSat. The unit-less function of magnetic latitude is 1 at magnetic equator, and the average value of 24414 km for the distance from the center of Earth is chosen. Thus, one can calculate the residual magnetic dipole torque:

$$T_m = 0.2 \cdot \frac{7.800 \cdot 10^{15}}{(24414 \cdot 10^3)^3} = 1.072 \cdot 10^{-7}\ Nm$$

Total magnitude of external disturbances

The estimated values obtained for each external disturbance have been calculated assuming the worst case scenario, but also keeping some realism. It is more complicated to obtain accurate values for a GTO orbit than a typical circular orbit in LEO. Still, the different torques can give an idea of the impacted magnitude the satellite will be subject to, and how powerful the selected actuator for attitude control will need to be. Table 3.1 summarizes the magnitude of all external disturbances and displays the total perturbation torque.

External disturbance	**Magnitude** $(\boldsymbol{Nm})$
Solar radiation pressure	$6.561 \cdot 10^{-8}$
Aerodynamic drag torque	$5.963 \cdot 10^{-6}$
Gravity gradient torque	$8.312 \cdot 10^{-11}$
Residual magnetic dipole torque	$1.072 \cdot 10^{-7}$
Total	$\mathbf{6.136 \cdot 10^{-6}}$

Table 3.1: Summary of external disturbances with their worst case magnitude.

3.3 Sensors

3.3.1 Sun sensors

The Sun can be used as a good attitude reference for satellites when they are orbiting Earth because of its high luminosity and small apparent size. Sun sensors consist of detectors (visible light or infrared) which measure one or several angles between the location where they are mounted and the incident sunlight. Nonetheless, ambiguity can appear in the measurements (see figure 3.3) since the incoming sunlight may lie anywhere along the mantle of a cone. [29]

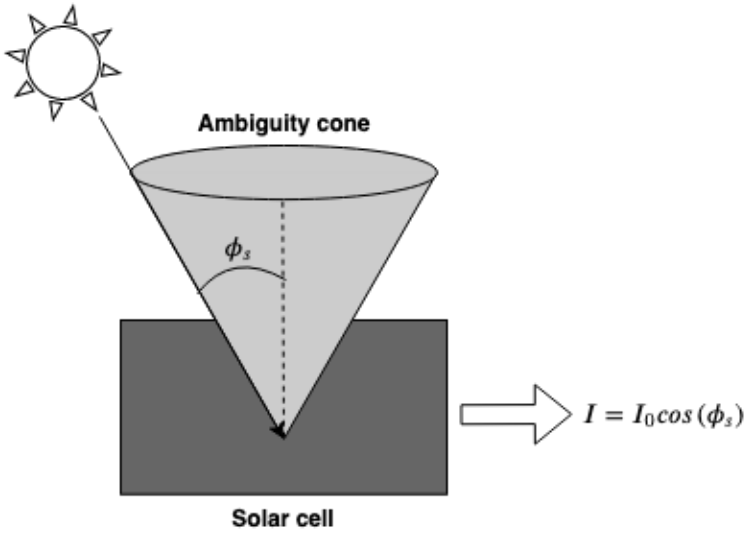

Figure 3.3: Incoming sunlight along the mantle of ambiguity cone. [29]

Sun sensors can be divided into three categories: the analog Sun sensor, the digital Sun sensor, and the Sun presence detector. The analog Sun sensors represents the most basic form of the technology where an electric signal is produced by a solar cell when this one one is being triggered (illuminated) by the Sun. The output current depends on the solar incidence angle ϕ_s according to the cosine rule. [26]

3.3.2 Earth sensors

To determine the orientation of a spacecraft, the Earth can be taken as a reference direction. An Earth sensor will scan the sky looking for the Earth's horizon. The latter is detected when a radiance having an uniform energy distribution is found. The Infrared region is generally used. As seen on figure 3.4, the sensor is composed of a signal processing unit alongside with an optical system detector. [26]

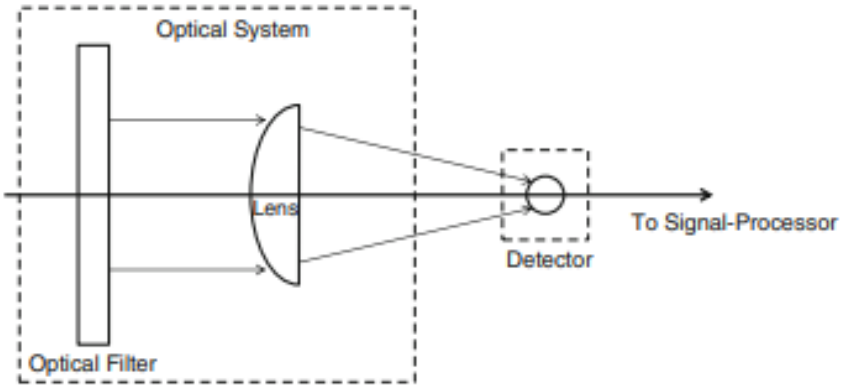

Figure 3.4: Component of an Earth sensor. [26]

Depending on the detector used, the sensitivity, and thus the accuracy of the Earth sensor will vary. Different types of detectors exist (thermopile, photodiode), but a bolomoter is the most common one. Earth sensors are typically used for body-stabilized satellites and provide an interesting solution since a completely autonomous Earth pointing system can be obtained. Nevertheless, such sensors are becoming less and less common (even among geostationary satellites) as the Earth's limb has a poor definition, making the potential accuracy to be limited to degree level. [25]

3.3.3 Star trackers

When using a star tracker, the attitude is determined relative to the inertial space. The technology consists of a digital camera alongside with a computer containing a catalogue (Hipparcos, Bright Star Catalog) of the most significant stars in the sky (about 10000). It works so that a picture is taken by the digital camera and then processed to identify and match stars with the catalogue. The Field of View and the star catalogue are selected to provide a unique determination of the attitude in the full sphere of the sky. A star tracker is the most accurate sensor compared to Sun sensors or Earth sensors, with a typical accuracy of 20 $arcsec$ or less. Two cameras can be mounted in a perpendicular system to improve the precision even more. [26]

The sensor is built (see figure 3.5 to have an example) in a way such that a baffle suppresses incoming information that could potentially affect the attitude determination (stray-light from the Sun, its reflections on the spacecraft, or light from the Earth limb). [29]

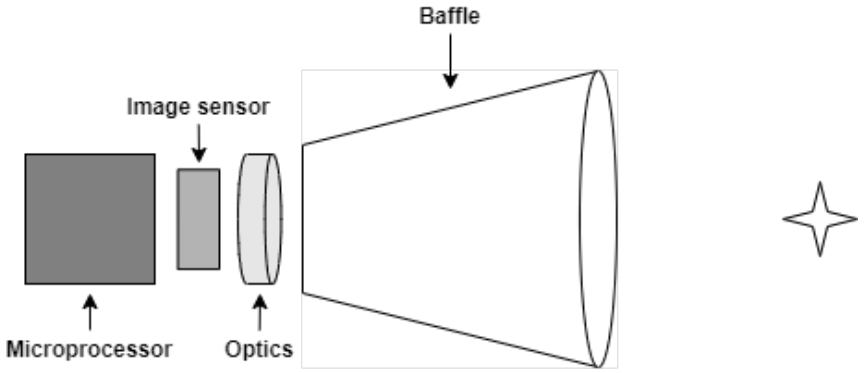

Figure 3.5: Basic star tracker schematic.

On the other hand, star trackers are more complex than the usual Sun or Earth sensors. They also are expensive, and involve numerous satellite system aspects such as mechanical and thermal stability, computers and data handling, software and others.

3.3.4 Gyros

Spinning gyros belong to the most established and well known sensors used on satellites. They measure the angular rates (or integrated angular rate) of a spacecraft without the need of knowing an absolute reference or any other information. For this reason, they are typically used when the designed mission requires to control the angular rate and position of a satellite. [26]

There are different technologies that exist. Ring Laser Gyros and Fibre Optic Gyros provide high precision measurements alongside with very low noise and high bias stability. Typically, they are used when high performances are required, to improve the attitude determination. On the other hand, MEMS technologies, Vibrating Structure Gyros, Hemispherical Resonator Gyroscopes provide low to medium precision measurements. They can support the attitude determination of a star tracker in case of temporary attitude measurement outages, or are being used for Safe Mode and detumbling. [25]

When integrating the noise and bias sources, the position being tracked can differ from the reality. That is why including accelerometers with three-axis gyro measurements (called an IMU) allows authentic measurements of the spacecraft's orientation and position.

3.3.5 Magnetometers

Magnetometers provide measurements of the Earth's magnetic field and are very common on-board satellites, especially in the LEO region.

Combined with a known orbit position, the attitude of spacecraft can be determined. [30] Magnetometers present several advantages compared to other sensors, making them to be an indispensable choice in almost all missions. Indeed, they are light, small and fairly inexpensive.

Nevertheless, because the Earth's magnetic field has many disturbances and does not act the same depending of the region where the satellite is at, magnetometers are generally used in combination with other sensors. Besides, they must be mounted and set up in an area free of noise, at the end of an extended boom for example.

3.3.6 GNSS/GPS

Global Navigation Satellite System and Global Positioning System signals are used for orbit determination and navigation. Antennas as a set connected to a GPS receiver facing the GNSS constellations in MEO allow to derive the attitude of a satellite by using the difference in phase between this same set of antennas. [26]

3.3.7 DPS

Deep Space Positioning System is a device that make possible the determination of a satellite's position and velocity and being located in interplanetary space. Optical navigation is used while DPS is basically the equivalent of GPS in the solar system. The position is obtained using images of objects from the solar system in combination with a one-way radio to the Earth. This instrument can be particularly useful for space missions going to Mars for instance (MarCO mission). [31]

3.4 Actuators

3.4.1 Magnetorquers

Magnetorquers work on the principle that a magnetic dipole can be generated using electromagnets. A torque is generated in presence of the Earth's magnetic field. This torque can change the angular momentum of the satellite and control momentum dumping of reaction wheels on CubeSats for example. A total of three units, with one magnetorquer per axis are needed to allow full control of the spacecraft. [29] Magnetorquers are very attractive as they offer a cheap attitude control solution for satellites being constrained in weight and volume.

Yet, magnetorquers have disadvantages. The first one being the decrease of the magnetic field strength with altitude. Magnetorquers will be very useful in LEO where the magnetic field is stronger than in GEO for instance. Additionally, a torque can only be produced about the local field direction and not in all directions depending on the orbital parameters needed for the designed mission. One can take the example of an equatorial orbit against a polar orbit. In the first one, the magnetic field only has one direction which can cause many problems depending on the mission. In the second one, any direction for the satellite can be achieved as the Earth's magnetic field (orientation) vary with the orbit. [26]

3.4.2 Reaction wheels

A reaction wheel consists of an electric motor driving a rotating mass where a moment of inertia is created in the process. The change of angular momentum within the rotating mass creates a reaction on the spacecraft body in the form of a torque. Reaction wheels are usually used for fine tuning and accurate attitude pointing. [26] They can have analog or digital interfaces. The last interface offers an internal loss torque compensation by comparing the wanted torque with the obtained change of angular momentum (or speed). [25] However, the use of reaction wheels is challenging and requires long lifetime tests. Accordingly, the current designs rely on old models where only a few parameters are changed.

Normally four reaction wheels are included in a redundant wheel configuration, that is to say either three nominal wheels plus one cold redundant wheel (as seen in figure 3.6) or four wheels used in hot redundancy (as seen in figure 3.7).

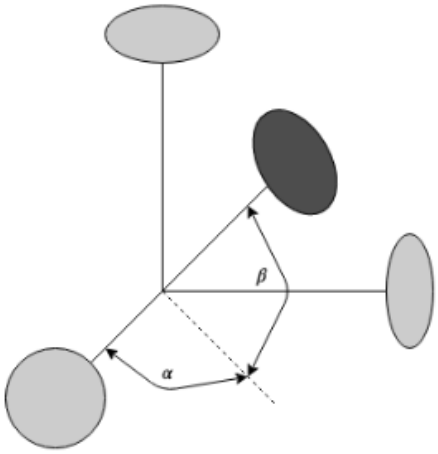

Figure 3.6: Configuration with three nominal reaction wheels plus one cold redundant reaction wheel.

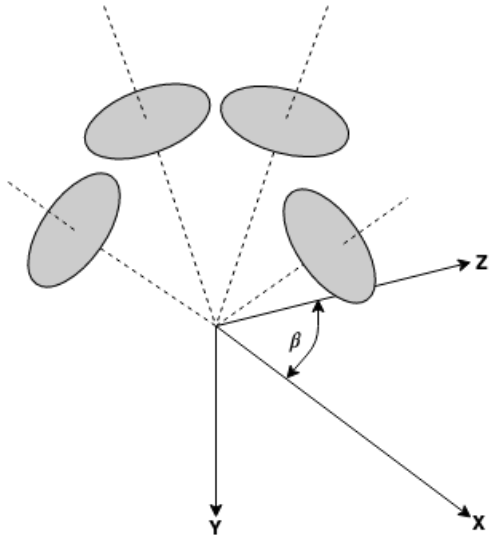

Figure 3.7: Configuration with four reaction wheels in hot redundancy.

3.4.3 Thrusters for attitude and orbit control

Thrusters provide a means to modify the angular momentum of a satellite, but also its orbit. They offer the possibility to counter external disturbances while being used in clusters. Many configurations exist depending on the mission design and the different maneuvers or orientation to be achieved, but a usual number of 12 is used to allow full and precise attitude control (a minimum of 6 is needed, but the resulting control accuracy will be less). Thrusters are needed when the Earth's magnetic field is too weak, so in other words with increased orbit altitudes. There exist different type of propulsion technologies (electric propulsion, cold gas or chemical) that enables attitude pointing systems to use various typed of throttleable micropropulsion. Pulse Width Modulation is normally used when thrusters for attitude and orbit control is chosen. [29]

Notwithstanding, using thrusters instead of other actuators means adding propellant in the budget that will increase the mass, the price, the volume taken but also more complexity on the system. Furthermore, thruster plume can contaminate or degrade spacecraft surfaces or equipment.

3.4.4 CMG

Control Moment Gyros are gimbaled wheels usually used for large satellites because of the possibility to store a high angular momentum in order to counteract external disturbances acting on the large surface area of the spacecraft. As seen on figure 3.8, CMGs consist of a momentum wheel mounted on a gimbal motor so that the angular momentum vector can achieve any desired direction. [26]

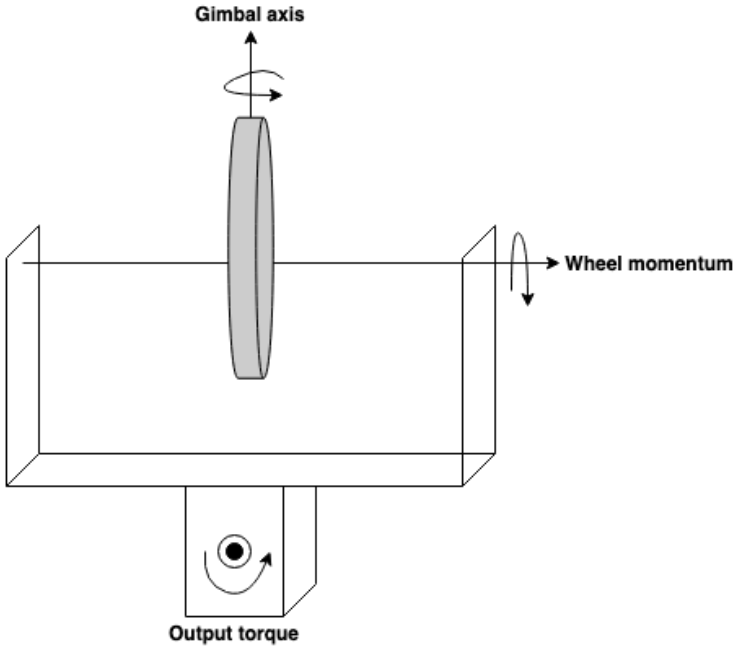

Figure 3.8: CMG diagram of a single gimbal. [26]

4 Trade studies

4.1 Methodology

As seen in the section 2, the number of missions designed to GTO is very low. That is high likely due to the harsh space environment surrounding the CubeSat. Indeed, the high energy radiations can cause critical damages to the on-board subsystems leading to a precipitated mission's end of life if not designed properly. Moreover, this orbit is often used as only a step when missions to GEO are launched. As a result, the orbit is filled with space objects coming from launch stage pieces or rocket fragmentation debris. The lack of scientific experiments at GTO is a motivation for the FORESAIL program alongside with demonstrating the feasibility of sending and using a CubeSat as a platform for experiments at this altitude. It has been studied that only few missions start to be designed for this type of orbit and some technology challenges still remain, the most challenging one being the AOCS probably. Undeniably, the design problem is based on the attitude control and on which actuators are best suited to solve the technology challenge. While the most common though is to use thruster based attitude control because of the lack of magnetic field strength, it seems like magnetorquers could be powerful enough to detumble the CubeSat when going closer to the perigee. The example of GTOSat and SpectroCube can be taken. They both are being designed so that magnetorquers will counter the momentum built up by the reaction wheels when passing by LEO when the strength of the magnetic field finally starts to be consequent. On the other hand, a similar system as for MarCO-A and MarCO-B (cluster of thrusters) could be used for attitude control solutions. In the trade studies, all actuators and sensors stated in section 2 will be studied for a potential selection. A special attention will be put on the tether deployment. Indeed, this is a crucial part of the mission, and rules the selection of the actuators. Thus, the attitude control actuators will be chosen accordingly after doing analyses on the maneuver time, the energy required, or the potential propellant mass needed. When the choice will be made, a configuration will be proposed, supposedly the best one in terms of efficiency, cost, weight, volume and mission requirements. In addition to that, mission design analyses will be performed to answer questions directly linked to AOCS design, such as the actual form factor of the CubeSat, the radiation dose accumulated by the satellite during its lifetime, or the compliance with the Space Debris Mitigation technical requirements (adopted by ESA, and defined in the standards ECSS-U-AS-10C / ISO 24113). The investigations in this thesis will be accomplished thanks to Systems Tool Kit by AGI, MASTER and DRAMA (both ESA's space debris software). Additionally, SPENVIS computed a pre-analysis of the space environment at GTO (see sections 2.1 and 2.2).

4.2 Major requirements

In this section, the mission requirements regarding the AOCS will be covered so that one can get a general overview of the objectives and constraints of the CubeSat design.

4.2.1 Attitude requirements

- *The spacecraft shall have the spin axis perpendicular to the magnetic field vector.*

  The Y-axis which will be spinning is normal to the 6U face of the CubeSat, always lies within the orbital plane, and is perpendicular to the orbit normal vector which was the defined constraint.

- *The attitude knowledge shall be better than* 3°.

- *The attitude control accuracy needs to be under 2°.*

- *The position knowledge shall be in the range of hundreds of meters.*

  This condition is needed in order to interpret scientifically the data in post processing.

- *The spin period of the CubeSat should range between 10 seconds and 30 seconds. An optimal value would be a spin period of 20 seconds.*

  If the spin axis is perfectly aligned, then half a spin (with 20 seconds period) already covers all pitch angles.

- *The attitude control system shall be able to increase the spin rate of the spacecraft in order to deploy the tether.*

  The CD tether, in addition to the science aspect, will be used as a de-orbiting system after mission completion to respect the 25 years orbit disposal guideline. An angular momentum of 25.510 Nms is needed to achieve this maneuver (total impulse of 48.150 Ns). See appendix A for more information.

- *The spacecraft must be able to calculate its attitude without the supervision or help from an external source.*

  For this aspiration, attitude sensors will be placed within the structure of the satellite to measure the angular velocities and momentum around each of the axis.

- *The spacecraft must be able to control its attitude without the supervision or help from an external source.*

  For this aspiration, attitude actuators will be placed within the structure of the satellite to control the angular velocities and momentum around each of the axis.

- *The AOCS shall be able to detumble the spacecraft if necessary before performing any control operation.*

  With the aim of detumbling the spacecraft, selected actuators will be used.

4.2.2 Orbit requirements

- *A GTO or HEO orbit shall be used. The minimum orbital altitude range shall be between two and five Earth radii.*

  Qualification to fulfill the scientific requirements, therefore, this is the type of orbit to be implemented.

- *The orbit inclination needs to be kept between* 0° *and* 30°. *The aimed inclination according to the launch options is* 28.5°.

  The magnetometer needs to fulfill those prerequisites to satisfy measurement requirements for the science goal regarding ULF waves.

- *The apogee shall reach an altitude of at least 2 to 3 Earth radii.*

- *The perigee shall reach an altitude between* 250 km *and* 500 km.

  For the sake of safe tether operations, the perigee shall not go lower than the numbers stated above. That is because the tether heats up to 165°C and 200°C and the tether tension from the atmospheric drag is 0.6 cN and 0.16 cN.

- *The expected lifetime of the CubeSat should be less than 25 years. If the satellite is not compliant with this rule, a disposal orbit has to be found, which guarantees an orbit decay within the next 25 years.*

4.3 Orbit propagation within STK

This section provides a gross characterization of the orbit. Unless stated otherwise, the analyses and simulations described in the next sections follow the initial parameters displayed in tables 4.1 and 4.2. The most likely to change parameters are the apogee, the perigee, the inclination, the orbital period, the semi-major axis, and the eccentricity depending on the running simulation.

Parameter	**Value**
Propagator	HPOP
Start of analysis period	12 Mar 2022 10:00:00 UTCG
End of analysis period	12 Mar 2023 10:00:00 UTCG
Apogee	37000 km
Perigee	300 km
Inclination	0°
Argument of perigee	0°
RAAN	0°
True anomaly	0°
Orbital period	10.94 $hours$
Semi-major axis	25021.00 km
Eccentricity	0.73

Table 4.1: Initial parameters for the orbital propagation of FS-2.

Perturbation force	Parameter	Input
Central body gravity	Gravity model	EGM2008
	Maximum degree	21
	Maximum order	21
	Solid tides	Full tide
	Use ocean tides	Yes
Drag	Use	Yes
	Model	Spherical
	CD	2.2
	Atmospheric density model	NRLMSISE 2000
Solar radiation pressure	Use	Yes
	Model	Spherical
	CR	1.0
	Shadow model	Dual cone
	Use boundary mitigation	Yes
Solar flux/Geomagnetic field	Flux/Ap File	SpaceWeather-All-v1.2.txt (provided by STK)
	Update rate	Daily
	Geomagnetic flux	Read Kp from file
	Eclipsing bodies	Sun and Moon

Table 4.2: Perturbation forces modelling parameters.

In addition to the perturbation forces showed in table 4.2, the Sun and the Moon have been added in the central body gravity perturbation force to take into consideration the third body gravity problem. The propagated orbit can be seen in figure 4.1 below.

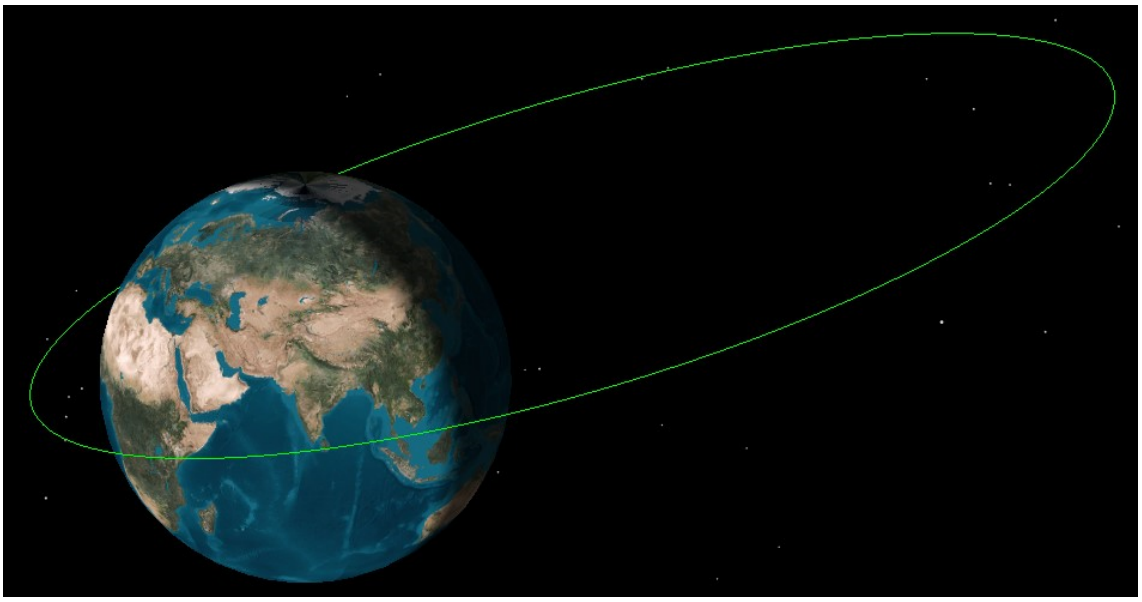

Figure 4.1: Propagated orbit by STK based on tables 4.1 and 4.2.

4.4 CubeSat form factor

The baseline form factor for FS-2 has always been 6U since the mission proposal. Nevertheless, this was an assumption based on the heritage mission FS-1. An important task is then to decide on the final size of the satellite before going further with simulations, as this is a crucial design aspect for the selection of sensors and actuators. One way to get a better idea of the final dimensions of FS-2 is to look at the illuminated cross-sectional area (theory and formulas from [32]). Power generation is a critical achievement in any designed space mission, and if one can prove that a 3U form factor won't be enough, then the final decision will be taken on the planned 6U baseline.

4.4.1 Solar illumination theory

Take the CubeSat is a cuboid with areas of the faces denoted as A_x, A_y, and A_z. One assumes that the spin axis is in the Z-direction. The solar direction is described as:

$$n = \begin{pmatrix} \sin(\theta)\cos(\varphi) \\ \sin(\theta)\sin(\varphi) \\ \cos(\theta) \end{pmatrix}$$

where θ is the angle between the spin and Sun vectors, and φ is the clock angle of the solar direction measured around the spin axis. One can deduce that the total projected area of the solar panels visible to the Sun is:

$$\begin{aligned} A_{illuminated} &= \mid ne_x \mid A_x + \mid ne_y \mid A_y + \mid ne_z \mid A_z \\ A_{illuminated} &= (A_x \mid \cos(\varphi) \mid + A_y \mid \sin(\varphi) \mid) \mid \sin(\theta) \mid + A_z \mid \cos(\theta) \mid \end{aligned} \tag{4.1}$$

In order to obtain the averaged spin area, one needs to average equation 4.1 over φ. Assuming that $0° \leq \theta \leq 90°$, the following derivation is obtained:

$$\begin{aligned} \langle A_{illuminated} \rangle_\varphi &= (A_x \langle \mid cos(\varphi) \mid \rangle_\varphi + A_y \langle \mid sin(\varphi) \mid \rangle_\varphi) sin(\theta) + A_z cos(\theta) \\ \langle A_{illuminated} \rangle_\varphi &= \frac{2}{\pi}(A_x + A_y) sin(\theta) + A_z cos(\theta) \end{aligned} \tag{4.2}$$

4.4.2 Simulation inputs and 3D models

Simulations for the CubeSat form factor have been done in STK, using a perigee of 400 km. They follow the requirements stated in section 4.2, and use the same setup described in section 4.3. The time step used for the area tool is 500 seconds and the simulation ran through the entire scenario (1 year). The angle between the spin axis and the Sun vector was created manually, and the viewed face was set to *FORESAIL-2 Sun vector*. Two form factors (3U and 6U) were compared during the simulations. A first simulation was done simulating attached solar panels to the body, and a second one simulating a deployed configuration. Both 3U and 6U models were modified using Blender to render the CubeSats with deployed solar panels.

Figure 4.2 displays the two different configurations for a 3U factor form (dimensions of $10\,cm \times 10\,cm \times 30\,cm$ set by ESA and NASA). Figure 4.3 displays the two different configurations for a 6U factor form (dimensions of $10\,cm \times 20\,cm \times 30\,cm$ set by ESA and NASA). The model used to simulate the 6U CubeSat with attached solar panels includes the extended boom, giving more accurate results. Unfortunately, as the general 6U model from STK was used to get the deployed solar panels, the extended boom will not be implemented. Nonetheless, the simulation still gives an idea about how much power could be produced and if the mission is feasible or not using this size and configuration.

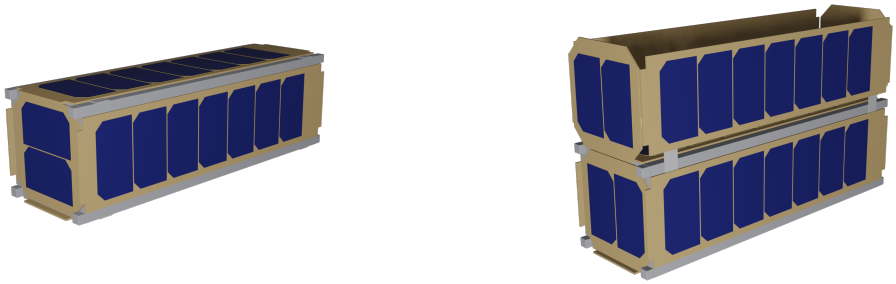

(a) 3U with attached solar .

(b) 3U with deployed solar panels.

Figure 4.2: 3U factor form configurations.

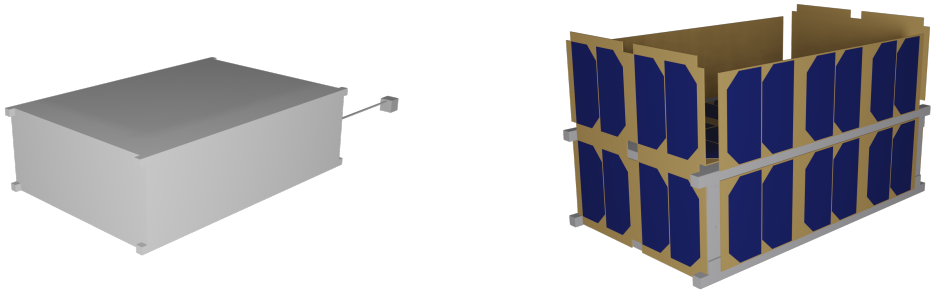

(a) 6U with attached solar .

(b) 6U with deployed solar panels.

Figure 4.3: 6U factor form configurations.

4.4.3 Decision on the form factor

Looking at figure 4.4, it can be seen that if the spin axis to Sun angle is kept within 60°, the 6U solution should be enough without deployable panels. However, if the angle gets larger than that, the available amount of power that can be produced by the solar panels will be quite low. The expected mission lifetime is of 6 months and could be difficult if deployable solar panels are not being used. Increasing the area of the surface facing the Sun might be a necessity and be set as a requirement. However, the only output needed here is the final size of the satellite. The potential power generated by the solar panels needs to be studied on the side, as this thesis is about AOCS considerations and mission design only.

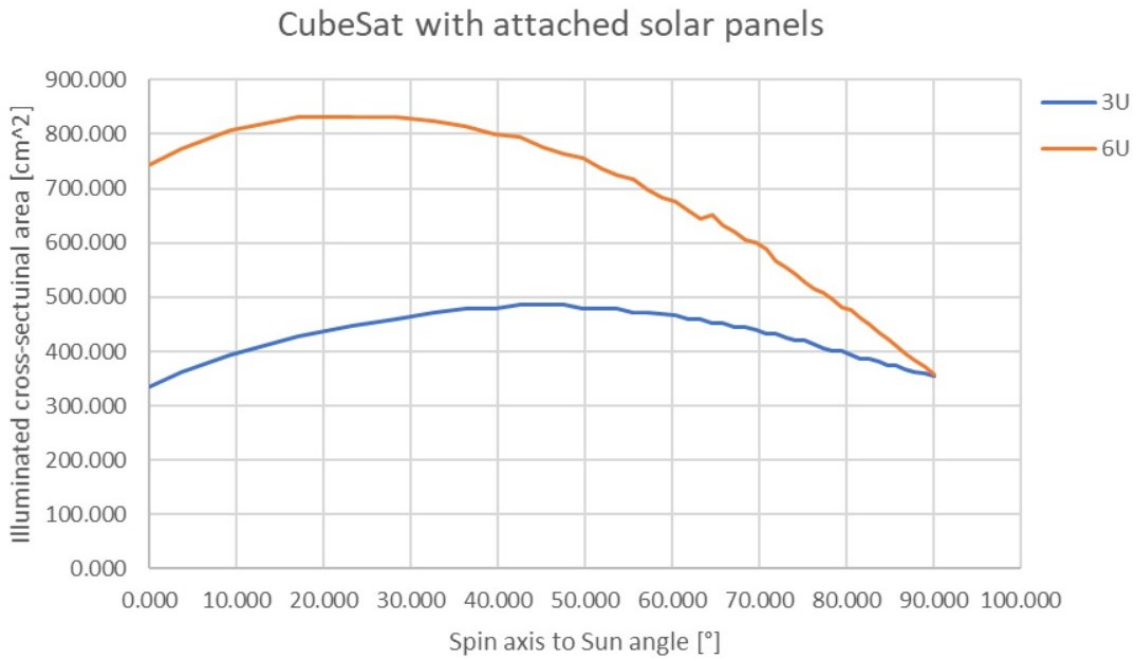

Figure 4.4: Illuminated cross-sectional area as a function of the spin axis to Sun vector angle for CubeSats with deployed solar panels.

The results obtained with a deployable solution for solar panels seem to fit better the mission lifetime of half a year. As a final decision, the 6U form factor is chosen over the 3U. Adding to the latter, the 6U dimensions fit better in case a propulsion system is chosen. The simulations continue to be done using the baseline dimensions set by the mission proposal, but this section was needed to confirm what was only an assumption before.

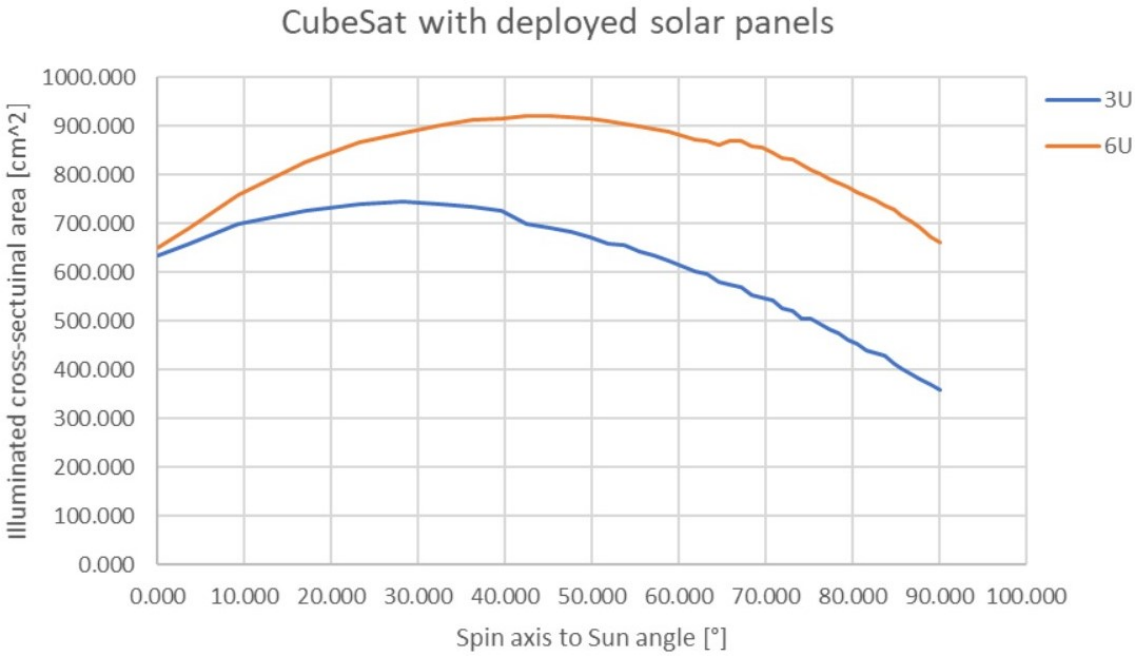

Figure 4.5: Illuminated cross-sectional area as a function of the spin axis to Sun vector angle for CubeSats with attached solar panels.

4.5 Orbital lifetime and decay

FS-2 will be orbiting through two protected regions (LEO protected region and GEO protected region) identified in the frame of IADC, followed as well by the UN COPUOS guidelines and ECSS and ISO standards. [33]

Guidelines	Standards to follow
Guideline 1	Limit debris released during normal operations
Guideline 2	Miminize the potential for break-ups during operational phases
Guideline 3	Limit the probability of accidental collision in orbit
Guideline 4	Avoid inatentional destruction and other harmful activities
Guideline 5	Minimize potential for post-mission break-ups resulting from stored energy
Guideline 6	Limit the long term presence of spacecraft and launch vehicle orbital stages in LEO region after the end of their mission
Guideline 7	Limit the long term interference of spacecraft and launch vehicle orbital stages with the GEO region after the end of their mission

Table 4.3: Space debris mitigation guidelines.

While the CubeSat should follow all guidelines stated in table 4.3, the ones of interest for the topic of this thesis are guidelines 6 and 7. They will serve as the constraints to define the final parameters for the orbit and refer to the ECSS-U-AS-10C / ISO 24113 standards. [34]

Aiming to a GTO orbit means to have a lot of variation depending on the time of the year when the satellite is being launched. To have a rough idea of the best possible launch time (even though dependent on the launch provider), four potential launch dates were simulated around the equinoxes and solstices as shown in table 4.4 below.

Launch dates simulated
21/03/2022 12:00:00
21/06/2022 12:00:00
21/09/2022 12:00:00
21/12/2022 12:00:00

Table 4.4: Potential launch dates simulated during the estimated launch year.

The decision on the simulated orbits was made according to the science requirements and the offers received so far by some launch providers. The perigee is the information that changes the most because of its importance. Setting the latter to 400 km or 250 km changes drastically the estimated lifetime of the satellite. Nonetheless, the perigee can't be too low because of the aluminum tether that can burn easily around Earth. A hard lower limit on the perigee is set to be around $200 - 250\,km$. The different orbits that were simulated using DRAMA can be seen in table 4.5.

For each orbit, four simulations were made taking into account the launch date during the year. A total of 80 simulations were conducted. Each orbit has an ID number to make the reference easier in this document. All orbits follow the setup explained in section 4.3, only the inclination changes and is set to 28.5°.

Apogee	Perigee	ID Number
35786 km	400 km	1
35786 km	350 km	2
35786 km	300 km	3
35786 km	250 km	4
30000 km	400 km	5
30000 km	350 km	6
30000 km	300 km	7
30000 km	250 km	8
25000 km	400 km	9
25000 km	350 km	10

Apogee	Perigee	ID Number
25000 km	300 km	11
25000 km	250 km	12
20000 km	400 km	13
20000 km	350 km	14
20000 km	300 km	15
20000 km	250 km	16
15000 km	400 km	17
15000 km	350 km	18
15000 km	300 km	19
15000 km	250 km	20

Table 4.5: Orbits studied during the simulation

An important parameter to obtain was the average cross-section for a 6U CubeSat, needed for simulating the orbital decay. The model for FS2 was designed directly inside DRAMA using the CROC tool to compute the orbital lifetime and assess post-mission disposal strategies (see figure 4.6).

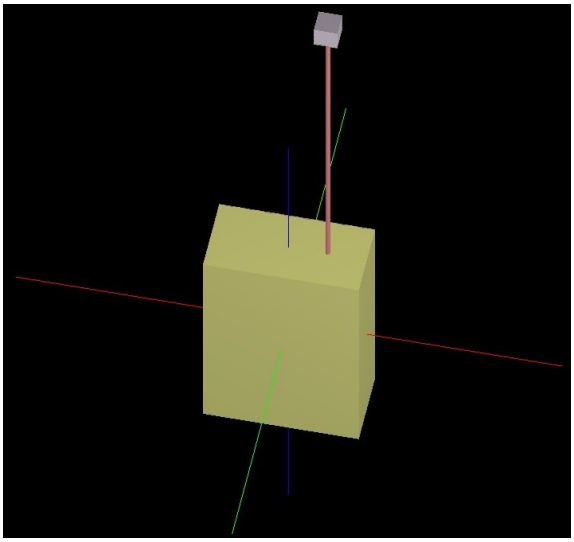

Figure 4.6: Designed model inside CROC tool. The red color refers to the X axis, the green color refers to the Y axis, and the blue color refers to the Z axis.

The dimensions of the CubeSat follow the standard dimensions set by NASA or ESA (10 $cm \times 20\ cm \times 30\,cm$). Regarding the dimensions of the extended boom (radius of 0.3 cm, height of 6 cm) and the magnetometer (3 $cm \times 3\ cm \times 3\ cm$, assimilated as a box here) were obtained discussion with the structure team. A dry mass of 7 kg was used. Running the CROC tool with the functionality set as *F3. Randomly tumbling satellite*, the average cross-section obtained is 571.590 cm^2. Figure 4.7 shows the cross-section of the model under the elevation and azimuth angles. This value was then implemented in the OSCAR tool, to compute the orbital lifetime and assess post-mission disposal strategies.

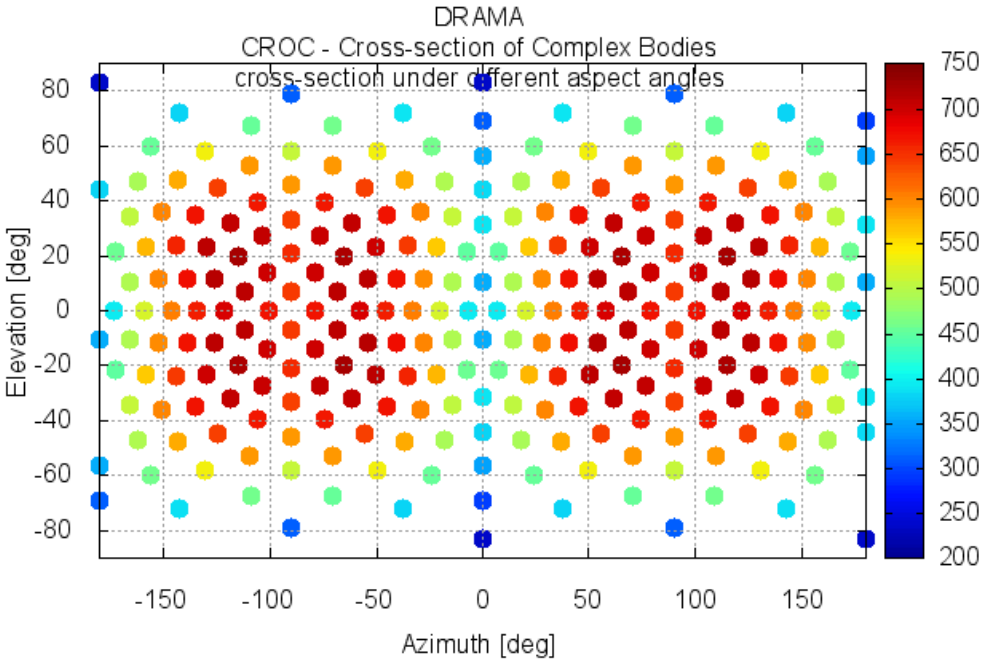

Figure 4.7: Cross-section of the designed model under different aspect angles.

After obtaining the average cross-section, the orbits specified in table 4.5 can be studied. The drag coefficient was set to 2.2 and reflectivity coefficient to 1.3. The disposal option was set to none as the purpose of this analysis is to see whether the CubeSat decays within 25 years without the help from a chemical propulsion system, an electric propulsion system, an electrodynamic tether system, or a drag augmentation device. Basically, the analysis is made for the worst case scenario where the CubeSat would not be able to use one of the devices stated previously for power or mechanical reasons for example. The lifetime margin is 5 %, and the propagation lasts for 100 years to verify the compliance with requirements related to the crossing of the protected regions in LEO and GEO. The OSCAR simulation run time is directly affected by this value, especially when searching for a specified lifetime orbit at higher altitudes in LEO. As for the solar and geomagnetic activity, the latest prediction scenario was chosen as it takes into account available up-to-date information on solar and geomagnetic activity from input files as provided by ESA. OSCAR requires up-to-date solar and geomagnetic activity data for its latest prediction. The update was done on May 26, 2020. Out of the 80 simulations, only 20 % were compliant with the 25 years limit through natural orbital lifetime. Table 4.6 displays only the orbits that match the 20 %, the others are not relevant.

ID Number	Apogee	Perigee	Launch date	Lifetime
3	35786 km	300 km	21/06/2022 12:00:00	1.20 years
3	35786 km	300 km	21/09/2022 12:00:00	24.23 years
3	35786 km	300 km	21/12/2022 12:00:00	1.33 years
4	35786 km	250 km	21/06/2022 12:00:00	1.17 years
4	35786 km	250 km	21/12/2022 12:00:00	2.65 years
11	25000 km	300 km	21/06/2022 12:00:00	23.18 years
12	25000 km	250 km	21/06/2022 12:00:00	23.76 years
15	20000 km	300 km	21/03/2022 12:00:00	20.60 years
15	20000 km	300 km	21/06/2022 12:00:00	20.74 years
15	20000 km	300 km	21/12/2022 12:00:00	6.94 years
16	20000 km	250 km	21/12/2022 12:00:00	5.20 years
16	20000 km	250 km	21/06/2022 12:00:00	5.20 years
20	15000 km	250 km	21/03/2022 12:00:00	6.24 years
20	15000 km	250 km	21/06/2022 12:00:00	3.01 years
20	15000 km	250 km	21/09/2022 12:00:00	4.22 years
20	15000 km	250 km	21/12/2022 12:00:00	2.05 years

Table 4.6: Orbits compliant with the 25 years limit through natural orbital lifetime.

One interesting fact is that not a single orbit with a perigee superior to 300 km complies with the guideline. Thus, a maximum threshold limit needs to be set for the perigee. The mission aims for a GTO orbit in the best-case scenario, therefore, the orbit with the ID number 3 looks the most suitable. In addition to that, three out of the four studied launch dates are compliant with the 25 years lifetime. Nonetheless, one important thing to keep in mind is the perigee during the mission. The expected mission lifetime is six months, and during this time, the perigee should not go lower than $200 - 250\,km$ as the tether will receive a drag force it can't sustain. With this information, one can eliminate all orbits with a perigee lower than 300 km. A hard constraint on the perigee is then to have it around 300 km, which seems to be the perfect altitude for the CubeSat. Now that an ideal orbit is selected, it is needed to select the best launching date, depending on the decreasing perigee. Figures 4.8, 4.9, and 4.10 display the behaviour of the perigee and apogee as a function of time, before the orbital decay of the satellite.

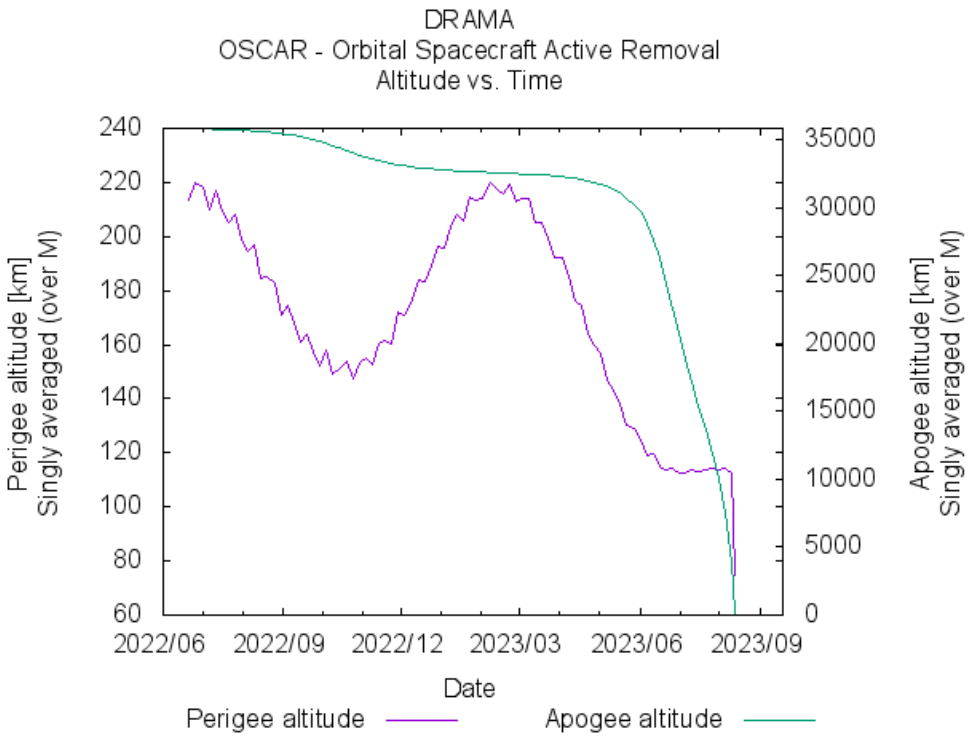

Figure 4.8: Altitude vs. Time, orbit number 3 for a launch in June.

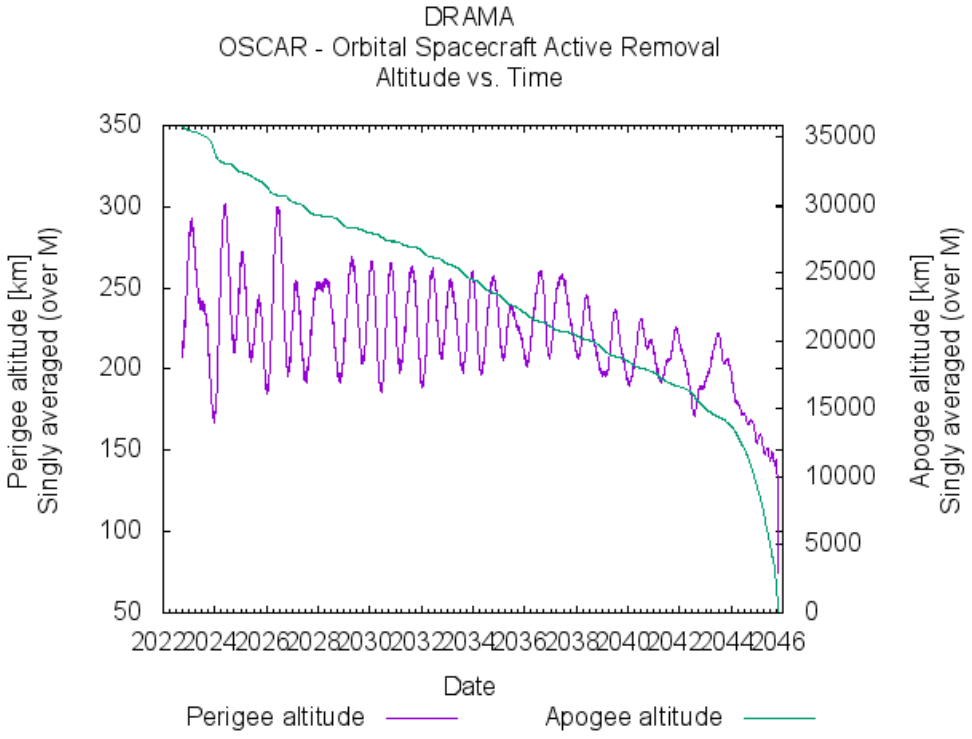

Figure 4.9: Altitude vs. Time, orbit number 3 for a launch in September.

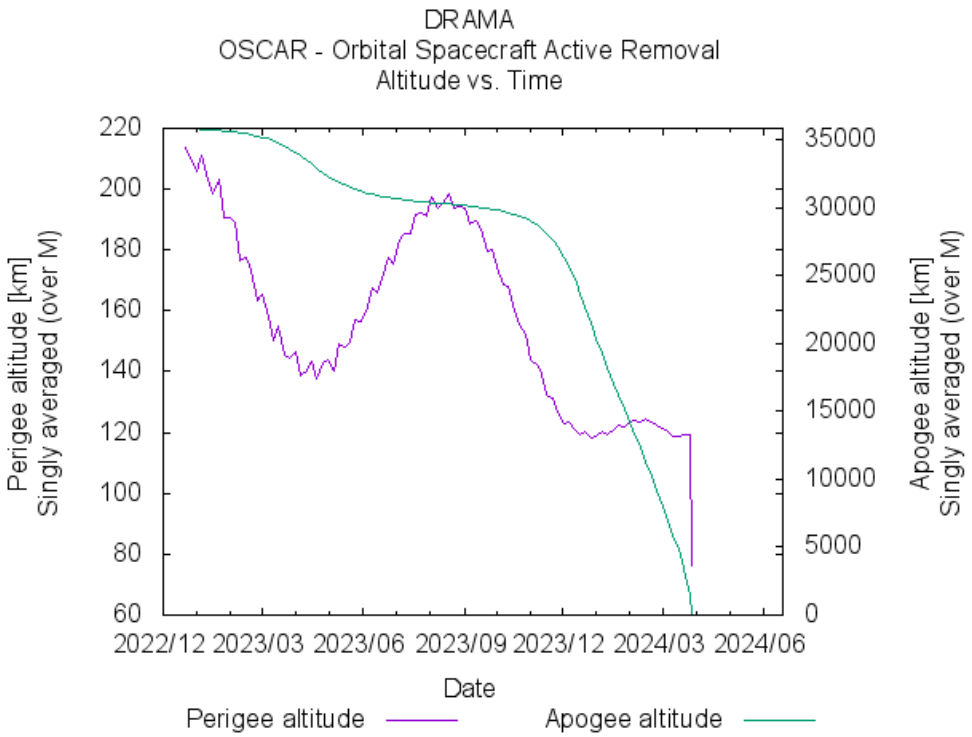

Figure 4.10: Altitude vs. Time, orbit number 3 for a launch in December.

Looking at the plots for a launch in June or December, it seems like the perigee decreases too much during the first 6 months of the expected lifetime, making it dangerous for the continuation of the mission once the tether is deployed (too much burning). However, a launch in September could work as the perigee remains around 300 km during the first months of the mission. The latter decreases when the mission is already finished, and the expected lifetime is just a bit less than 25 years, which works perfectly. This analysis can be conclude on using the orbit number 3 (apogee of 35786 km, perigee of 300 km, launch in September) as a baseline for the future simulations. This knowledge is valuable, especially for conducting the analysis on the total dose accumulated by the CubeSat during its mission lifetime. The last-mentioned being a significant aspect when selecting the sensors and actuators for the AOCS.

4.6 Total radiation dose

4.6.1 Radiation environment model

The SEET radiation tool (see table 4.7 for simulation setup) from STK was defined taking into account the resulting orbit from section 4.5. The default energy levels when using the NASA computational mode will be those from the CRRESS models.

The CRRESELE database model returns electron flux at discrete energies in the range $0.5 - 6\ MeV$, reporting electron fluxes for a specific set of energy levels only (0.65, 0.95, 1.60, 2.00, 2.35, 2.75, 3.15, 3.75, 4.55, 5.75 MeV).

Similarly, the CRRESPRO database model computes proton flux at discrete energies in the range $1 - 100\ MeV$, reporting proton fluxes only for a specific set of energy values only (1.5, 2.1, 2.5, 2.9, 3.6, 4.3, 5.7, 6.8, 8.5, 9.7, 10.7, 13.2, 16.9, 19.4, 26.3, 30.9, 36.3, 41.1, 47.0, 55.0, 65.7, 81.3 MeV). [35]

The material chosen for shielding is aluminum as it is the most common solution used by space companies. The latter is varying from $1\ mm$ to $10\ mm$, because it was determined that higher shielding thicknesses do not apply for small satellites such as CubeSats usually. [36]

Model	**Parameter**	**Input**
CRRES Activity	Proton	Active
	Radiation	Average
NASA Electron and Proton activity	Activity	Solar Max
Magnetic field model	Main field	IGRF
	External field	Olson-Pfitzer
	IGRF Update rate	1 day
South Atlantic Anomaly (SAA)	Channel	$> 23\ MeV$
	Flux level	Background + 3 Sigma
SEET Radiation	Computational mode	NASA
	Dose channel	Total
	Detector type	Silicon
	Detector geometry	Spherical
	Dose integration step	60 seconds
	Dose report step	6 hours
	Nuclear attenuation	Yes
	Neutrons in nuclear attenuation	Yes

Table 4.7: Initial parameters for modelling the radiation environment using STK.

4.6.2 Accumulated dose

The main goal of this simulation was to determine the possibility to use available AOCS sensors and actuators on the market. Indeed, they will be of no use if the radiation threshold value is too low. The accumulated doses for different aluminum shielding thicknesses are displayed on figure 4.11. The interest here is to determine the maximum dose FS-2 will accumulate during the mission lifetime. This one is supposed to be six months, but for estimation purposes, the simulation ran during one year. Table 4.8 zooms on those final numbers. If the shielding protection is not thick enough, then the CubeSat will have to sustain quite a lot of radiation making it a problem for the subsystems, the different components, and especially the electronics.

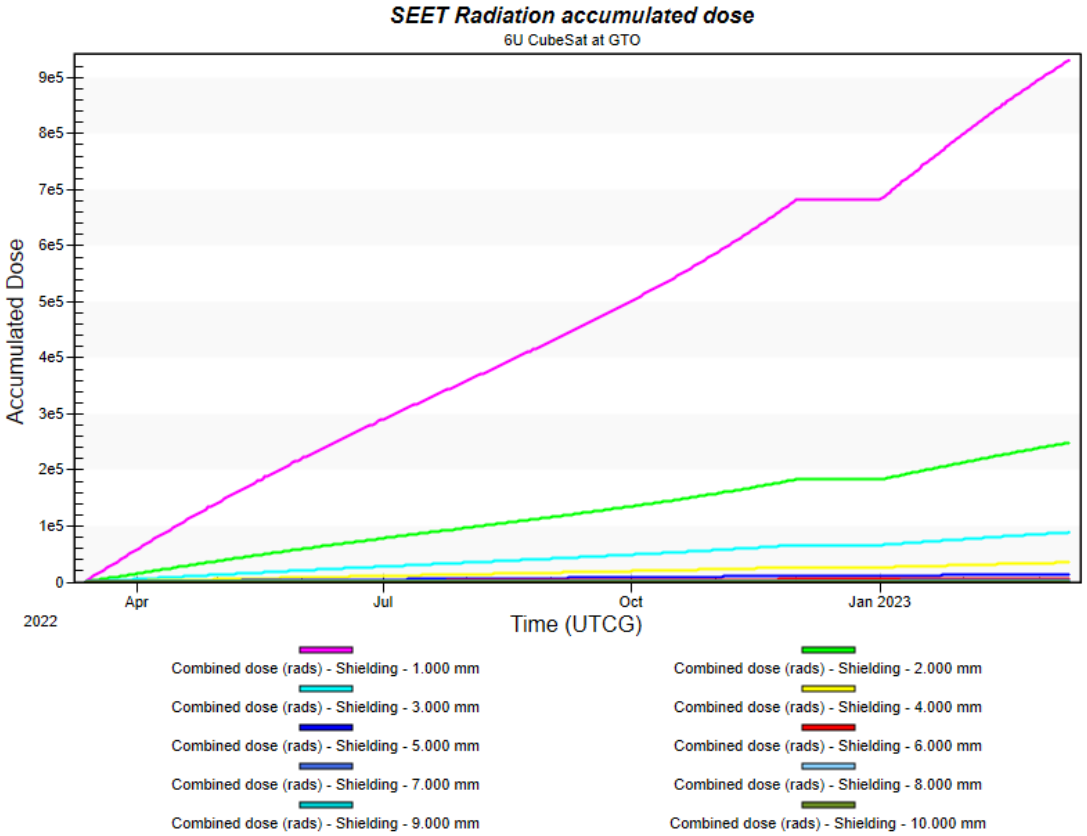

Figure 4.11: Accumulated dose as a function of time and shielding thicknesses.

Shielding thickness (Aluminum)	**Accumulated dose**
1 mm	933.500 $krads$
2 mm	249.200 $krads$
3 mm	89.160 $krads$
4 mm	35.310 $krads$
5 mm	14.740 $krads$
6 mm	6.566 $krads$
7 mm	3.021 $krads$
8 mm	1.677 $krads$
9 mm	1.097 $krads$
10 mm	0.799 $krads$

Table 4.8: SEET Radiation accumulated dose after on year in space.

Most of the COTS available on the market can sustain a total dose of about 10 $krads$, if not 20 $krads$ for some of them. Still, it is always safer to go for the worst case scenario, especially in the space industry. By setting an upper limit on the accumulated radiation dose at 10 $krads$, one can deduce that a shielding thickness of 6 mm using aluminum provides sufficient protection for on-board components and subsystems. In order to be sure, a margin is taken, and the shielding thickness is risen up to a minimum of 7 mm.

As an example, GTOSat by NASA (see section 2.4.2) will go through a very similar environment and is targeting the severe radiation of GTO. As a protection, it will feature a 7 mm thick vault for electronics. Additionally, SpectroCube by ESA (see 2.4.2) is using another approach and will add radiation shielding to radiation-sensitive components. The latter mainly includes the electronics of the science payload, communication, and power subsystem. The expected total ionizing tolerance dose of most electronics components on their mission is approximately 20 $krads$, and after doing a design study, it was proven that a 6 mm aluminum shielding is sufficient. Those two examples confirmed the assumption stated earlier looking at the number of the simulation.

4.7 Feasibility analysis

4.7.1 Sensors selection

First of all, it is needed to get the potential accuracy and performances of each sensor in order to determine which one can fulfill the requirements imposed by the scientific payloads. Those information can be seen in tables 4.9, 4.10 and 4.11. Different sources were found to compare the different solutions and have a general picture of the technologies.

SENSORS	
Component	**Potential accuracy**
Sun sensors	1 $arcmin$ ($\sim 0.017°$)
Earth sensors	6 $arcmin$ ($\sim 0.1°$)
Star trackers	1 $arcsec$ ($\sim 0.0002°$)
Magnetometers	30 $arcmin$ ($\sim 0.5°$)
GPS	6 $arcmin$ ($\sim 0.1°$)

Table 4.9: Potential accuracies of some AOCS sensors. [25]

SENSORS			
Component	**Performance**	**COTS**	**TRL**
Sun sensors	$0.1°$ accuracy	> 8	9
Earth sensors	$0.25°$ accuracy	> 2	9
Star trackers	25 $arcsec$ ($\sim 0.007°$) pointing knowledge	> 8	9
Gyroscopes	$1°h^{-1}$ bias stability $0.1°h^{-\frac{1}{2}}$ random walk	> 4	9
Integrated units	$0.002°$ pointing capability	> 8	9
Magnetometers	10 nT resolution	> 6	9
GPS	1.5 m position accuracy	> 4	9
DPS	N/A	> 2	9

Table 4.10: State of the art and accuracy of AOCS sensors 1. [30]

SENSORS			
Component	**Performance**	**Application**	**Price**
Sun sensors			
Solar cell	5°	Sun acquisition	€
V-slit	0.1°	Sun maintenance	€€€
Digital	0.05°	Sun maintenance	€€€
Earth sensors			
Static	5°	Earth acquisition	€
Horizon crossing	0.1°	Earth maintenance	€€€
Star trackers	0.01°	Substitute for sun or earth sensor	€€
Magnetometers	3°	LEO satellites	€
Gyroscopes			
Spinning	0.01°	During eclipse transits	€€
Ring laser	0.005°	During eclipse transits	€€€
GPS	0.5°	Experimental for autonomous onboard attitude determination	€€

Table 4.11: State of the art and accuracy of AOCS sensors 2. [29] The classification of the price goes as follow: relatively cheap €, mid price €€, quite expensive €€€.

Sun sensors

According to the potential accuracy provided, sun sensors are fully applicable for the mission. Besides, numerous technologies are available on the market making this component very easy to acquire and rather cheap. Nonetheless, Sun sensors cannot be used to determine the spin rate of the CubeSat as they cannot detect any rotation about the Sun vector. That is the reason why, if Sun sensors are chosen as attitude sensors for the spacecraft, they need to be put additionally in combination with another sensor that can postulate the CubeSat's rotation. It is also needed to keep in mind that Sun sensors can be used all the time at GTO apart from the eclipse region.

Earth sensors

Earth sensors have a a low accuracy compared to other sensors such as Sun Sensors or star trackers and start to become less common on modern space missions. One advantage though is that they are cheap compared to other technologies. Notwithstanding, the further away the CubeSat goes from the Earth, less useful Earth sensors become as they work the best around the perigee in LEO.

Star trackers

Star trackers are the most powerful and accurate attitude sensor and are a good replacement option over Sun sensors and Earth sensors. They can be used all the time, even during the eclipse (not possible for Sun sensors) but compared to more typical sensors, they are convoluted and expensive as well. In addition to that, they need thermal and mechanical stability, optics alongside with data handling. Finally, another aspect to take into account is the potential harm that radiations can cause

to such sensors resulting into a less accurate pointing knowledge. Since star trackers require exposure time, the spin rate of the satellite must also be limited.

Gyroscopes

Gyroscopes provide a measurement of angular velocity. It is a measurement that is needed for the mission because of the constraints set by the payloads. Thus, it is essential for them to be implemented in the AOCS in combination with another sensor that will provide continued control of satellite's attitude. Gyros are one of the most popular option when it comes to attitude sensors as they provide a simple and cheap solution to mission design.

Magnetometers

Magnetometers have several advantages, some being the simplicity of the use, the cheap cost but also the robustness they can have. Yet, the magnetic field is not well mapped filled with abnormalities limiting the accuracy of this type of sensor. On top of that, magnetometers are very sensitive to noises that could be generated by the other subsystems and most of the configuration are set so that they are located the furthest away possible from any disturbances that could occur, sometimes even placed on a extendable boom. Nevertheless, as star trackers have a limited tracking rate on a spinning satellite, summed up with the fact that the tether deployment will happen in LEO region, it might be a good idea to back up the sun sensors with three one-axis magnetometers or one three-axis magnetometer.

GPS

Even though GPS receivers are now the primary method for performing orbit determination in LEO region, they have limitations to their accuracy as they were primarily designed to be used on Earth. Thus, it is easy to conclude that the further away from Earth the CubeSat is, the weaker the signal will be affecting the attitude knowledge. As for magnetometers, they can be very useful around the perigee, and sometimes (depending on the mission requirement) enough to propagate the orbit when associated with a good antenna.

DPS

This new class of sensors, innovative that is to say, cannot be used for the simple reason that GTO is not considered as deep space. Using DPS navigation would not lead anywhere and would be quite expensive.

Integrated units

Integrated units are a combination of attitude sensors and actuators that can provide an easy single component solution for AOCS. They are usually composed of gyros, accelerometers, reaction wheels, magnetometers or magnetorquers. Such units can be used depending on the composition of the AOCS cube. While reaction wheels and gyros are surely needed for FS-2, magnetometers will be of no use and different options need to be studied so that money is not wasted in unsuitable components.

The table 4.12 below lists the selected sensors. The selection is made based on the performance, the cost and the applicability of the sensors. The colors shows if the condition of the potential sensor is a good option or not for the AOCS, going from green (good), yellow (average) and red (not good). The classification of the price goes as follow: € (relatively cheap), €€ (mid price), €€€ (quite expensive).

SENSORS				
Component	**Performance**	**Cost**	**Applicability**	**Selection**
Sun sensors	YES	€	FULLY APPLICABLE Apart from the eclipse region, they can be used all the time.	YES
Earth sensors	YES	€	PARTLY APPLICABLE Only useful when approaching the perigee.	NO
Star trackers	YES	€€	NOT APPLICABLE Limited by the tracking rate.	NO
Gyroscopes	YES	€€	FULLY APPLICABLE The spin rate of the CubeSat is a crucial information.	YES
Magnetometers	YES	€	PARTLY APPLICABLE Useful in LEO region during tether deployment.	YES
GPS	YES	€€	PARTLY APPLICABLE Network available in LEO region.	YES
DPS	YES	€€€	NOT APPLICABLE Only useful in deep space and GTO is not part of it.	NO
Integrated units	YES	€	FULLY APPLICABLE If a combination of useful sensors is found, they can be used.	YES

Table 4.12: List of selected sensors.

4.7.2 Actuators selection

First of all, it is needed to get the potential torque ranges and performances of each actuator in order to determine which one can fulfill the requirements imposed by the scientific payloads. Those information can be seen in tables 4.13 and 4.14. Different sources were found to compare the different solutions and have a general picture of the technologies.

ACTUATORS	
Component	**Torque range**
Magnetorquers	$10^{-2} - 10^{-1}\ Nm$
Reaction wheels	$10^{-1} - 1\ Nm$
Reaction Control System (RCS)	$10^{-2} - 10\ Nm$
CMG	$10^{-2} - 10^{3}\ Nm$

Table 4.13: Range of torques available from AOCS actuators. [37]

ACTUATORS			
Component	**Performance**	**COTS**	**TRL**
Magnetorquers	$0.001 - 0.3\ Nm$ peak torque $0.015 - 8\ Nms$ storage	> 8	9
Reaction wheels	$0.1\ Nm$ peak torque $1.5\ Nms$ storage	> 13	9
Thrusters	N/A (each option needs to be studied individually)	> 10	9

Table 4.14: State of the art and accuracy of AOCS actuators. [30]

Magnetorquers

They are often used as the primary actuator nowadays on CubeSats. It can be explained by the simplicity of use but also by the cheap cost of magnetorquers. Moreover, they have an unlimited lifetime, which is not the case for thrusters for example. On the other hand, they can cause magnetic interference and no torque can be provided about the local field direction. Because of the mission requirements, it is indisputable that magnetorquers cannot be used as a primary actuator. With the increasing altitude, the same conclusion as for magnetometers will be obtained, that is, as magnetorquers are only useful in LEO where the magnetic field strength is high, they can't be chosen (primary actuator) here as most of the orbital time will be happening at altitudes superior to LEO characteristics. Still, it can be possible for magnetorquers to be powerful enough when passing by the perigee for momentum dumping of reaction wheels for instance as the magnetic field gets stronger.

Reaction wheels

Reactions wheels can produce precise pointing but also a high torque if necessary. They are not limited by the environment and can provide with continuous control over the mission's lifetime. A minimum of three reaction wheels will be necessary in

order to get full three-axis control over the CubeSat. This type of actuator can be chosen as one attitude control tool because of its high reliability and its specifications that match perfectly the mission design of the spacecraft. One disadvantage however is that when the momentum builds up, a secondary actuator is needed for momentum dumping. To detumble the CubeSat, either thrusters or magnetorquers can be used.

Thrusters

Thrusters provide a good solution to modify the spacecraft orbit and angular momentum. Unlike magnetorquers, they are not dependent of the magnetic field and, therefore, by extension not dependent of the altitude either. One of the main use of thrusters is actually when missions are designed to high orbits where the magnetic field is weak. Nevertheless, even though they can produce a high torque, thrusters are expensive, more complicated to use than magnetorquers for example. They also consume quite a lot of power and add weigh in the mass budget. Eventually, they don't have an infinite lifetime as they depend on the propellant brought on-board the CubeSat.

CMG

CMGs are mainly used for large spacecrafts because of the high torque they can generate, and would be far too expensive and heavy for a CubeSat mission. For this reason, it is not necessary to go further as this type of actuator will not be selected for the AOCS.

The table 4.15 below lists the selected actuators that will go through further analysis. The selection is made the same way as for the sensors and is explained in section 4.7.1.

ACTUATORS				
Component	**Performance**	**Cost**	**Applicability**	**Selection**
Magnetorquers	YES	€	PARTLY APPLICABLE In combination with reaction wheels, it can be useful in LEO region.	YES
Reaction wheels	YES	€€	FULLY APPLICABLE In combination with magnetorquer or thrusters.	YES
Thrusters	YES	€€€	FULLY APPLICABLE In combination with reaction wheels.	YES
CMG	YES	€€€	NOT APPLICABLE Too heavy and too expensive for just a CubeSat mission.	NO

Table 4.15: List of selected actuators.

4.8 Trade-off study - Magnetorquers

4.8.1 Geomagnetic field model and calculation

The main field was modeled using IGRF while the external field was modeled using Olson-Pfitzer (see table 4.7 for the modeling parameters). The simulation follows the guidelines stated in table 4.1 and is coherent with the results obtained in the previous sections. Because of the inclination of the Earth magnetic field at the equator (0°), it was important to keep the orbit inclination near the equator in order to estimate the highest torques that could result from using magnetorquers. The aim of this analysis is fundamentally to prove that this type of actuator cannot provide the necessary angular momentum needed for the mission.

Three methods have been used to determine if magnetorquers can be used to deploy the tether but also how fast could they detumble potential reaction wheels. The first method is based on the magnetic field integration over the entire scenario and gives the most accurate results. The second method is based on choosing periods when the magnetic field is consequent enough to have an impact on the generated torque produced by the magnetorquers. A threshold value of $> 1000\,nT$ was chosen arbitrarily. Finally, the third method is based on focusing on one orbit only, and assuming the same behavior for the entire mission lifetime. The orbit when the magnetic field is at its peak was chosen to simulate the the best case scenario.

The formula below [29] expresses the magnetic dipole generated by a magnetorquer:

$$\overrightarrow{m_{mag}} = nIA_{mag} \tag{4.3}$$

When interacting with the magnetic field, the magnetic dipole generates a torque [29] (perpendicular to the magnetic field vector of the Earth), evidenced below by:

$$\overrightarrow{T_{mag}} = \overrightarrow{m_{mag}} \times \vec{B} \tag{4.4}$$

Looking at equation 4.4, one can see the resulting torque actually depends on the magnetic dipole of the magnetorquer. Thus, the latter will vary from $0.2\,A \cdot m^2$ to $1.2\,A \cdot m^2$ in the analysis to estimate the maneuver times depending on the size of the air coil. The time step used in the simulation to get the magnetic field vector of the Earth was 60 seconds. To calculate the maneuver time, one can have a look at the unit of the required momentum to be achieved and find a formula that will get the time needed. The goal is to obtain $N \cdot m \cdot s$ expressed as $kg \cdot m^2 \cdot s^{-1}$ in International System of units. Only a quick observation is needed to derive the following formula:

$$Maneuver\ time = \frac{Angular\ momentum\ goal}{Torque\ generated} \tag{4.5}$$

4.8.2 Integration over the entire scenario

The first method gives the most accurate results (although the simulation time is rather long). A mean intensity of 1641.826 nT was obtained from the model in STK, and using the formula derived in section 4.8.1, the maneuver time for a zero degree inclination ranges from 899 days to 149 days. The results can be seen in table 4.16 and figure 4.12. The time limit for deploying the tether is set to be one month. The first method of this simulation clearly shows such a maneuver using magnetorquers as main actuators is not possible. In the best case scenario, the maneuver time is almost 5 times larger than the threshold limit. Moreover, a single magnetorquer having a magnetic dipole of 1.2 $A \cdot m^2$ has a consequent size already, of about 94 $mm \times 15\,mm \times 13\,mm$ taking the example of NCTR-M012 from NewSpace Systems. [38] The requirements on the sizing of potentially usable magnetorquers (for tether deployment) are simply not suitable for a 6U CubeSat.

Another part of the analysis was to study the usefulness of magnetorquers to detumble the CubeSat controlled by reaction wheels. The situation is so that the spacecraft is spinning because of the reaction wheels but those ones can't be used anymore. Magnetorquers would be the only option to detumble the spacecraft then. The reaction wheels chosen for the example are the RW-0.03 from Sinclair Technology with a peak momentum of 0.04 Nms. [39] Looking at table 4.16 and 4.13, it can be seen that it would take between 33 days and 5 days depending on the magnetic moment. Thus, magnetorquers could be used as second actuators when passing in the perigee region, but it is important to keep in mind that the time spent in LEO is very brief, and the velocity is very high (around 10 $km \cdot s^{-1}$) which can result in difficulties with the spacecraft's maniability.

Magnetic dipole ($A \cdot m^2$)	**Maneuver time (days)**	
	Tether deployment	**Detumbling**
0.2	899.166	33.838
0.3	599.444	22.558
0.4	449.583	16.919
0.5	359.366	13.535
0.6	299.722	11.279
0.7	256.904	9.668
0.8	224.791	8.459
0.9	199.815	7.519
1.0	179.833	6.768
1.1	163.485	6.152
1.2	149.861	5.640

Table 4.16: Maneuver times for tether deployment and detumbling (method 1).

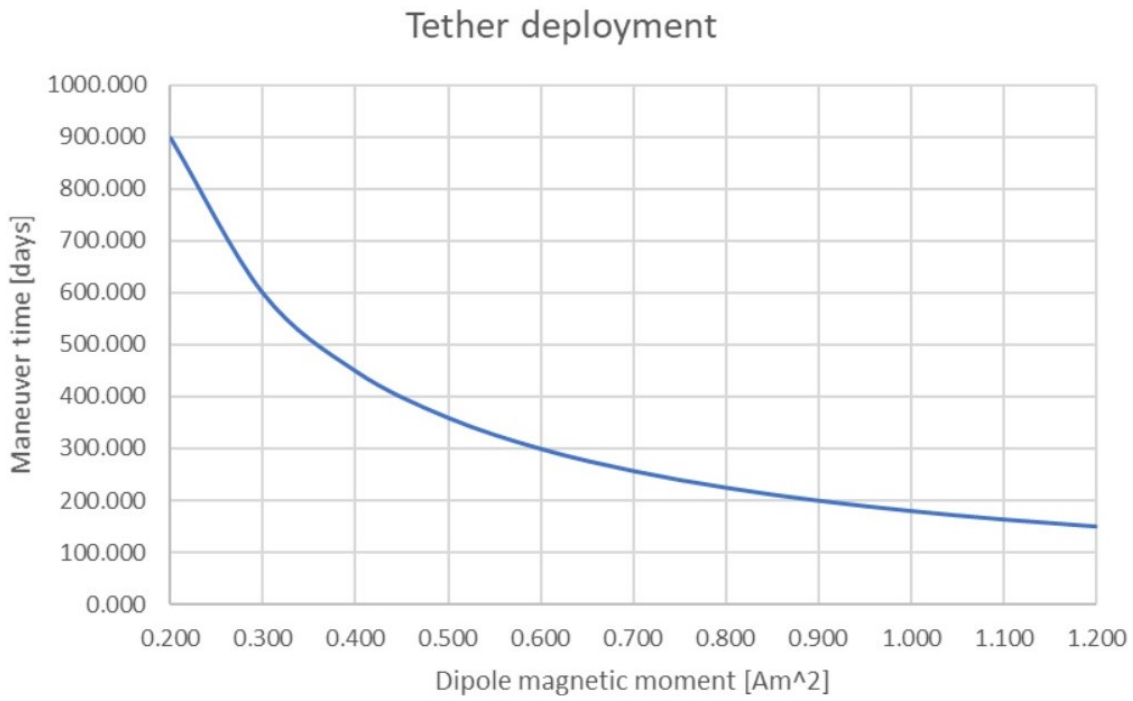

Figure 4.12: Tether deployment using magnetorquers as a function of magnetic dipole (method 1).

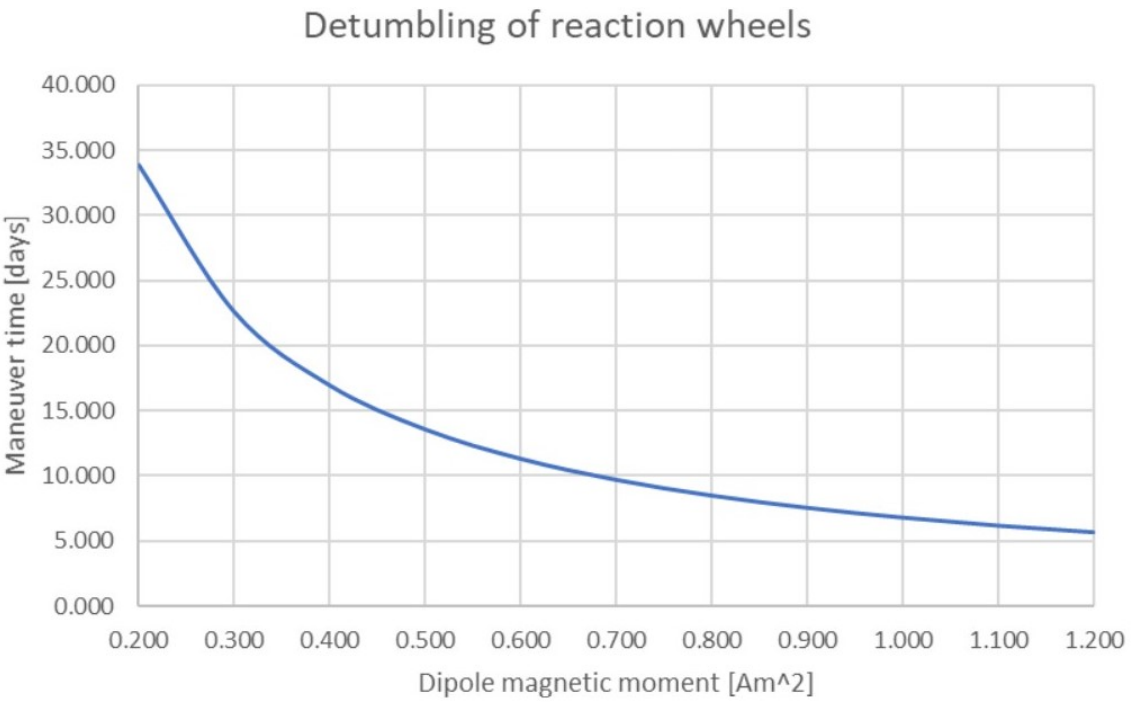

Figure 4.13: Detumbling using magnetorquers as a function of magnetic dipole (method 1).

4.8.3 Integration over consequent magnetic field periods

During the simulation, the orbital period was estimated to be 10.920 $hours$, and a total of 802 $orbits$ were performed. As said previously in section 4.8.1, only the periods with a magnetic field strength superior to 1000 nT were chosen. For one orbit, the latter lasts for 1.950 $hours$, which represents 65.153 $days$ during the entire scenario of one year in STK. A mean intensity of 9073.658 nT was obtained, which is much higher than for the first method. Nonetheless, this mean intensity was obtained only for the periods with a consequent magnetic field. Thus, adding back the 8.97 $hours$ remaining of the orbit time, one quickly goes back to similar results as for the first method (see table 4.17, figures 4.14 and 4.15). This method has the advantage of being fast to simulate, but gives less accurate results as the margin error is higher and assumptions are taken. Nevertheless, it is a good way of verifying the better results of the first method to conclude on the exactitude of the latter. The same conclusions are therefore deduced, and magnetorquers cannot provide an adequate solution for the tether deployment.

Magnetic dipole ($A \cdot m^2$)	**Maneuver time (days)**	
	Tether deployment	**Detumbling**
0.2	911.113	34.287
0.3	607.409	22.858
0.4	455.557	17.144
0.5	364.445	13.715
0.6	303.704	11.429
0.7	260.318	9.796
0.8	227.778	8.572
0.9	202.470	7.619
1.0	182.223	6.857
1.1	165.657	6.234
1.2	151.852	5.715

Table 4.17: Maneuver times for tether deployment and detumbling (method 2).

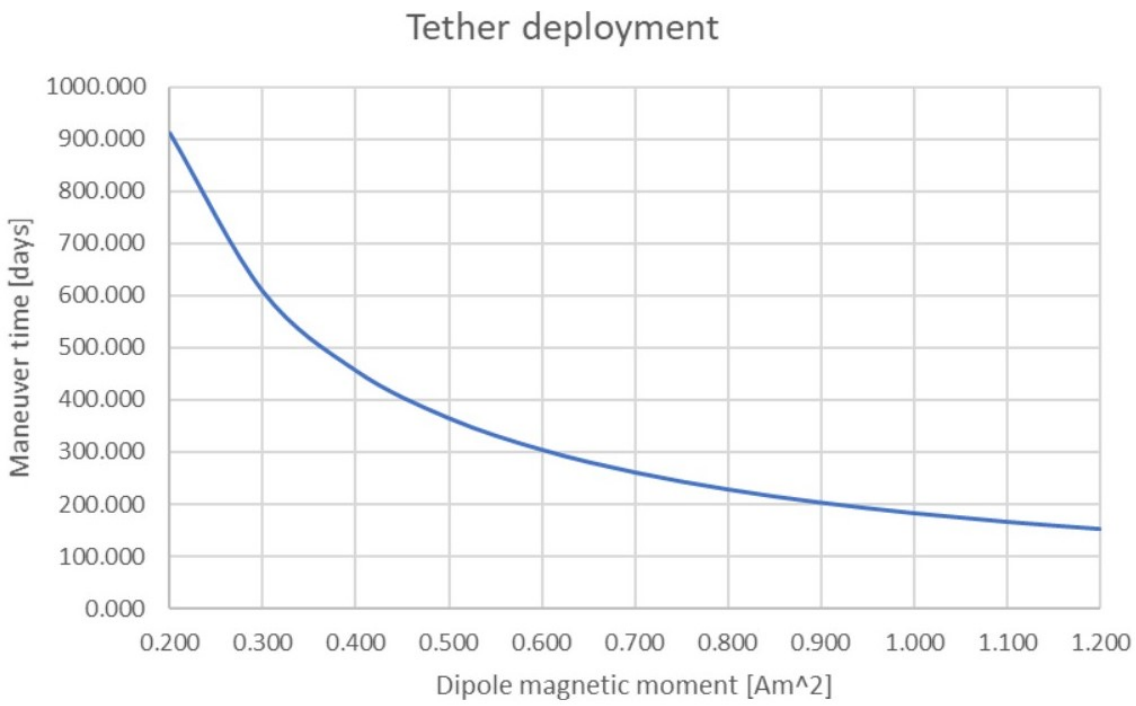

Figure 4.14: Tether deployment using magnetorquers as a function of magnetic dipole (method 2).

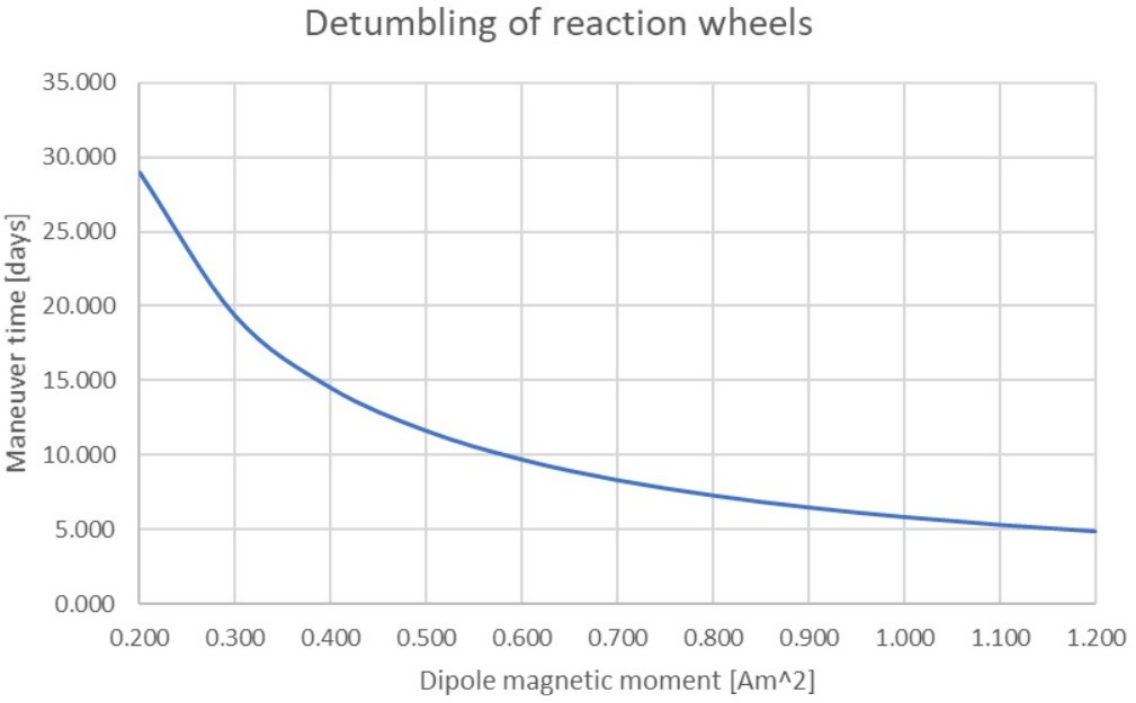

Figure 4.15: Detumbling using magnetorquers as a function of magnetic dipole (method 2).

4.8.4 Integration over one orbit

This method is probably the best one to conclude on the usefulness of magnetorquers as main actuators. It goes without saying that this does not provide accurate results, but highlights the highest performances achievable when using the magnetic field as an energy source. Needless to say, the orbit when the magnetic field is at its peak was taken as an assumption for the entire scenario. It was simulated that the peak would happen on the 5th of January 2023, reaching a maximum of 35140 nT as it can be seen on figure 4.16. The obtained maneuver times are faster than for the two first methods, yet not good enough (see table 4.18, figures 4.17 and 4.18). Indeed, even when the best scenario is happening, it would take up to 128 days to deploy the tether using the highest magnetic dipole usually available for magnetorquers. It is more than 69% of the entire mission lifetime of the satellite, and is more than four times longer than the maximum allocated time. As fo the detumble of the spacecraft, the maneuver times do not change much compared to the other two methods, but it still proves that if magnetorquers are being used, it would be for momentum management of reaction wheels.

In a nutshell, one can conclude that magnetorquers are not powerful enough in the desired GTO environment. They cannot be used as the main actuators of the CubeSat as they can't provide the necessary means to achieve the main requirements imposed by the mission design (see section 4.2). Furthermore, because of the restricted area and time where and when magnetorquers could be used, the risk of a potential failure to provide attitude control might be increased. A total shut down of the mission might then happen as most of the scientific payloads won't be able to perform their tasks.

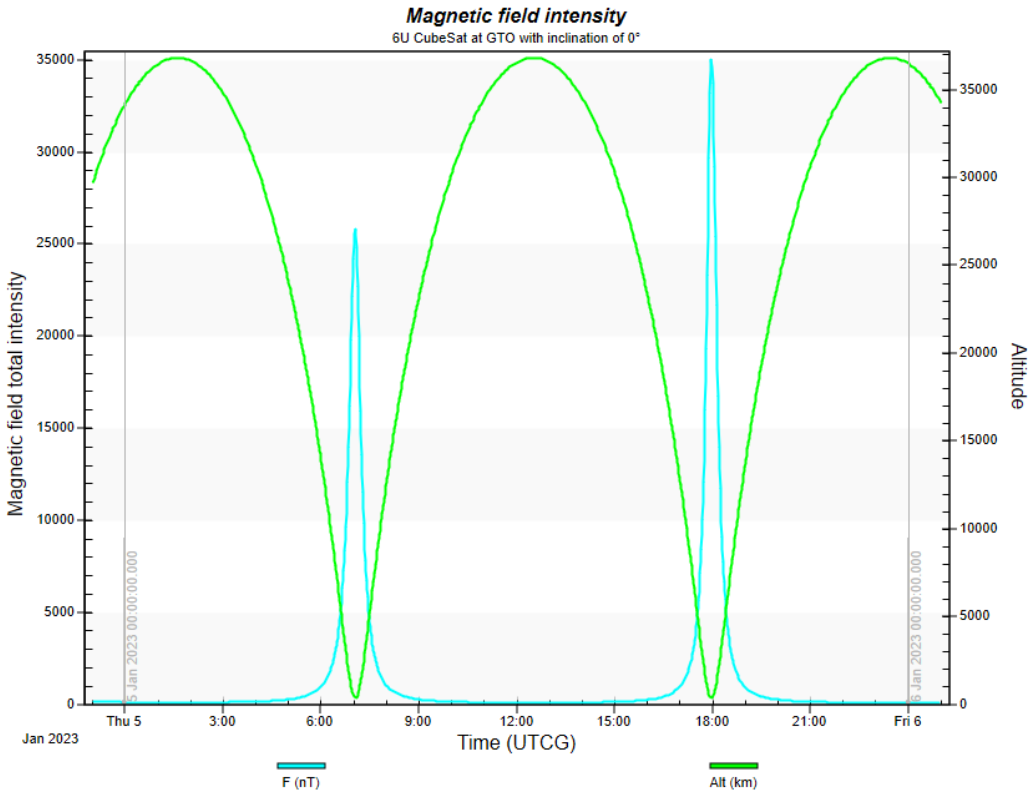

Figure 4.16: Magnetic field intensity (at its peak) and altitude as a function of time.

Magnetic dipole ($A \cdot m^2$))	Maneuver time (days)	
	Tether deployment	Detumbling
0.2	770.637	29.001
0.3	513.758	19.334
0.4	385.318	14.500
0.5	308.255	11.600
0.6	256.879	9.667
0.7	220.182	8.286
0.8	192.659	7.250
0.9	171.253	6.445
1.0	154.127	5.800
1.1	140.116	5.273
1.2	128.439	4.833

Table 4.18: Maneuver times for tether deployment and detumbling (method 3).

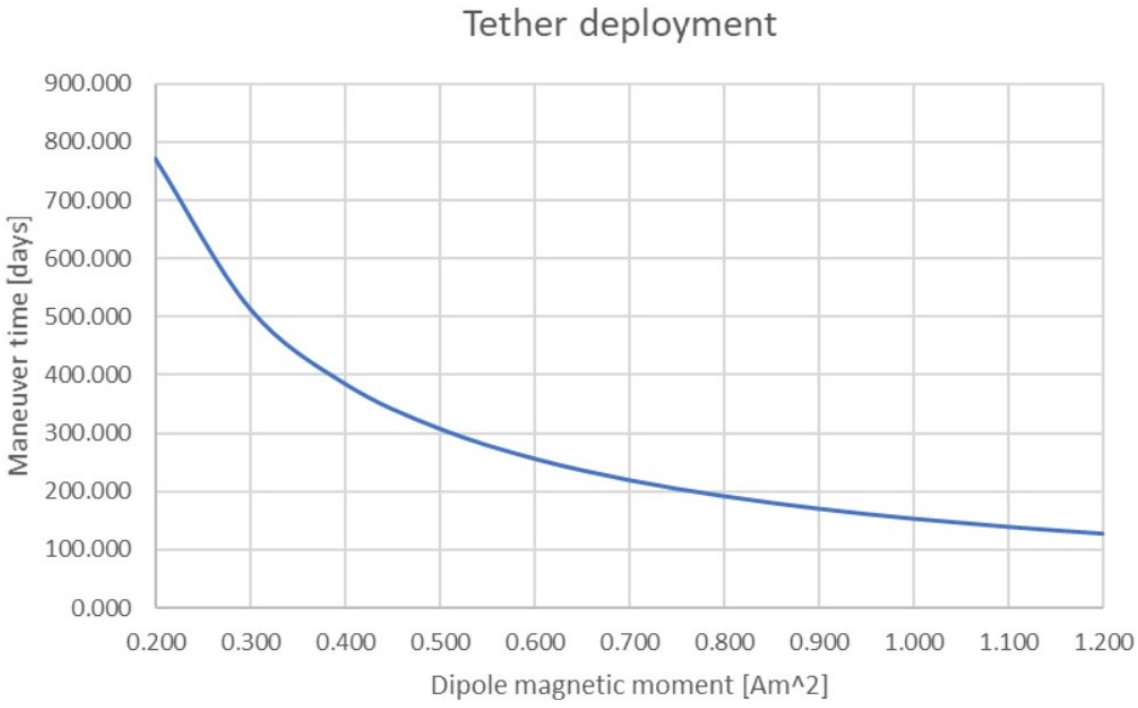

Figure 4.17: Tether deployment using magnetorquers as a function of magnetic dipole (method 3).

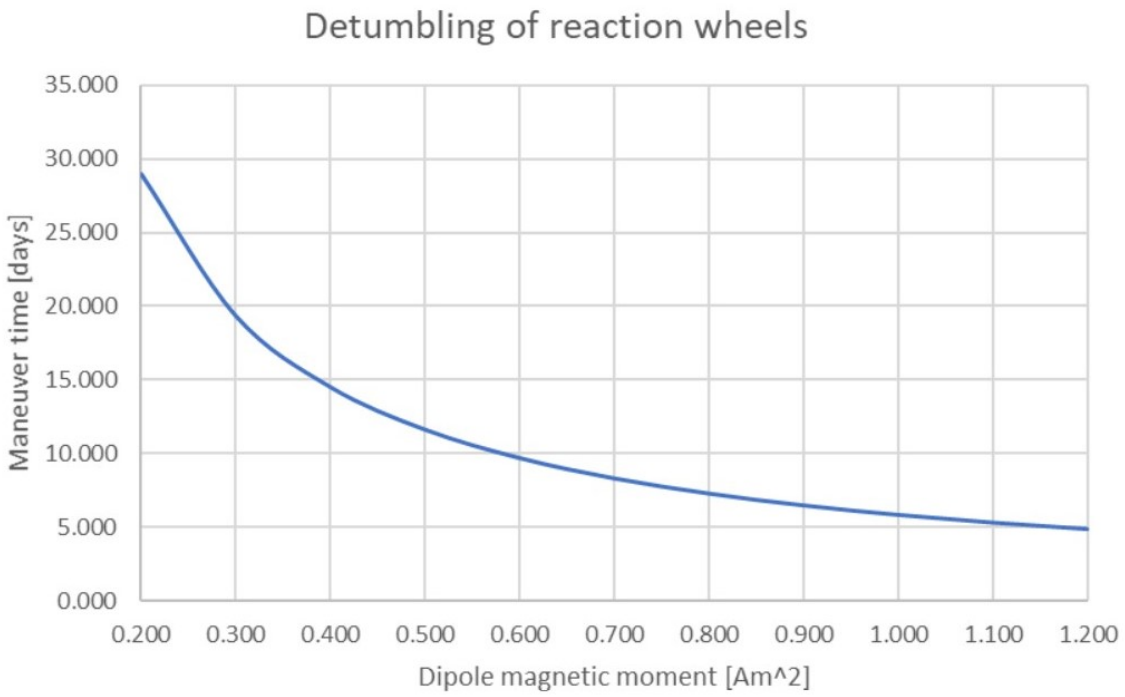

Figure 4.18: Detumbling using magnetorquers as a function of magnetic dipole (method 3).

4.9 Trade-off study - Reaction wheels

4.9.1 Mass and volume limitations

To determine the usefulness of reaction wheels for deploying the tether, one can simply have a look at the available models available on the market and see that in order to achieve an angular momentum of 25.510 Nms, a minimum mass of 6 kg per unit of reaction wheel seems to be needed. Indeed, the model RSI 25-75/60 from Rockwell Collins [40], and the model W18ES from Bradford Space [41] are both capable of providing a momentum of 25 Nms, but weigh 6.3 kg and 6.02 kg respectively. Both models are not only too heavy for a 6U CubeSat, but also too big. As a matter of fact, it was discussed by the project managers of the mission that an ideal size of the ADCS system within the satellite would be to accommodate every sensor and actuator in a 1.5 U volume. The latter leads to have an available volume of $10\,cm \times 10\,cm \times 15\,cm = 1500\,cm^3$ while the RSI 25-75/60 model has a form factor 2.73 times bigger, and the W18ES model has a form factor 2.46 times bigger. It goes without saying that those are the volumes needed by one reaction wheel only, making it simply impossible accommodate a full control attitude system using 3 reaction wheels of the models stated above.

4.9.2 Reaction wheel design

Having said that, it is still interesting to prove mathematically if reaction wheels should be used as main actuators or not.

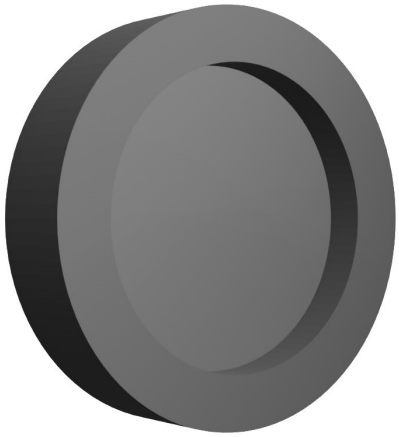

Figure 4.19: Designed model of the reaction wheel.

One way to do that is to design a reaction wheel unit taking into account the requirements and constraints of the satellite and the mission. [42] The goal is to obtain the final momentum a reaction wheel unit can provide taking into consideration the volume and mass constraints. In the following design (see figure 4.19), the reaction wheel should have a maximum mass of 3 kg, and a maximum diameter of 15 cm. The allocated space for the motor is not taken into account here as the purpose of the analysis is to evaluate the impossibility of using a reaction wheel for the critical maneuver needed for the mission.

The unit consists of a disc and a ring, so the mass of one reaction wheel can be decomposed as:

$$m_{RW} = m_{disc} + m_{ring} \tag{4.6}$$

Using the expressions of mass for a cylinder and a ring, equation 4.6 can be derived into:

$$m_{RW} = \rho_{mat}\pi r_{disc}^2 h_{disc} + \rho_{mat}\pi \left(r_{ring}^2 - r_{disc}^2\right) h_{ring} \tag{4.7}$$

Iron has been chosen as the material because of its high density ($7.85 \cdot 10^3\, kg \cdot m^{-3}$). This was done as the goal of the reaction wheel design is to obtain the highest momentum capability. Another material like urethane could have been chosen, but it has a density much lower than iron, meaning that in order to reach the momentum achievable with a reaction wheel made of iron, the reaction wheel made of urethane would need to be much bigger. That is not possible due to the volume constraint imposed by the design here. Thus, iron was the right material to go with for complying with the volume and mass limitations. In order to solve equation 4.7, empirical calculation were made (see below), and the final design parameters are displayed in table 4.19.

Parameter	Value
Radius of the disc	$0.055\,m$
Radius of the ring	$0.075\,m$
Height of the disc	$0.005\,m$
Height of the ring	$0.035\,m$
Mass of the disc	$0.373\,kg$
Mass of the ring	$2.244\,kg$
Mass of the reaction wheel	$2.617\,kg$

Table 4.19: Design parameters of the reaction wheel.

Putting the values of the parameters in, the mass of the disc and the mass of the ring are obtained as:

$$m_{disc} = 7.85 \cdot 10^3 \cdot \pi \cdot 0.055^2 \cdot 0.005 = 0.373\,kg$$

$$m_{ring} = 7.85 \cdot 10^3 \cdot \pi \cdot \left(0.075^2 - 0.055^2\right) \cdot 0.035 = 2.244\,kg$$

Summing up the two masses calculated above, one can get the mass of the reaction wheel unit for the given size parameters:

$$m_{RW} = 0.373 + 2.244 = 2.617\,kg$$

Now that all design parameters are known, the next step is to calculate the inertial momentum of the reaction wheel unit. Using equations 4.8 and 4.9 below [43], one can derive the inertias produced by the two elements that compose the reaction wheel (the disc and the ring):

$$I_{disc} = \frac{m_{disc} r_{disc}^2}{2} \tag{4.8}$$

$$I_{ring} = \frac{m_{ring}\left(r_{ring}^2 + r_{disc}^2\right)}{2} \tag{4.9}$$

The inertial momentums obtained are $5.642 \cdot 10^{-4}\,kg \cdot m^{-2}$ for the disc, and $9.706 \cdot 10^{-3}\,kg \cdot m^{-2}$ for the ring. Finally, one can simply derive the total inertial momentum of the reaction wheel by summing up the results obtained for the two components:

$$I_{RW} = I_{disc} + I_{ring} \tag{4.10}$$

Thus, the designed reaction wheel will have a total inertial momentum of $1.027 \cdot 10^{-2}\,kg \cdot m^{-2}$. To finalize the design of the reaction wheel, it is needed to calculate the maximum angular momentum that the unit can provide using the following equation:

$$h_{max} = I_{RW}\omega_{max} \tag{4.11}$$

Looking at the available reaction wheels on the market, it seems that for the targeted angular momentum, the operational speed of the motor oscillates between 4300 RPM and 6000 RPM. A motor with an operational speed of 6000 RPM is chosen here as the goal is to get maximum angular momentum that can be provided to the satellite. Using equation 4.11 [44], the latter has the following value:

$$h_{max} = 1.027 \cdot 10^{-2} \cdot 6000 \cdot \frac{2\pi}{360} = 1.076\ Nms$$

The calculated value is far from being enough compared to the angular momentum needed to deploy the tether. Thus, it is needless to say that reaction wheels cannot be used as the main actuator on-board the satellite. However, looking at the requirements in section 4.2, it is stated that an ideal spin period of 20 seconds is wanted by the science teams. This means that when the satellite will operate in fine pointing mode, the actual spin rate of the spacecraft will be $18\ deg \cdot s^{-1}$, or $0.314\ rad \cdot s^{-1}$. This spin-rate is easily achievable by reaction wheels much smaller than the one designed in this section. Consequently, using reaction wheels as second actuator on-board of FS-2 seems to be a better fit already then magnetorquers, taking into consideration the instability of the magnetic field on the targeted orbit. Moreover, the reaction wheel designed was limited by two constraints which where the mass and the volume, yet it was only one unit. It is well known that three reaction wheels are needed to get full control of the satellite attitude. In this case, it would mean having a total mass of $7.851\ kg$ when a total targeted mass of the satellite including all subsystems is $7\ kg$. Additionally, the size constraint is not respected either as accommodating three reaction wheels having a diameter of $15\ cm$ into a 6U CubeSat is not possible. Accordingly, the only option remaining is using a propulsion system for the tether deployment, which will be studied in the next section.

4.10 Trade-off study - Thrusters

The analysis here will focus on the use of propulsion units as a mean for accomplishing the critical mission phase. As a matter of fact, the latter sets key points on the maneuver time, the propellant mass needed, and the energy required for a trade-off study.

4.10.1 Propulsion theory and formulas

Specific impulse

The specific impulse, noted I_{sp} and expressed in seconds, is the total impulse per unit weight of propellant. It is a significant aspect of the propulsion system of a rocket or a spacecraft, and highlights how efficient it actually is. [45] If one assumes constant propellant flow and constant thrust, the equation can be expressed as:

$$I_{sp} = \frac{I_t}{m_p g_0} \tag{4.12}$$

where I_t is the total impulse (thrust force integrated over a burning time), and m_p is the total effective propellant mass.

Energy required

One important factor to look at is the energy required for the planned maneuver. It was already shown that generating power will be a challenge on the designed mission. As a consequence, making an estimation of the required energy for the tether deployment is needed. One can calculate the required energy using the equation below:

$$E_{required} = P_{thruster} \cdot t_{maneuver} \tag{4.13}$$

where $P_{thruster}$ is the power consumption of the propulsion unit, and $t_{maneuver}$ is the time needed to deploy the tether.

Maneuver time

To calculate the maneuver time, a similar analysis as in section 4.8.1 is done to derive a formula. Thus, the following equation expresses the way to calculate the maneuver time:

$$t_{maneuver} = \frac{I_{t_{required}}}{T} \tag{4.14}$$

where $I_{t_{required}}$ is the total impulse required to deploy the 300 meters long tether, and T is the thrust generated by the chosen propulsion unit.

4.10.2 Inputs and analysis set-up

The first task was to have a look at the available thrusters for CubeSats in the market. There are numerous models, using different types of propulsion, but only two were selected: cold gas propulsion and electric propulsion.

Cold gas systems are usually simple able to provide a consequent propulsion for small satellites. Moreover, the technology of such systems belong to the most mature ones. They are used quite often for small buses because of their low complexity, their robustness, and their cheap prices. One advantage of this technology is the low energy that is required for maneuvers. When missions (such as FORESAIL-2) have a small power budget, it is generally unwise to use electric propulsion because of the high risks this technology brings in special mission cases. However, the propellant and the fuel tank adds not only more weight to the final mass of the satellite, but also complexity. On the other hand, during the last few years, electric propulsion has seen its technology maturity to be improved, but also its availability as more providers are able to work on such systems. Some missions require high specific impulses to generate the required total impulse to accomplish a maneuver. Electric propulsion provides the means for that. Notwithstanding, the trade-off is done on the maneuver time and results in very long propulsion periods (meaning a higher power consumption as well). [46]

Tables 4.20 and 4.21 below display which thrusters have been selected for the analysis. For both types of propellant, five thrusters from different providers were chosen in order to make a good comparison and have a clear idea on the maneuver time, propellant mass, and required energy. The important parameters to obtain from the datasheets for each model were the specific impulse, the thrust, and the power consumption. The models have been selected setting an important limit on the weight, and only propulsion units that can be accommodated on a 6U CubeSat such as FS-2.

Propulsion unit	**Manufacturer**
IFM Nano Thruster [47]	Enpulsion
BIT-1 [48]	Busek
nanoFEEP [49]	Morpheus Space
Tile 50 [50]	Accion
NanoPPT [51]	Clyde Space Ltd

Table 4.20: Selected electric propulsion units.

Propulsion unit	**Manufacturer**
OT [52]	Aurora Propulsion Technologies
NanoProp 6U [53]	GOMspace
POPSAT-HIP1 [54]	Micro Space
PUC [55]	VACCO
MiPS [56]	VACCO

Table 4.21: Selected cold gas and water-based propulsion units

As the tether deployment needs to be done in the Z-axis only, a minimum of two propulsion units is needed to provide accurate and stable thrust generation. Figure 4.20 displays such a configuration.

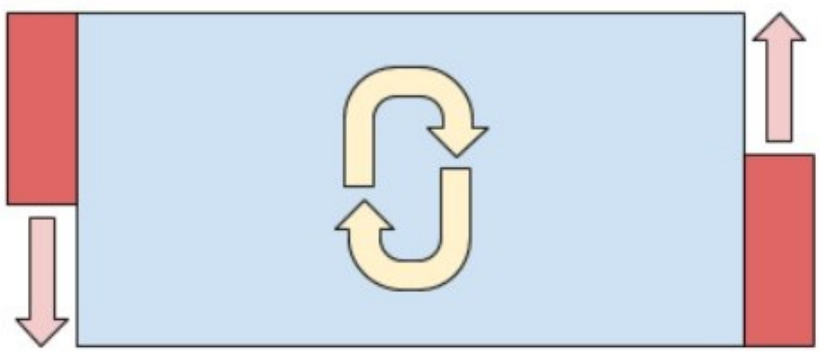

Figure 4.20: Thrusters configuration view from below the satellite. The blue box represents the CubeSat, the red boxes the propulsion units, the red arrows the direction of the generated thrust, and the yellow arrows the rotation that results.

4.10.3 Results

Cold gas and water-based propulsion

As expected from the propulsion units using cold gas (and liquid) technology, the maneuver time is rather low. Indeed, it was already stated in section 4.8 that a maximum maneuver time of one month is allowed for the mission. Here, this limt is far from being exceeded, with a maximum maneuver time of 66.875 hours using POPSAT-HIP1. The most efficient unit in terms of maneuver time is the MiPS model, being able to deploy the tether entirely in less than an hour (0.669 hours, that is around 40 minutes). The difference between the maneuver times can be explained by the size of some thrusters. OT and POPSAT-HIP1 are part of the smallest propulsion units available on the market, therefore reducing the maximum specific impulses and thrusts they can generate. One can wonder what is the most important aspect to tale from this analysis. As all thrusters provide an efficient way of deploying the tether in less than a month, the trade off will not take this factor into account here. Regarding the energy required, all models seem to be efficient in this way, as the technology is not based on power generation unlike electric propulsion. MiPS is the most efficient in terms of maneuver time and energy required, but needs a propellant mass of 122.706 g, which is much larger than the other models. On the other hand, OT from Aurora Propulsion Technology is a model that requires only 49.083 g of propellant (it is actually the best one in that sense), and would consume 33.438 Wh for the entire maneuver. Compared to the other models of the list, it seems like this model is the perfect balance between all the points stated above. In addition to that, the university of Aalto and Aurora Propulsion Technology work in collaboration on the FS-1 and FS-2 projects, thus making them the favoured manufacturer. All numbers and results of the analysis can be seen in table 4.22, figures 4.21, 4.22 and 4.23.

Propulsion unit	$t_{maneuver}$ **(hours)**	m_p **(g)**	$E_{required}$ **(Wh)**
OT	33.438	49.083	33.438
NanoProp 6U	6.688	81.804	26.750
POPSAT-HIP1	66.875	98.165	66.875
PUC	1.338	70.118	40.125
MiPS	0.669	122.706	13.375

Table 4.22: Maneuver time, propellant mass, and energy required for each cold gas and water-based propulsion unit chosen for the analysis.

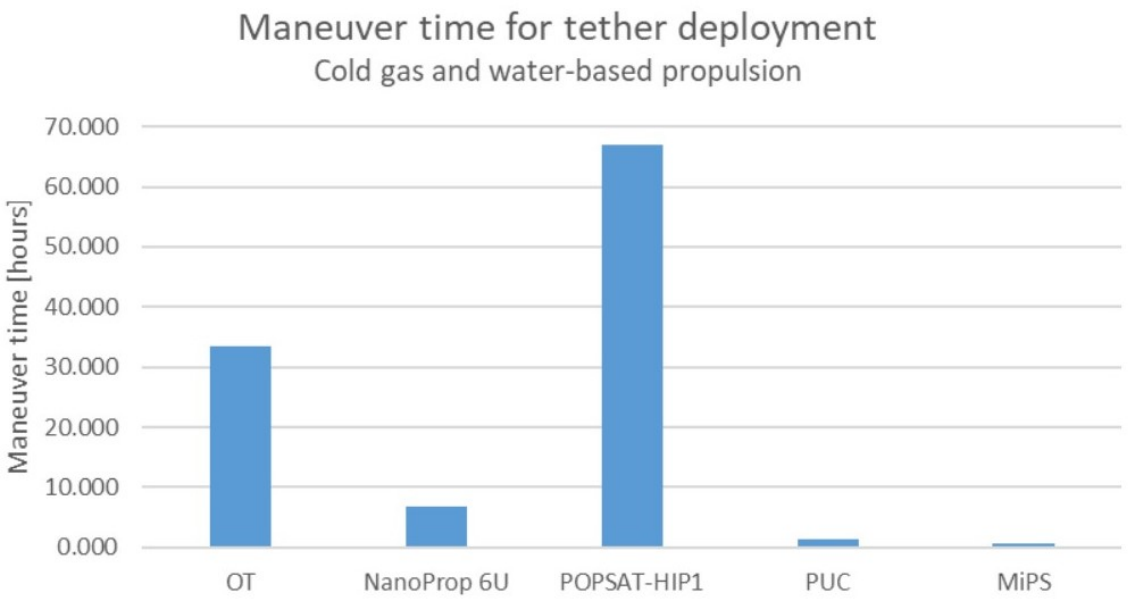

Figure 4.21: Maneuver time needed for tether deployment when using cold gas and water-based propulsion technology.

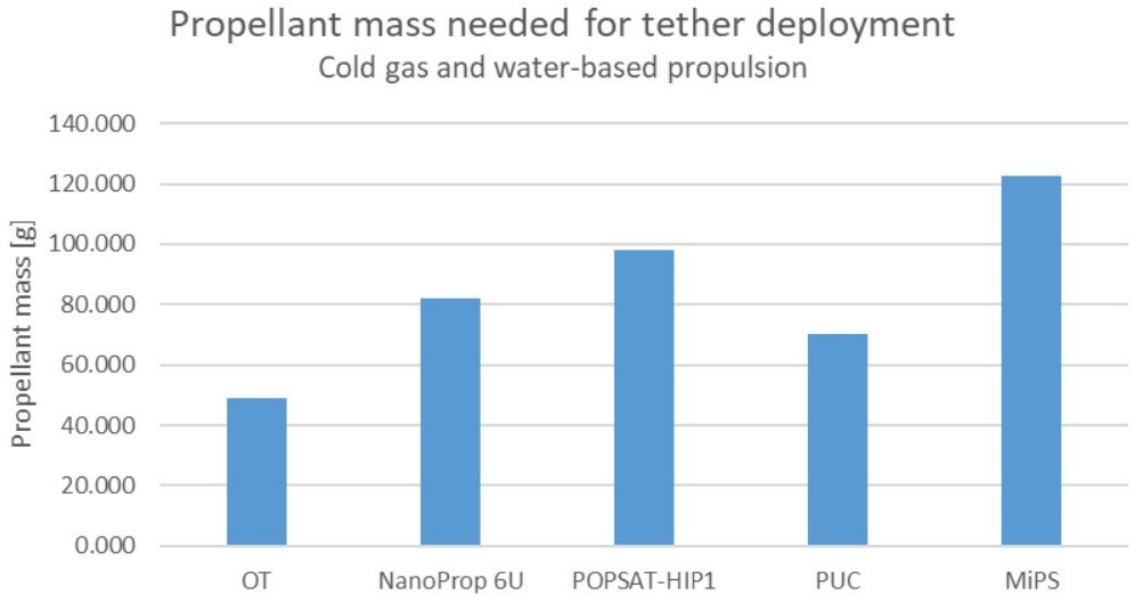

Figure 4.22: Propellant needed for tether deployment when using cold gas and water-based propulsion technology.

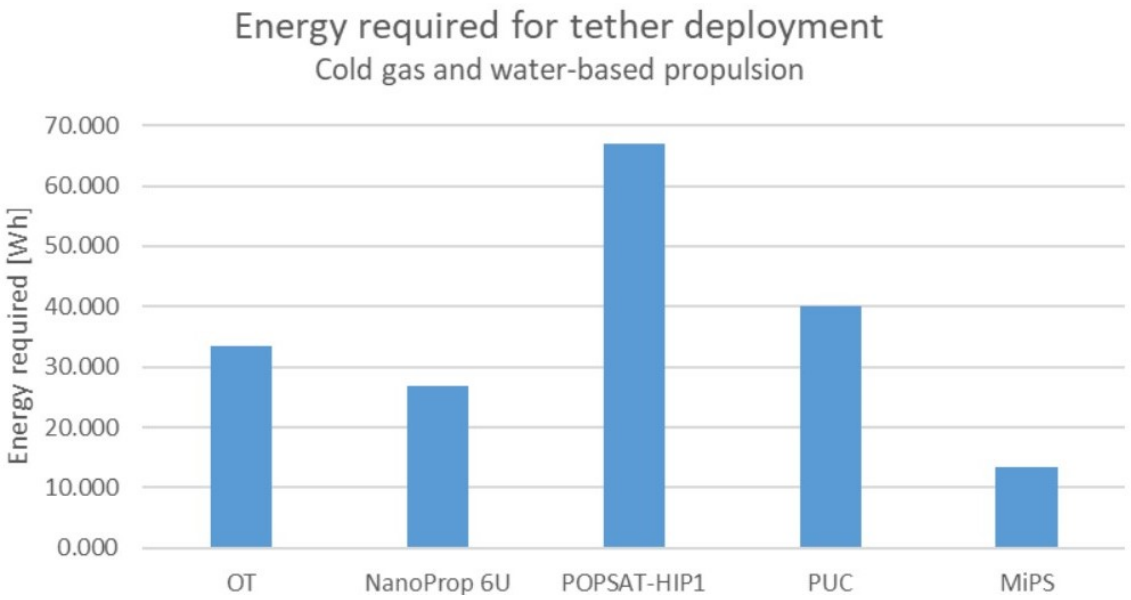

Figure 4.23: Energy required for tether deployment when using cold gas and water-based propulsion technology.

Electric propulsion

Compared to cold gas and water-based technology, the maneuver time for tether deployment is longer when electric propulsion units are used. However, they still comply with the time limit of one month imposed by the mission design, with maneuver times ranging from 19.107 hours with IFM Nano Thruster to 167.188 hours with nanoFEEP. Because of the technology that is used, the propellant mass needed is close to zero, saving a few hundreds of grams that could result in less money spent for the launch. Thus, the latter will not be taking into account when selecting the potential thruster unit as it can be negligible. Nevertheless, the important information to look at here is the energy required for the maneuver. It can be seen that using electric propulsion consumes much more than for cold gas, which could be a problem as specified in section 4.4.3. The power generation on-board FS-2 is yet to be analysed by the EPS team, and the decision on using deployable solar panels is yet to be taken as the mission budget is still rather unsure at the moment. As a result, the available power to be fed to the electric propulsion unit could be very low, resulting in the impossibility of accomplishing the desired maneuver. Nonetheless, if one assumes deployable solar panels, then it seems like Tile 50 is a good compromise. The latter achieve the maneuver quite fast, in 133.750 hours, does not require much propellant as it uses tiled liquid electrospray, and consumes less than the other electric propulsion units, with a total of 401.250 Wh for the tether deployment. All numbers and results of the analysis can be seen in table 4.23, figures 4.24, 4.25 and 4.26.

Propulsion unit	$t_{maneuver}$ $(hours)$	m_p (g)	$E_{required}$ (Wh)
IFM Nano Thruster	19.107	2.454	1528.571
BIT-1	36.149	3.068	2024.324
nanoFEEP	167.188	1.636	1003.125
Tile 50	133.750	3.927	401.250
NanoPPT	74.306	7.669	743.056

Table 4.23: Maneuver time, propellant mass, and energy required for each electric propulsion unit chosen for the analysis.

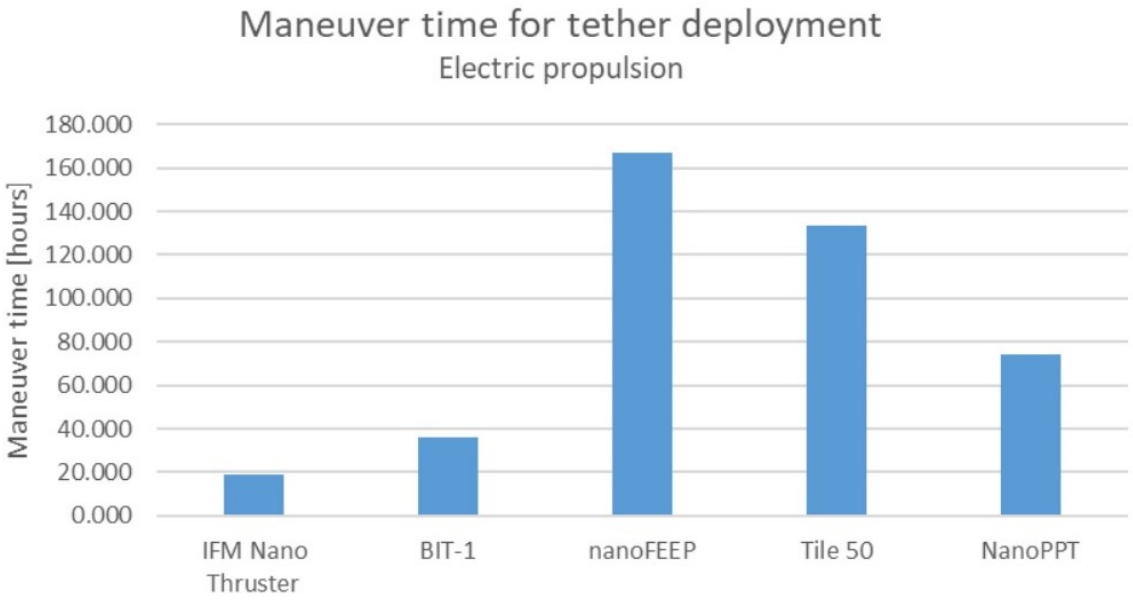

Figure 4.24: Maneuver time needed for tether deployment when using electric propulsion technology.

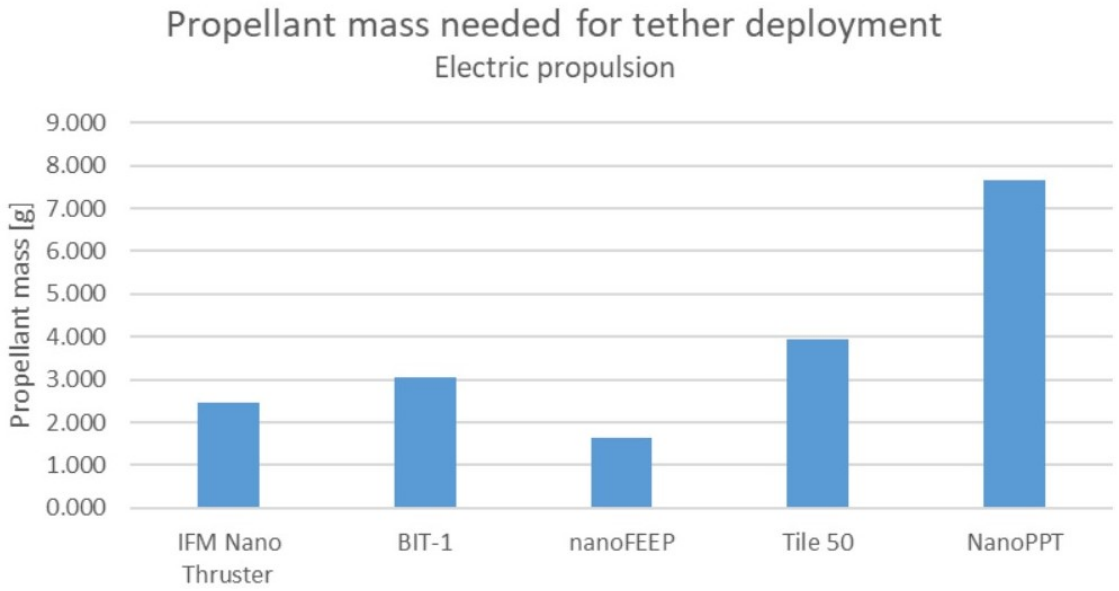

Figure 4.25: Propellant needed for tether deployment when using electric propulsion technology.

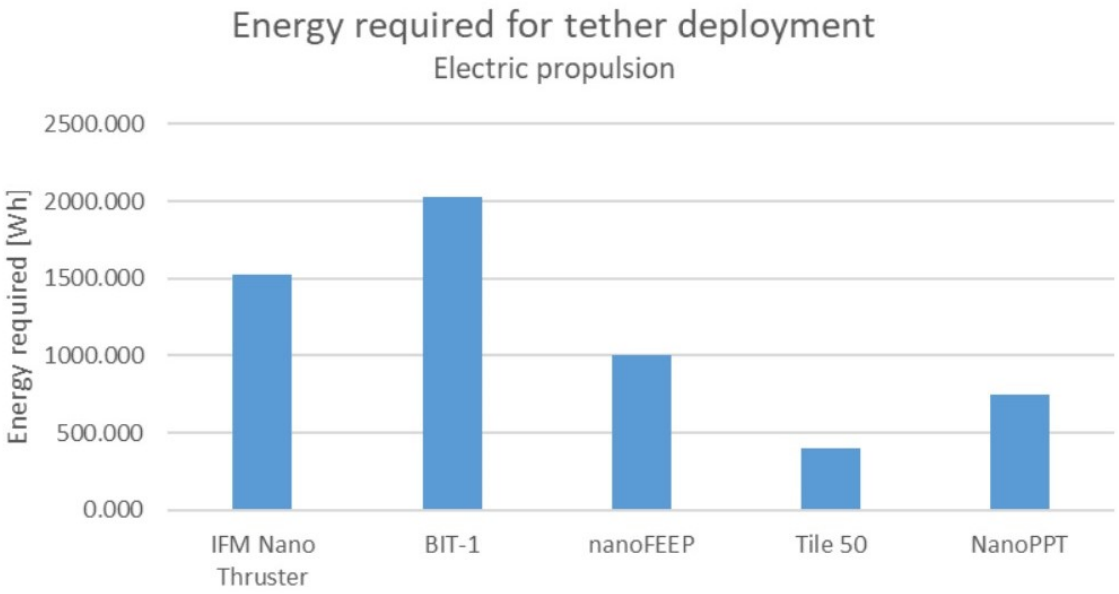

Figure 4.26: Energy required for tether deployment when using electric propulsion technology.

This analysis proved that using propulsion for deploying the tether seems to be the right choice. Not only does it save time on the deployment maneuver, it also allows more time for the science team to make measurements. Two units, using different propulsion technologies, are chosen for a potential use in the AOCS configuration: OT from Aurora Propulsion Technology, and Tile 50 from Accion. They both fulfill the time requirement for the maneuver, and while OT saves energy for the other subsystems of the CubeSat, Tile 50 saves approximately 100 g of mass to be added to the final mass budget of the satellite. The next section will enumerate the final list of sensors and actuators (in an AOCS configuration) needed in order to fulfill the mission requirements (section 4.2).

4.11 AOCS Configurations

4.11.1 Attitude sensor set

The main considerations for choosing the sensors that will be accommodated on FORESAIL-2 is the ability to provide the required accuracy of 3° while the satellite is spinning. Other considerations are the mass, the volume, the power consumption, and the radiation dose limit. As seen in section 4.7.1, Earth sensors and DPS are excluded from the configuration because of the technologies not matching with the mission. Star trackers are excluded as well because of the tracking rate they have. Indeed, the maximum limit is usually of about 10 degrees per second. FORESAIL-2 has a desired spin rate of 18 degrees per second when working in normal mode, which is already almost twice the maximum threshold value stated earlier. Moreover, the optics and the baffle add a mass contribution that is not negligible for a 6U CubeSat. Sun sensors provide the satellite with the necessary attitude determination accuracy. Nonetheless, because they can't be used in the eclipse region, they have to be placed on all faces of the CubeSat to maximise the FoV. The angular rate is one of the

most important measurements, therefore, gyroscopes in an IMU will be added in the configuration. An IMU is preferred over simple gyroscopes because of the low gyro noise and low gyro bias instability it can provide. Magnetometers have a low accuracy compared to other sensors, yet provide the necessary accuracy for the mission as this one is quite large. They can back up the Sun sensors in LEO region and during tether deployment as the FoV is not limited. Even though the GPS network is limited above the LEO region, the constraint on the position knowledge is of hundreds of meters. After a discussion with the team, it was decided to use a GPS to propagate the satellite when this one will be able to reach the signal. Finally, a radiation sensor and a temperature (housekeeping sensors) will be added to keep an eye on the subsystem. The satellite will go though environments where those two elements will change drastically, thus it is important to include them to foresee any complications that would put the mission at risk.

4.11.2 Attitude actuator set

The different actuators were tested for the specific maneuver that is the tether deployment. The outcome of those analyses was that only a propulsion system is able to provide the required momentum. Reaction wheels are added in combination with the propulsion system to provide the satellite with attitude control before the tether deployment. Because of the external disturbances that impact the satellite, detumbling the reaction wheels will be needed over time. This will be accomplished by a set of additional thrusters added on the spacecraft. In total, a minimum of eight propulsion units should be set on the CubeSat. A mimimum of two thrusters for the tether deployment maneuver, and a mimimum of six thrusters for detumbling the three reaction wheels put in all three axes.

4.11.3 Summary of the AOCS set

Table 4.24 below displays the recommended AOCS configuration for FORESAIL-2.

Element	Number	Role
Sun sensors	6	Attitude determination
Magnetometers	3	Attitude determination
GPS	1	Attitude determination
IMU	1	Attitude determination
Radiation sensor	1	Housekeeping
Temperature sensor	1	Housekeeping
Reaction wheels	3	Attitude control
Propulsion units	8	Attitude control

Table 4.24: Recommended AOCS configuration for FORESAIL-2.

4.12 COTS availability

This section displays which components are chosen to define a baseline of the attitude determination and attitude control hardware.

4.12.1 Attitude determination

Sun sensors

FORESAIL-2 will be using the same Sun sensors as FORESAIL-1. They are developed by Aalto University based upon the Hamamatsu S5990-1 PSD.

Characteristic	Specification	Unit
Field of view	90	°
Accuracy	0.056	°
Update rate	100	Hz
Sampling time	4	ms
Operating voltage	$2-5$	V
Power consumption	0.004	W
Mass	0.004	kg
Dimensions	$26 \times 14 \times 4$	mm^3
Cost	50	€
Number of units	6	N/A

Table 4.25: Characteristics of the PSD Sun sensor designed by Aalto University.

Magnetometers

FORESAIL-2 will be using the NMRM-001-485 tri-axial magnetometer from NewSpace Systems as a baseline. The latter provides measurements in all axes, with an included temperature sensor. Because of the inability to place this unit at the end of a rigid boom, it includes precision processing, low noise and analogue to digital conversion which improve the linearity and reduce the sensitivity drifting effect. [57]

Characteristic	Specification	Unit
Orthogonality	± 1	°
Measurement range	± 60000	nT
Resolution	8	nT
Update rate	18	Hz
Dimensions	$96 \times 45 \times 20$	mm^3
Mass	0.067	kg
Operating voltage	5	V
Power consumption	0.550	W
Temperature range	-25 to $+70$	$°C$
Radiation tolerance	10	$krads$
Cost	15000	$
Number of units	1	N/A

Table 4.26: Characteristics of the NMRM-001-485 3-axial magnetometer by NewSpace Systems.

GPS

The information about the position of the satellite is needed to compute the orbital velocity and position vectors, but also for the science team so that the measurements done by the payloads can be processed. The current solution is provided by NovAtel and PCTEL with the OEM7600 dual-frequency GNSS receiver [58] and the 3961D embedded GPS antenna. [59]

Characteristic	**Specification**	**Unit**
Horizontal position accuracy	1.5	m
Velocity accuracy	< 0.03	$m \cdot s^{-1}$
Update rate	$1 - 100$	Hz
Dimensions	$35 \times 55 \times 13$	mm^3
Mass	0.031	kg
Operating voltage	3.3	V
Power consumption	$0.9 - 1.3$	W
Temperature range	-40 to $+85$	$°C$
Number of units	1	N/A

Table 4.27: Characteristics of the OEM7600 dual-frequency GNSS receiver by NovAtel.

Characteristic	**Specification**	**Unit**
Frequency range	1575.42 ± 10	MHz
Noise figure	$0.5dB$	$m \cdot s^{-1}$
LNA Gain	28 at $3.3\,V$	dB
Nominal impedance	50	$Ohms$
Dimensions	$47 \times 8 \times 1$	mm^3
Mass	0.016	kg
Operating voltage	$2.7 - 5$	V
Current draw	7.5 at $3.3\,V$	mA
Temperature range	-40 to $+85$	$°C$
Number of units	1	N/A

Table 4.28: Characteristics of the 3961D embedded GPS antenna by PCTEL.

IMU

The STIM300 model is the current choice for the IMU and is manufactured by Sensonor. It contains three highly accurate MEMS gyros, three high stability accelerometers and three inclinometers. [60] Here the focus is only put on the gyroscopes as the angular rate of the satellite is a key point for the succeeding the mission.

Characteristic	Specification	Unit
Input range	± 400	$^\circ \cdot s^{-1}$
Resolution	0.22	$^\circ \cdot h^{-1}$
Bias	± 250	$^\circ \cdot h^{-1}$
Bias instability	0.3	$^\circ \cdot h^{-1}$
Dimensions	$38.6 \times 44.8 \times 21.5$	mm^3
Mass	0.055	kg
Operating voltage	$4.5 - 5.5$	V
Power consumption	$1.5 - 2$	W
Temperature range	-40 to $+85$	$^\circ C$
Number of units	1	N/A

Table 4.29: Characteristics of the STIM300 IMU by Sensonor.

4.12.2 Attitude control

Propulsion units

Two different propulsion units will be needed on-board the satellite. One unit composed of two thrusters use as main actuators for tether deployment only, and another one composed of six thrusters minimum for attitude control only (detumbling of the reaction wheels). Aurora Propulsion Technologies offers the current solution by providing both units, Orbital Thruster [52] and Attitude and Orbit Control System. [61] The latter is composed of an array of 12 individual thrusters able to provide scalable and efficient thrust for spacecraft control. It is capable of attitude adjustments and orbital control maneuvers.

Characteristic	Specification	Unit
Thrust	$0.2 - 2$	mN
Specific Impulse	$100 - 130$	s
Power consumption	$0.5 - 5$	W
Dry mass	0.100	kg
Dimensions	$30 \times 100 \times 100$	mm^3
Number of units	2	N/A

Table 4.30: Characteristics of the Orbital Thruster propulsion unit by Aurora Propulsion Technologies.

Characteristic	Specification	Unit
Thrust	$0.2 - 2$	mN
Specific Impulse	$100 - 130$	s
Power consumption	$0.5 - 5$	W
Dry mass	0.250	kg
Dimensions	$100 \times 100 \times 30$	mm^3
Number of units	1	N/A

Table 4.31: Characteristics of the Attitude and Orbit Control System propulsion unit by Aurora Propulsion Technologies.

Reaction wheels

The reaction wheels will provide the required torque in safe and normal modes. They are used as secondary actuators for fine pointing maneuvers, and especially for delivering the required spin rate for the instruments on-board the satellite. The required momentum storage can be integrated using the formula proposed by Wertz and Larson [62] for the worst-case disturbance torque over one full orbit:

$$h_{max} = T_{dist} \frac{1}{\sqrt{2}} \frac{t_{orbit}}{4} \tag{4.15}$$

It is assumed that the momentum us built up in one quarter of an orbit. Using the calculation from section 3.2.1 for the external disturbances, and the period stated in 4.3, one can obtain the desired reaction wheel's size:

$$h_{max} = 6.136 \cdot 10^{-6} \cdot \frac{1}{\sqrt{2}} \cdot \frac{39384}{4} = 42.719\, mNms$$

The AOCS design includes three reaction wheels located in all axes of the satellite frame. The reaction wheel unit chosen as a baseline is the RW3-0.06 model from Sinclair Interplanetary. [39]

Characteristic	Specification	Unit
Angular momentum	$0.060 - 0.180$	Nms
Maximum torque	± 20 at $0.12\, Nms$	mNm
Dimensions	$77 \times 65 \times 38$	mm^3
Mass	0.226	kg
Operating voltage	$7.5 - 34$	V
Power consumption	0.5 at $0.060\, Nms$	W
Temperature range	-40 to $+70$	$°C$
Radiation tolerance	20	$krads$
Cost	35000	\$
Number of units	3	N/A

Table 4.32: Characteristics of the RW3-0.06 reaction wheel by Sinclair Interplanetary.

4.13 System budgets - SWaP

With the selection of the different sensors and actuators from available COTS, the system budgets simplified in SWaP for CubeSats can be seen in table 4.33. It is an efficient way to keep track of the different budgets of the satellite, and follow the ECSS-E-ST-10C (system engineering general requirements).

Item	Size (cm^3)	Weight (kg)	Peak power (W)
AOCS Platform	**1628.663**	**1.471**	**20.374**
Reaction wheels	570.570	0.678	1.500
Propulsion	900.00	0.600	15.000
Sun sensors	8.736	0.024	0.024
Magnetometer	86.400	0.067	0.550
GPS	25.025	0.031	1.3
Antenna	0.752	0.016	N/A
IMU	37.180	0.055	2.000

Table 4.33: AOCS Platform budgets simplified in SWaP for FORESAIL-2.

4.14 Modes and functional architecture

4.14.1 Functional architecture

The modes for FS2 will follow the architecture shown in figure 4.27. The safe mode (usually used for detumble and Sun acquisition) includes two modes named Safe Mode (SM) and Coarse Pointing Mode (CPM). The normal mode will be used for mission execution and includes two modes named Fine Pointing Mode (FPM) and Tether Pre-Deployment Mode (TPDM). Finally, the Orbit Maintenance and Deorbit Mode (OMDM) is defined but its use is still to be determined depending on the launching options available. It should be used for the acquisition and maintenance of the operational orbit alongside a deorbit process as one has to make sure that the presence of the satellite after the end of its nominal mission does not exceed 25 years.

Following what was said in section 4.11, the Sun sensors, the IMU and the reaction wheels are used in SM, CPM and FPM. Magnetic measurements for AOCS are realized using the three-axial magnetometer unit while the radiation and temperature sensors are used for housekeeping purposes. A dual-frequency GPS receiver is used to obtain the orbit position knowledge. The propulsion units are used in TPDM and OMDM (with the exception of using the thrusters in FPM for detumbling the reaction wheels).

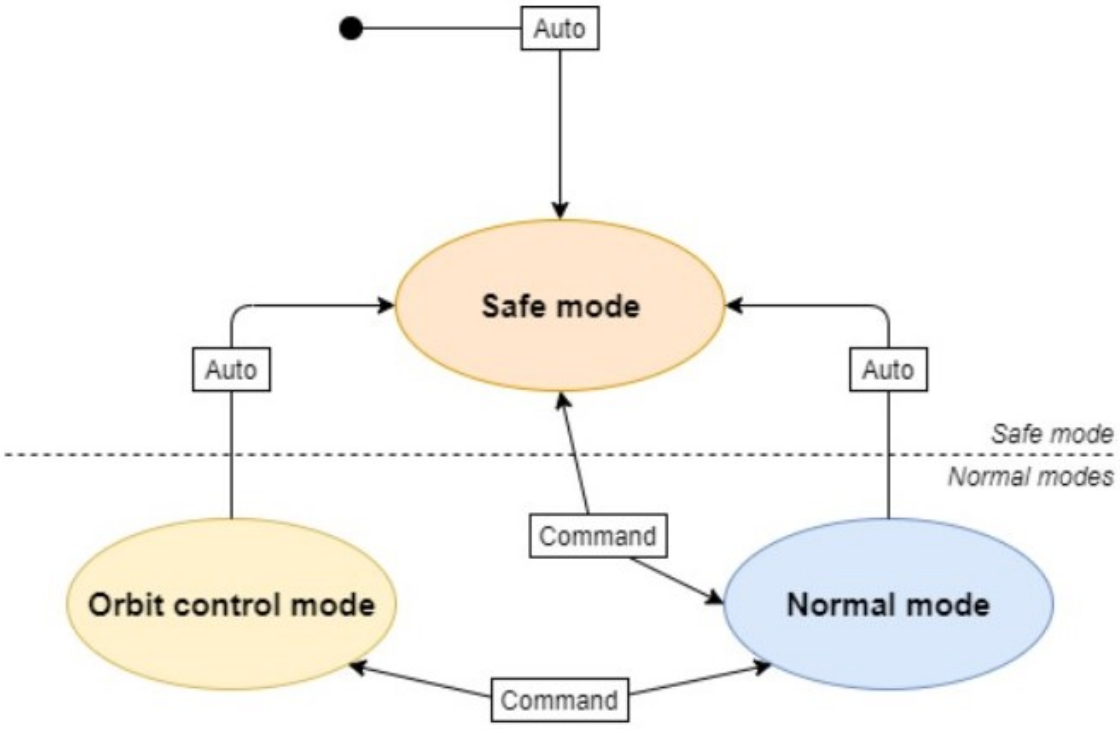

Figure 4.27: FORESAIL-2 Mode architecture

4.14.2 Safe Mode

In this mode, the system will boot up and start sending telemetry. It will receive commands, and data from housekeeping sensors will be available. The control actuators and determination sensors are turned off.

Booting up	YES
AOCS sends telemetry	YES
AOCS receives commands	YES
Data available	Housekeeping sensors
Actuators for attitude control	OFF
Actuators for tether deployment	OFF
Actuators for orbit control	OFF
Sensors for attitude and orbit determination	OFF

Table 4.34: Safe Mode's key points

4.14.3 Coarse Pointing Mode

In this mode, the functionalities of the previous mode will keep on being effective. Additionally, the three-axial magnetometer unit and the IMU sensors will be turned on. The GPS data will be available and the control over the CubeSat momentum only will be possible.

AOCS sends telemetry	Yes
AOCS receives commands	Yes
Data available	Housekeeping sensors, GPS, IMU, Sun sensors, 3-axial magnetometer
Actuators for attitude control	ON for momentum management only
Actuators for tether deployment	OFF
Actuators for orbit control	OFF
Sensors for attitude and orbit determination	ON

Table 4.35: Coarse Pointing Mode's key points

4.14.4 Fine Pointing Mode

This is the mission execution mode. All sensors will be on in order to provide the CubeSat with an accuracy of less than 3° in all axes. The reaction wheels will be on as well and able to provide control over the satellite with a pointing accuracy of less than 2° in all axes. The actuators will also provide control over the spin rate of the CubeSat, with a period of 20 seconds in the best-case scenario.

AOCS sends telemetry	Yes
AOCS receives commands	Yes
Data available	Housekeeping sensors, GPS, IMU, Sun sensors, 3-axial magnetometer
Actuators for attitude control	ON
Actuators for tether deployment	OFF
Actuators for orbit control	OFF
Sensors for attitude and orbit determination	ON

Table 4.36: Fine Pointing Mode's key points

4.14.5 Tether Pre-Deployment Mode

This mode will mostly provide the satellite with sufficient momentum in order to deploy the tether. All actuators and sensors are on to provide the same attitude determination and control accuracies as in the Fine Pointing Mode.

AOCS sends telemetry	Yes
AOCS receives commands	Yes
Data available	Housekeeping sensors, GPS, IMU, Sun sensors, 3-axial magnetometer
Actuators for attitude control	ON
Actuators for tether deployment	ON
Actuators for orbit control	OFF
Sensors for attitude and orbit determination	ON

Table 4.37: Tether Pre-Deployment Mode's key points

4.14.6 Orbit Maintenance and Deorbit Mode

If the acquisition and maintenance of the operational orbit are needed, this mode will be activated. To comply with the 25 years lifetime limit, a deorbiting maneuver might be necessary depending on the final orbit of the CubeSat.

AOCS sends telemetry	Yes
AOCS receives commands	Yes
Data available	Housekeeping sensors, GPS, IMU, Sun sensors, 3-axial magnetometer
Actuators for attitude control	ON
Actuators for tether deployment	ON
Actuators for orbit control	ON
Sensors for attitude and orbit determination	ON

Table 4.38: Orbit Maintenance and Deorbit Mode's key points

4.14.7 Function Enabling Scheme per Mode

See appendix B for the detailed figure.

"X" denotes that the function is actively used in the loop.

"(X)" denotes that the function is active for monitoring only and not used actively.

5 Conclusion

5.1 Conclusion

This thesis describes the AOCS trade studies and design of a CubeSat mission to GTO. The current research was done for the FORESAIL-2 satellite organized by the Finnish Centre of Excellence in Research of Sustainable Space. The final design presented in this work was intended to be rather generic since the mission itself is still at an early stage of development, and the other subsystems are not fully established. Based on the literature review, it was shown that the GTO environment is a location of interest to accomplish science, but is yet to be touched by nanosatellites because of the difficulties for them to survive. Consequently, the theoretical background was meant to inspect the technologies available for CubeSats, alongside with a survey of the potential disturbances that will affect the spacecraft.

A detailed list of major requirements for the attitude and orbit was written with the intent to get a general overview of the objectives and constraints that come with the designed mission. From this list, few requirements seem to be more crucial than others for one mission phase specifically, which is the tether deployment. Accordingly and among others, FORESAIL-2 shall have an attitude knowledge better than 3°, an attitude control accuracy better than 2°, its spin axis perpendicular to the Earth's magnetic field vector, a spin period of 20 seconds, and a method to increase drastically its spin rate.

After characterizing the orbit propagation within STK, mission design analyses were performed to conclude on the form factor of the CubeSat, the orbital lifetime and decay, and the total radiation dose expected to impact the satellite. It was found that FORESAIL-2 shall be a 6U CubeSat because of the potential lack of power generation crucial for all subsystems if a 3U factor form is chosen. Not a single orbit studied with a perigee superior to 300 km was compliant with the 25 years guideline. Thus, a maximum threshold limit for the perigee was set to this value, while the apogee remains at 35786 km. Another interesting outcome when looking at the decreasing perigee in the first months of the satellite's lifetime was that the best launch times occur around the months of June and September. This parameter depends mostly on the launch providers, but still is valuable. The study of the radiation environment in the desired orbit let to the conclusion that a shielding thickness of 7 mm (using Aluminium) seems to be sufficient to provide enough protection against the radiation dose. By using such a protection, a total dose of less than 20 $krads$ for the planned mission lifetime is assured for the on-board components and subsystems.

To study the ideal AOCS configuration, a particular attention was set on the actuators as the decision actually depended on the possibility to deploy the tether or not. It was decided that magnetorquers cannot provide the required angular momentum even when the best-case scenario was simulated, exceeding the maneuver time limit allowed by the science team. The design of a reaction wheel unit using a threshold constraint on the size showed that this type of actuators cannot be use for tether deployment because of the poor momentum that could potentially be provided. A propulsion unit is the only type of actuators that can provide the required angular momentum. An analysis on different propulsion units was done in order to obtain the maneuver time, the propellant mass needed, and the energy required. The electric propulsion units studied had a longer maneuver time but less propellant needed. Nonetheless, the results for the required energy were too high (especially knowing that the power generation might be a problem on-board FORESAIL-2), with an average value of 1.2 kWh. From there, the baseline configuration took the Orbital Thruster propulsion unit from Aurora Propulsion Technologies as the current solution for the AOCS set. As the tether deployment needs to be done in the Z-axis only, a minimum of two propulsion units is needed to provide accurate and stable thrust generation.

With the results obtained from the mission design analyses and the trade-off study on the actuators, it was found that the AOCS configuration will be composed of a Sun sensor on each face of the CubeSat, making a total of six Sun sensors. They shall act as the main attitude determination sensors and provide the desired accuracy. The use of a star tracker was discarded after finding out that the maximum limit on the tracking rate was in the order of 10° per second. A three-axial magnetometer should provide information regarding the evolution of the Earth's magnetic field at any point in the orbit. A GPS will give the information about the position of the satellite in the inertial frame in order to compute the orbital velocity and position vectors. Because the angular rates are one of the most important measurements, an IMU composed of three gyros is to be accommodated in the AOCS set. An IMU is preferred over simple gyroscopes because of the low gyro noise and low gyro bias instability it can provide. A radiation sensor and a temperature sensor shall also be put for housekeeping purposes. For the actuators, reaction wheels will provide the means to spin the satellite at the desired spin rate. Two propulsion units will provide the means to deploy the tether, and a minimum of six other propulsion units are needed in order to detumble the reaction wheels.

From this configuration, a study on different models available on the market was conducted to obtain a mass and volume budgets. The Sun sensors should be the same as in FORESAIL-1 and developed by Aalto University. The GPS and antenna models would be provided by NovAtel and PCTEL. The IMU, from Sensonor, is composed of three highly accurate MEMS, three high stability accelerometers and three inclinometers. The reaction wheels were chosen using the Wertz and Larson formula, and the RW3-0.06 from Sinclair Interplanetary was the best fit in terms of mass and available momentum. Finally, two Orbital Thruster units for tether deployment and one Attitude and Orbit Control System unit from for detumbling from Aurora Propulsion Technologies are chosen as a baseline. Correspondingly, the proposed AOCS configuration should have a final volume of 1628.663 cm^3, and a final mass of 1.471 kg.

Finally, based on the constraints collected from the major requirements, the mission design analyses, and the trade-off study on the AOCS configuration, five main pointing modes have been established: Safe Mode, Coarse Pointing Mode, Fine Pointing Mode, Tether Pre-Deployment Mode, and Orbit Maintenance and Deorbit Mode.

5.2 Future developments

It is recommended by the author of this thesis to start analyzing the other subsystems in order to establish the overall system budgets of the satellite. An in-depth simulation on the power requirements needs to be conducted to conclude on the use of deployable solar panels or attached solar panels.

For each defined modes, the needed algorithms for estimation, control, and filtering need to be identified. This can be done by doing a trade-off between different methods, and by conducting stability and performance analysis.

Once the components have all been selected and ordered after discussions with the manufacturers, the complete AOCS configuration should undergo a verification process. Step by step verification logic from numerical models to real hardware should be carried out in order to validate the behavior of the subsystem. The typical steps include the AOCS design and performance verification, the AOCS software and hardware verification, the verification at satellite level, the ground interface verification, and the in-flight verification.

Ultimately, it is recommended to involve more employees to the FORESAIL-2 project once FORESAIL-1 will have been launched to increase the efficiency of the satellite's development.

Bibliography

[1] H. Li. *Geostationary Satellites Collocation*. Springer, 2014. ISBN: 978-3-642-40798-7.

[2] AJ. Valverde Sacristan. *Thermal Control in Space: Heat Sources*. 2016. URL: https://www.techforspace.com/spaceflight/thermal-control-heat-sources/.

[3] J. Meseguer et al. *Spacecraft Thermal Control*. Woodhead Publishing, 2012. ISBN: 978-1-84569-996-3.

[4] H. Curtis. *Orbital Mechanics for Engineering Students*. Elsevier, 2005. ISBN: 0-7506-6169-0.

[5] ESA Space Debris Office. *ESA's Annual Space Environment Report*. 2019. URL: https://www.sdo.esoc.esa.int/environment_report/Space_Environment_Report_latest.pdf.

[6] Alan C. Tribble. *The Space Environment: Implications for Spacecraft Design*. Princeton University Press, 2003. ISBN: 978-0-691-10299-3.

[7] TJ. Patrick. "Space environment and vacuum properties of spacecraft materials". In: *Vacuum* (1981). DOI: 10.1016/S0042-207X(81)80042-5.

[8] ESA Operated by Belgian Institute for Space Aeronomy. *SPENVIS - Space Environment, Effects, and Education System*. 2018. URL: https://www.spenvis.oma.be/.

[9] E. Howell. *Van Allen Radiation Belts: Facts & Findings*. 2018. URL: https://www.space.com/33948-van-allen-radiation-belts.html.

[10] D. Hastings and H. Garrett. *Spacecraft-Environment Interactions*. Cambridge University Press, 1996. ISBN: 978-0-511-52503-2.

[11] L. Keesey. *NASA's New Dellingr Spacecraft Baselined for Pathfinding CubeSat Mission to Van Allen Belts*. 2018. URL: https://www.nasa.gov/feature/goddard/2018/nasa-s-new-dellingr-spacecraft-baselined-for-pathfinding-cubesat-mission-to-van-allen-belts.

[12] E. Mabrouk. *What are SmallSats and CubeSats?* 2015. URL: https://www.nasa.gov/content/what-are-smallsats-and-cubesats.

[13] G. Konecny. "Small satellites – A tool for Earth observation?" In: *XXth ISPRS Congress Technical Commission* 4 (2004), pp. 580–582.

[14] E. Kulu. *Nanosats Database*. 2019. URL: https://www.nanosats.eu/.

[15] K. Shubber. *Constellations of CubeSats are revolutionising how we use satellites*. 2013. URL: https://www.wired.co.uk/article/viva-los-cubesats.

[16] NASA Jet Propulsion Laboratory. *Mars Cube One Demo*. URL: https://www.jpl.nasa.gov/news/press_kits/insight/launch/appendix/mars-cube-one/.

[17] A. Elsaesser et al. "SpectroCube: a European 6U nanosatellite spectroscopy platform for astrobiology and astrochemistry". In: *Acta Astronautica* (2020). DOI: https://doi.org/10.1016/j.actaastro.2020.01.028.

[18] L. Kepko et al. *GTOSat: A Pathfinder for a Smallsat-Based Operational Space Weather Program*. URL: https://www.swpc.noaa.gov/sites/default/files/images/u59/04%20Larry%20Kepko%20Official.pdf.

[19] C. Goodloe. *DellingrX: SmallSat Architecture and Platform Enabling Planetary Science*. 2018. URL: https://cubesats.gsfc.nasa.gov/symposiums/2018/presentations/Day2/0915_Goodloe.pdf.

[20] S. Clarke, J. Moses, and L. Blum. *GTOSat: A 6U CubeSat in Geosynchronous Transfer Orbit to Study Radiation Belt Dynamics*. URL: https://techport.nasa.gov/view/94406.

[21] Finnish Centre of Excellence in Research of Sustainable Space (FORESAIL). *FS-1 Mission paper*. 2018.

[22] A. Alho. *FORESAIL-1 Renders*. 2018.

[23] Finnish Centre of Excellence in Research of Sustainable Space (FORESAIL) et al. *FORESAIL-2 Mission Objectives and Requirements*. 2019.

[24] H. Goldstein and C.P. Poole. *Classical Mechanics*. Addison-Wesley Publishing Company, 1980. ISBN: 978-0-201-02918-5.

[25] P. Fortescue, J. Stark, and G.G. Swinerd. *Spacecraft Systems Engineering*. 2005. DOI: 10.1002/9781119971009.

[26] M. Macdonald and V. Badescu. *The International Handbook of Space Technology*. 2014. ISBN: 978-3-642-41100-7.

[27] C. Young-Keun et al. "Design and development of HAUSAT-1 picosatellite system (CubeSat)". In: (2003).

[28] J. O'Sullivan. *European Missions to the International Space Station*. Springer, 2019. ISBN: 978-3-030-30326-6.

[29] P. Berlin. *Satellite Platform Design*. Lulea University of Technology, 2014. ISBN: 978-91-637-5330-5.

[30] National Aeronautics and Space Administration NASA. *State of the Art of Small Spacecraft Technology*. 2018. URL: https://sst-soa.arc.nasa.gov/05-guidance-navigation-and-control.

[31] W. Homer Mark. *Deep-Space Positioning System (DPS)*. URL: https://ntts-prod.s3.amazonaws.com/t2p/prod/t2media/tops/pdf/NPO-TOPS-26.pdf.

[32] R. Vainio. *Spin-averaged Illuminated Panel Area*. 2020.

[33] United Nations Office For Outer Space Affairs. *Space Debris Mitigation Guidelines of the Committee on the Peaceful Uses of Outer Space*. 2007.

[34] European Cooperation for Space Standardization. *ECSS-U-AS-10C Rev.1 – Adoption Notice of ISO 24113: Space systems – Space debris mitigation requirements*. 2019.

[35] K.A. Pfitzer and W.P. Olson. "Olson-Pfitzer field model (1974)". In: *Planetary and Space Science - PLANET SPACE SCI* (1992). DOI: 10.1016/0032-0633(92)90229-H.

[36] N.J. Pelton and F. Allahdadi. *Handbook of Cosmic Hazards and Planetary Defense*. Springer, 2015. ISBN: 978-3-319-03952-7.

[37] *Attitude Determination and Attitude Control*. URL: http://oberon.roma1.infn.it/metodiastrofisicaspaziale/lezione_7_2015.pdf.

[38] NewSpace Systems. *Magnetorquer Rod*. 2020. URL: http://www.newspacesystems.com/wp-content/uploads/2020/04/NewSpace-Magnetorquer-Rod_7b.pdf.

[39] Sinclair Interplanetary. *Nanosatellite Reaction Wheels (RW-0.03)*. 2019. URL: http://www.sinclairinterplanetary.com/reactionwheels.

[40] Rockwell Collins. *RSI 68 Momentum and Reaction Wheels 14 – 68 Nms with integrated Wheel Drive Electronics*. 2007. URL: http://www.electronicnote.com/RCG/RSI%2068_A4.pdf.

[41] Bradford Space. *REACTION WHEEL UNIT*. 2019. URL: https://www.bradford-space.com/assets/pdf/be_datasheet_rwu_2019dec.pdf.

[42] E. Oland and R. Schlanbusch. "Reaction wheel design for CubeSats". In: *ResearchGate* (2009). DOI: 10.1109/RAST.2009.5158296.

[43] H. D. Young and R. A. Freedman. *University Physics, 11th Edition*. Pearson Education, 2004. ISBN: 978-3-319-58914-5.

[44] M. J. Sidi. *Spacecraft Dynamics and Control: A Practical Engineering Approach*. Cambridge University Press, 1997. ISBN: 978-0-521-55072-7.

[45] G.P. Sutton and O. Biblarz. *Rocket Propulsion Elements*. Wiley, 2001. ISBN: 978-0-471-32642-7.

[46] P.M. Sforza. *Theory of Aerospace Propulsion*. Elsevier Science, 2011. ISBN: 978-1-856-17912-6.

[47] Enpulsion. *IFM NANO THRUSTER*. 2020. URL: https://www.enpulsion.com/wp-content/uploads/ENP2018-001.F-IFM-Nano-Thruster-Product-Overview.pdf.

[48] Busek. *Ion Thrusters*. 2020. URL: http://busek.com/technologies__ion.htm.

[49] Morpheus Space. *nanoFEEP*. 2020. URL: https://www.morpheus-space.com/static/MSWeb/documents/M-Space%20Products.pdf.

[50] Accion. *Tile 50*. 2020. URL: https://www.accion-systems.com/tile.

[51] Clyde Space Ltd. *Pulsed Plasma Thruster (PPT) projects*. 2018. URL: https://mars-space.co.uk/ppt.

[52] Aurora Propulsion Technology. *ORBITAL THRUSTER (OT)*. 2020. URL: https://auroraptfi/wp-content/uploads/2020/05/Aurora-OT.pdf.

[53] GOMspace. *NanoProp 6U*. 2019. URL: https://gomspace.com/UserFiles/Subsystems/flyer/gomspace_nanoprop_cgp6_flyer.pdf.

[54] POPSAT. *POPSAT-HIP1*. 2020. URL: http://www.pop-sat.com/.

[55] VACCO. *Propulsion Unit for CubeSats*. 2020. URL: https://www.cubesat-propulsion.com/wp-content/uploads/2016/03/11044000-01_PUC_2019update.pdf.

[56] VACCO. *End-Mounted Standard MiPS*. 2020. URL: https://www.cubesat-propulsion.com/wp-content/uploads/2015/08/X14029003-1X_MiPS_standard_end-mounted-2019update.pdf.

[57] NewSpace Systems. *NewSpace Magnetometer NMRM-001-485*. 2020. URL: http://www.newspacesystems.com/wp-content/uploads/2020/04/NewSpace-Magnetometer_8b.pdf.

[58] NovAtel. *OEM7600 Dual-Frequency GNSS Receiver*. 2020. URL: https://hexagondownloads.blob.core.windows.net/public/Novatel/assets/Documents/Papers/OEM7600-Product-Sheet/OEM7600-Product-Sheet.pdf.

[59] PCTEL. *Low Noise Embedded GPS Antenna — 3961D*. 2020. URL: https://www.pctel.com/wp-content/uploads/2018/11/Product-Datasheet-63.pdf.

[60] Sensonor. *Inertial Measurement Unit - STIM300*. 2020. URL: https://www.sensonor.com/products/inertial-measurement-units/stim300/.

[61] Aurora Propulsion Technologies. *Attitude and Orbit Control System (AOCS)*. 2020. URL: https://auroraptfi/wp-content/uploads/2020/05/Aurora-AOCS-v5.pdf.

[62] J.R. Wertz and W. Larson. *Space Mission Analysis and Design*. Springer, 1999. ISBN: 978-0-7923-5901-2.

A Tether deployment

The required angular momentum and total impulse to fulfill the tether deployment were obtained from a fist analysis done using MATLAB by the department working on FORESAIL-2. As the goal of the thesis was not to study the structural and attitude dynamics of the tether, the numbers were just taken and assumed to be correct. As a matter of fact, the author of this thesis was instructed to use those numbers for calculation and analyses as a baseline.

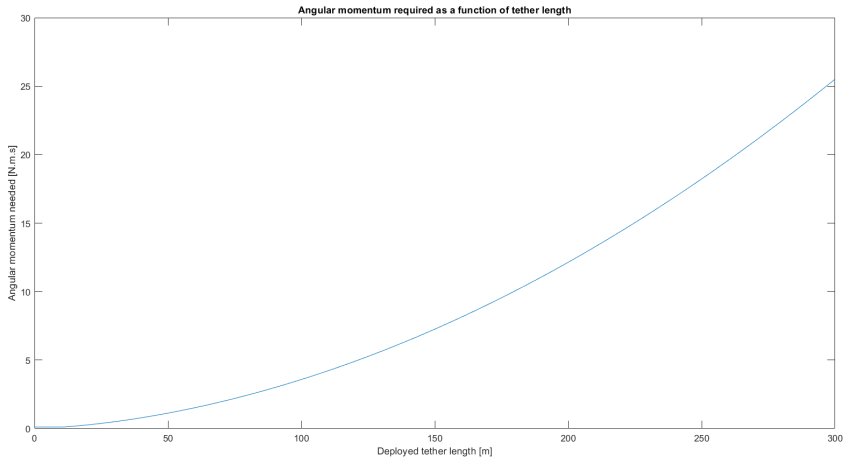

Figure A.1: Angular momentum required as a function of tether length.

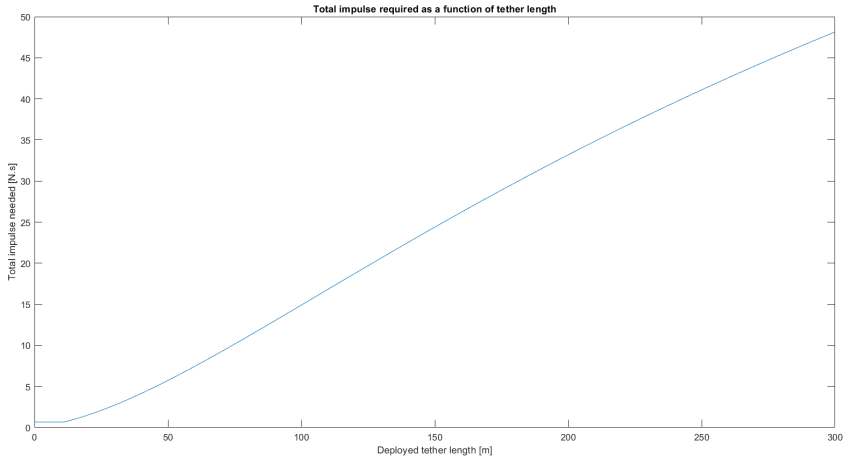

Figure A.2: Total impulse required as function of tether length.

B Scheme per Mode

Category	Function name	SM	CPM	FPM	TPDM	OMDM
Signal conditioning	GPS signal conditioning		(X)	(X)	(X)	X
	IMU signal conditioning	(X)	X	X	X	X
	Magnetometer signal conditioning	(X)	(X)	(X)	(X)	(X)
	Radiation sensor signal conditioning	(X)	(X)	(X)	(X)	(X)
	Sun sensors signal conditioning		X	X	X	X
	Temperature sensor signal conditioning	(X)	(X)	(X)	(X)	(X)
Navigation and estimation	Sun vector estimation		X	X	X	X
	Body rate estimation	(X)	X	X	X	X
	Orbit propagator		(X)	(X)	(X)	X
Guidance	Attitude guidance		X	X	X	X
	Orbit guidance					X
Control	Detumble control		X			
	Sun acquisition control		X			
	Momentum management control		X	X	X	X
	Reaction wheel attitude control		X	X	X	X
	Thruster attitude control		X	X	X	X
	Orbit control					X
Command distribution	Reaction wheel command distribution		X	X	X	X
	Thruster command distribution		X	X	X	X

Figure B.1: Function Enabling Scheme per Mode for FORESAIL-2.